Wave-influenced deltas grow through cyclical accretion of barrier-spits

Connor Broaddus[1], Jaap H Nienhuis[2], Douglas Arthur Edmonds[3], and Efi Foufoula-Georgiou[1]

[1]University of California, Irvine
[2]Utrecht University
[3]Indiana University

November 27, 2024

Abstract

Wave-influenced deltas are the most abundant delta type and are also potentially the most at-risk to human-caused changes, owing to the effects of wave-driven sediment transport processes and the short timescales on which they operate. Despite this, the processes controlling wave-influenced growth are poorly understood, and the role of fine-grained cohesive sediment (mud) is typically neglected. Here we simulate idealized river deltas in Delft3D across a range of conditions to interrogate how relative wave-influence and fluvial sediment composition impact delta evolution on decadal-millennial timescales. Our simulations capture the barrier-spit formation and accretion process characteristic of prograding wave-influenced deltas, such as those of the Red (Vietnam), Sinu (Colombia), and Coco (Nicaragua) rivers. Barrier-spit accretion exhibits multi-decadal cyclicity driven by subaqueous accumulation of fluvial sediment near river mouths. Using a range of metrics, we quantify how waves and mud influence delta morphology and dynamics. Results show that waves stabilize and simplify channel networks, smooth shorelines, increase shoreline reworking rates, reduce mud retention in the delta plain, and rework mouth bar sediments to form barrier-spits. Higher fluvial mud concentrations produce simpler and more stable distributary networks, rougher shorelines, and limit back-barrier lagoon preservation without altering shoreline reworking rates. Our findings reveal distinct controls on shoreline change between river-dominated and wave-influenced deltas and demonstrate that mud plays a critical role in delta evolution, even under strong wave influence. These insights could enhance paleoenvironmental reconstructions and inform predictions of delta responses to climate and land-use changes.

Hosted file

`ms05.gif` available at https://authorea.com/users/573566/articles/1243878-wave-influenced-deltas-grow-through-cyclical-accretion-of-barrier-spits

Hosted file

`ms01.gif` available at https://authorea.com/users/573566/articles/1243878-wave-influenced-deltas-grow-through-cyclical-accretion-of-barrier-spits

Hosted file

`ms02.gif` available at https://authorea.com/users/573566/articles/1243878-wave-influenced-deltas-grow-through-cyclical-accretion-of-barrier-spits

Hosted file

`ms04.gif` available at https://authorea.com/users/573566/articles/1243878-wave-influenced-deltas-grow-through-cyclical-accretion-of-barrier-spits

Hosted file

`ms03.gif` available at https://authorea.com/users/573566/articles/1243878-wave-influenced-deltas-grow-through-cyclical-accretion-of-barrier-spits

Wave-influenced deltas grow through cyclical accretion of barrier-spits

Connor Broaddus[1], Jaap H. Nienhuis[2], Douglas A. Edmonds[3], Efi Foufoula-Georgiou[1,4]

[1]Department of Civil and Environmental Engineering, University of California Irvine, USA
[2]Department of Physical Geography, Utrecht University, NL
[3]Department of Earth and Atmospheric Sciences, Indiana University, USA
[4]Department of Earth System Science, University of California Irvine, USA

Key Points:

- Barrier-spits are the primary constructional elements of wave-dominated deltas and leave distinct signatures (lagoons) on the delta plain.
- Accretion of barrier-spits is a cyclical autogenic process controlled by accumulation of fluvial sediment near the delta front.
- Mud exerts important controls barrier-spit accretion and distributary channel network morphodynamics, even in wave-dominated deltas.

Corresponding author: Connor Broaddus, `cbroaddu@uci.edu`

Abstract

Wave-influenced deltas are the most abundant delta type and are also potentially the most at-risk to human-caused changes, owing to the effects of wave-driven sediment transport processes and the short timescales on which they operate. Despite this, the processes controlling wave-influenced growth are poorly understood, and the role of fine-grained cohesive sediment (mud) is typically neglected. Here we simulate idealized river deltas in Delft3D across a range of conditions to interrogate how relative wave-influence and fluvial sediment composition impact delta evolution on decadal-millennial timescales. Our simulations capture the barrier-spit formation and accretion process characteristic of prograding wave-influenced deltas, such as those of the Red (Vietnam), Sinu (Colombia), and Coco (Nicaragua) rivers. Barrier-spit accretion exhibits multi-decadal cyclicity driven by subaqueous accumulation of fluvial sediment near river mouths. Using a range of metrics, we quantify how waves and mud influence delta morphology and dynamics. Results show that waves stabilize and simplify channel networks, smooth shorelines, increase shoreline reworking rates, reduce mud retention in the delta plain, and rework mouth bar sediments to form barrier-spits. Higher fluvial mud concentrations produce simpler and more stable distributary networks, rougher shorelines, and limit back-barrier lagoon preservation without altering shoreline reworking rates. Our findings reveal distinct controls on shoreline change between river-dominated and wave-influenced deltas and demonstrate that mud plays a critical role in delta evolution, even under strong wave influence. These insights could enhance paleoenvironmental reconstructions and inform predictions of delta responses to climate and land-use changes.

Plain Language Summary

Humans have disrupted sediment delivery to river deltas globally, and deltas with strong wave climates (wave-influenced deltas) may be the most vulnerable to these disruptions. However, wave-influenced deltas are poorly understood. To address this, we developed computer models of wave-influenced delta growth and used them to investigate how the processes involved in delta formation are affected by waves and by the type of sediment delivered by the river. Our models show that wave-influenced delta growth is fundamentally different from deltas with weak wave-climates; wave-influenced deltas are made up of shore-parallel sand bodies, which we call "barrier-spits". Each barrier-spit takes multiple decades to form, and they are added to the delta at regular intervals. Our models also show that mud affects the way in which deltas form, even when waves are large. Mud is deposited between barrier-spits, affecting delta deposits. Mud also impacts the way that river channels grow and move around the delta, where more mud leads to fewer and more stable channels. Overall, our models are useful for understanding how waves and mud impact the growth of river deltas, which may help us to predict how deltas will respond to changes in sediment delivery caused by humans.

1 Introduction

In the absence of tides, river deltas exhibit a spectrum of processes and forms thought to be the result of varying degrees of fluvial and wave influence. At one end of this spectrum are fully "river-dominated" deltas with complex distributary networks and large, lobate shoreline protrusions (L. D. Wright, 1973; Galloway, 1975; Broaddus et al., 2022; ?, ?). These systems grow through a combination of avulsion and mouth-bar driven bifurcation, both of which can be driven by channel elongation and resultant reductions in local sediment transport capacity (Jerolmack & Swenson, 2007; Edmonds & Slingerland, 2007, 2010; Fagherazzi et al., 2015). At the other end of this spectrum are "wave-dominated" deltas, which lack distributary networks and have smooth, cuspate shorelines with limited protrusions (L. D. Wright, 1973; Galloway, 1975; Anthony, 2015; Broaddus et al., 2022; Vulis et al., 2023). Wave-dominated deltas grow through onshore-directed

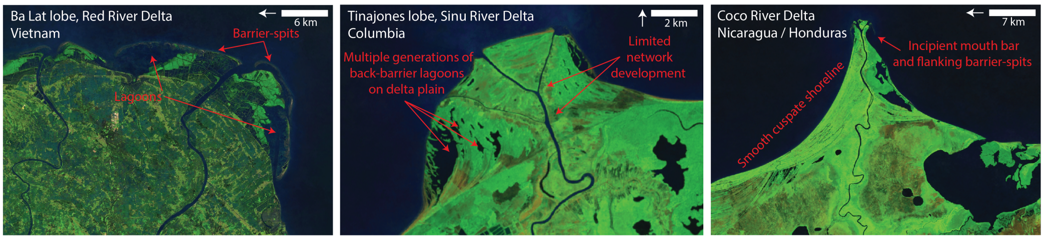

Figure 1. Examples of real-world wave-influenced deltas. Note the ubiquitous presence of shore-parallel barriers and associated lagoons, which are unique to wave-influenced systems. Other diagnostic features include simple distributary networks and smooth shorelines ranging from lobate to cuspate.

wave-driven reworking of fluvial sediment deposited in the shoreface and through impoundment of non-deltaic littoral sediment carried from updrift locations by longshore currents (Komar, 1973; L. D. Wright, 1973; Galloway, 1975; Dominguez, 1996; Ashton & Giosan, 2011; Anthony, 2015).

While the processes governing the evolution of the above-described end-members are well understood, intermediate, “wave-influenced” deltas have received considerably less attention, despite being the most abundant category of deltas (Nienhuis et al., 2020). These deltas have morphologies that vary between river and wave-dominance, but also include unique features such as barriers, spits and lagoons (Figure 1). Questions remain concerning the morphological transitions between river and wave-dominated deltas, and especially the role of mud. Do deltaic processes and morphology vary monotonically with wave-influence? And are the transitions gradual, or abrupt?

Addressing these questions is of urgent importance, as the driving forces that control delta morphology and dynamics are changing rapidly (Giosan et al., 2014; Tessler et al., 2015; Hoitink et al., 2020). Changes in land use and climate are affecting the volumes of water and sediment that reach deltas (Nienhuis et al., 2020; Tessler et al., 2018), while sea level rise and land subsidence threaten to drown existing delta deposits (J. P. Syvitski et al., 2009; Ericson et al., 2006; Ibáñez et al., 2014). Understanding how delta morphology and dynamics vary across a range of environmental forcing conditions is the first step toward predicting how deltas will respond to the plethora of anthropogenic pressures which they currently face.

2 Background

2.1 Physics-based modeling of wave influenced delta growth across scales

Physics-based numerical models provide a promising path toward predicting how wave-influenced deltas will respond to change by facilitating investigation into the interactions between river flow, wave-action, and longshore currents which govern sediment transport across a range of scales. Models such as Delft3D and MIKE (coupled with spectral wave models) provide an avenue for exploring the development and modification of river mouth bars in the presence of waves on timescales relevant to engineering (years to decades). Nardin and Fagherazzi (2012) used an idealized Delft3D model of a river mouth to show that waves impact mouth bar development by enhancing bed shear stress, changing the direction of the river jet (in the case of non-frontal waves), and increasing jet spreading. They showed that bar morphology is modulated by these processes, and bar formation is inhibited in the presence of large waves that approach from high angles. Nardin et al. (2013) used a similar model to demonstrate that the jet spreading effect dominates over increased bed shear stress in the presence of small frontal waves, which actually increases the propensity of bars to form closer to the river mouth. They suggested that a non-monotonic relation exists between wave energy and mouth bar formation; small waves enhance mouth bar formation over cases with no waves, while larger waves inhibit mouth bar formation. More recently Zăinescu et al. (2021) developed idealized river mouth models in MIKE21 FM to simulate interactions between longshore currents, mouth bars, and fluvial jets, finding that jet behavior and flow circulation patterns near the river mouth can be predicted by the momentum or discharge balances between the fluvial jet and longshore currents. A detailed review of the controls on river mouth morphodynamics is presented in Fagherazzi et al. (2015).

Physics-based numerical models are also capable of simulating the growth and evolution of wave-influenced river deltas over longer timescales (decades to centuries). Historically, wave-dominated deltas have been simulated primarily using so called ”1-line” shoreline models (Komar, 1973; Ashton & Giosan, 2011; Gao et al., 2018). These models work well to simulate shoreline evolution but cannot capture the transition to river dominance due to their inability to simulate mouth bars. In this transition, mouth bars are expected to appear as fluvial sediment supply outpaces potential longshore transport (Nienhuis et al., 2015). Geleynse et al. (2011) developed idealized delta-scale simulations in Delft3D to show that waves act to limit sequestration of fine-grained sediment on the delta plain, and reduce the number of active distributaries, leading to smoother (less rugose) delta shorelines. In a similar effort, Liu et al. (2020) showed that deltas subject to wave-action produced shallower topset gradients and reduced distributary avulsion frequency, leading to smoother shorelines. Willis et al. (2021, 2022) used the Chevron CompStrat model (which, similar to Delft3D and MIKE, is governed by the shallow water equations) to explore wave-influenced delta deposit stratigraphy under conditions of changing sea level. Their simulations develop morphologies that are remarkably similar to real-world wave-influenced delta systems, including dual clinoform delta fronts with large subaqueous platforms. Sloan et al. (2024) used idealized Delft3D models to explore the conditions under which waves completely inhibit delta accretion. Recently, Zăinescu et al. (2024) used idealized delta-scale simulations in Delft3D to investigate morphodynamics in asymmetrical wave-influenced deltas. They found that increasing degrees of wave-influence lead to channel stabilization and a reduction in avulsion frequency compared to river-dominated deltas, paralleling results from Liu et al. (2020) and morphodynamic models (Swenson, 2005; Ratliff et al., 2018; Gao et al., 2018; Hu et al., 2022). They also demonstrate that the trade-off between trapping and bypassing of updrift sediment around the river mouth is highly sensitive to the relative strengths of fluvial and longshore sediment transport, and that this relationship determines the morphology of asymmetric wave-influenced deltas.

These efforts collectively demonstrate the efficacy and utility of using physics-based numerical models to reproduce the dynamics and morphologic features common to wave-influenced deltas. Despite these advances, substantial knowledge gaps remain, particularly on the role of mud and the morphologic transition from mouth bars to barrier-spits as the dominant delta constructional element.

2.2 Barrier-spits

Among the most characteristic features of wave-influenced and wave-dominated deltas are barriers and spits (Anthony, 2015). Both barriers and spits form through a combination of cross-shore and longshore sediment transport processes, and differ primarily in that barriers are true islands while spits are connected to an adjacent landmass at one end. These features were historically associated with phases of delta abandonment, and their deposits interpreted to represent an allogenic response to changes in sedimentary (upstream) or marine (downstream) forcing. The best known example is the Chandeleur Islands of the Mississippi River delta, a set of barriers which formed by headland erosion of delta lobes (Penland et al., 1988) or onshore transport of shelf deposits (Stapor & Stone, 2004) following abandonment during large scale avulsions. Another example is the visually striking system of paired spits that flank the Ebro River delta, which have been shown through historical reconstructions and numerical modeling to be a result of decreases in fluvial sediment flux following a river avulsion (Ibàñez et al., 1997; Nienhuis et al., 2017).

More recently, a separate category of deltaic barriers and spits have been recognized which are genetically distinct from those formed as a result of marine transgression or delta lobe abandonment. This category is associated with punctuated progradation in wave-influenced environments, and may be the most common genetic mode for these features on river deltas (Stutz & Pilkey, 2002; Bhattacharya & Giosan, 2003). Furthermore, progradational barrier-spit accretion may be the dominate process by which wave-influenced deltas build new land (Vespremeanu-Stroe & Preoteasa, 2015), as evidenced by the unique geometry and sedimentary character of their deposits. While river-dominated deltas have deposits characterized by systems of mouth bars, crevasses and abandoned distributary channels (Olariu & Bhattacharya, 2006; Edmonds & Slingerland, 2010; Esposito et al., 2013; Willis et al., 2021; Nota et al., 2024), wave-influenced delta deposits are typically composed of series of regularly-spaced, elongate, shore-parallel sand bodies. These sand bodies may amalgamate to form "beach-ridge plains", or may be separated by back-barrier deposits of fine-grained sediment, forming "cheniers" (Otvos, 2000; Tamura, 2012).

The mechanisms and sediment sources responsible for the formation of barrier-spits (and their subsequent incorporation into the delta plain) are thought to vary between symmetric and asymmetric wave-influenced deltas. Asymmetric deltas form under wave climates that exhibit a dominant angle of approach, setting up unidirectional longshore currents that impart distinct processes and sedimentary facies on the updrift and downdrift flanks of the delta (Bhattacharya & Giosan, 2003; Korus & Fielding, 2015; Vespremeanu-Stroe et al., 2016; Preoteasa et al., 2016). Barrier-spits can develop on the updrift flank and morphologically "deflect" distributary outlets due to blocking of longshore currents by the fluvial jet (Todd, 1968; Komar, 1973; Nienhuis, Ashton, & Giosan, 2016; Gao et al., 2020). Barrier-spits can also develop on the downdrift flank of asymmetric deltas as a result of several different processes, including high wave approach angles that cause instabilities in the longshore transport field (Ashton & Giosan, 2011), or by gradual development of a subaqueous sediment platform followed by wave-driven onshore transport (Vespremeanu-Stroe & Preoteasa, 2015; Preoteasa et al., 2016; Zainescu et al., 2016).

Barrier-spits and their associated deposits (beach-ridges / cheniers) are also prevalent in symmetric wave-influenced deltas. The mechanisms involved in the formation and evolution of these features, however, as well as their overall role in the progradation of symmetric deltas, have received less attention than those on asymmetric systems, and are still poorly understood (Zainescu et al., 2016). One well studied example is the Red River Delta of Vietnam, where cyclical barrier-spit development is characterized by a multi-phase process consisting of subaqueous fluvial sediment accumulation, onshore transport due to wave asymmetry, and reworking by longshore currents (Van Maren, 2005; van Maren, 2007). The process is similar to that described for the downdrift flank of the asymmetric Sfantu Gheorge lobe of the Danube delta (Vespremeanu-Stroe & Preoteasa, 2015; Preoteasa et al., 2016). A similar process is thought to describe the development of the Goro spit system in the Po River delta of Italy (Simeoni et al., 2007).

Despite a likely similar origin of mouth bars (on river dominated deltas) and barrier-spits (on wave dominated deltas), they have historically been considered separately. Perhaps the conditions under which barrier-spit formation dominates over mouth bar accretion would determine the resulting morphology, and thereby also affect beach ridge spacing, and the timescales of barrier-spit formation.

2.3 Role of fine-grained cohesive sediment

There is also significant uncertainty surrounding the role of fluvial sediment composition in the formation of wave-influenced deltas. Several studies have highlighted the crucial role of fine-grained cohesive sediment (mud) in shaping the morphology and dynamics of river-dominated deltas. Higher proportions of mud in fluvial effluent reduces channel mobility, enhances the formation of levees, deepens channels and inhibits bifurcations and avulsions, limiting the total number of active distributaries on a delta (Edmonds & Slingerland, 2010; Martin et al., 2009; Li et al., 2017). The effects of mud on the channel network propagate to the overall shape of the delta and its shoreline; fluvial sediment flux is distributed less evenly across the delta shoreline, leading to enhanced growth of local shoreline protrusions and producing more elongate delta plains with rougher shorelines (Geleynse et al., 2011; Caldwell & Edmonds, 2014).

By contrast, the role of fine-grained cohesive sediment (mud) in wave-influenced delta evolution has received significantly less attention and is commonly ignored in numerical modeling efforts due to long settling timescales and the high degree of turbulence associated with surf-zone environments (Geleynse et al., 2011; Nardin et al., 2013; Nienhuis, Ashton, Nardin, et al., 2016; Broaddus et al., 2022; Sloan et al., 2024; Zăinescu et al., 2024). However, large portions of the delta front can be sheltered from wave action by barriers and spits, permitting deposition of fine-grained sediment in these locations (Rodriguez et al., 2000; Bhattacharya & Giosan, 2003; Stutz & Pilkey, 2002; Van Maren, 2005). Both channel geometry and network dynamics are strongly dependent on the character of fluvial sediment (Orton & Reading, 1993; Hoyal & Sheets, 2009; Martin et al., 2009; Edmonds & Slingerland, 2010; Caldwell & Edmonds, 2014). Furthermore, phase differences between periods of peak discharge and significant wave events are common in deltas with large drainage basins (Anthony, 2015), which could allow fluvial mud to be incorporated in the shoreface regardless of the long-term average wave conditions.

To address the knowledge gaps outlined above we developed physics-based numerical simulations capable of resolving the complex interactions between fluvial and wave processes that control morphodynamics in wave-influenced deltas. Our simulations reproduce emergent features considered to be characteristic of wave-influenced deltas, such as mouth bars, barriers, and spits (which we refer to collectively as barrier-spits), at the timescales on which deltas grow and evolve. They differ from previous efforts (Geleynse et al., 2011; Liu et al., 2020; Willis et al., 2021; Sloan et al., 2024; Zăinescu et al., 2024) by focusing on the role of mud. We characterize the barrier-spit accretion process and its temporal characteristics using quantitative frequency analysis. We present metrics to quantify delta morphology and dynamics and show how the processes controlling delta evolution vary with wave-influence and the proportion of cohesive sediment in fluvial effluent. Finally, we discuss the implications of our findings for management actions, paleoenvironmental interpretation, and general knowledge of wave-influenced delta morphodynamics.

3 Methods

3.1 Model Setup

Delft3D is a hydro-morphodynamic modeling package capable of simulating fluid flow (Reynolds-averaged Navier-Stokes equations), wave action (SWAN model), sediment transport, and morphological change. It has been validated for a wide range of hydrodynamic conditions and has been shown to be capable of simulating idealized delta development (Storms et al., 2007; Edmonds & Slingerland, 2010; Geleynse et al., 2011; Burpee et al., 2015; Caldwell & Edmonds, 2014; Rossi et al., 2016; Liu et al., 2020; Broaddus et al., 2022; Xu & Plink-Björklund, 2023; Anderson et al., 2023; Nota et al., 2024; Sloan et al., 2024; Zăinescu et al., 2024), as well as the morphodynamics at wave-influenced river mouths (Edmonds & Slingerland, 2007; Nardin & Fagherazzi, 2012; Nardin et al., 2013; Nienhuis, Ashton, & Giosan, 2016; Gao et al., 2018; Zăinescu et al., 2021).

Using Delft3D we set up an idealized model of river delta growth and evolution in the presence of waves. For simplicity we ignore the effects of tides, wind, density gradients, Coriolis forces, and other factors that may impact delta morphodynamics. The flow equations are solved on a rectilinear grid of 25 m square cells covering an area of 189 km^2 (21 km in the cross-shore direction, 9 km in the long shore direction) (Figure 2a). Initial bed levels in all simulations consist of a river with a trapezoidal geometry (width = 300 m, depth = 3 m) that cuts through a bluff-backed beach (bluff height = 10 m, bluff width = 500 m, beach height = 2 m, beach width = 500 m) and terminates into a sloping basin (Figure 2b). The basin slope follows an equilibrium shoreface profile for 200 µm sand (Equation 1), as defined by Dean (1991).

$$z(x) = ax^{2/3} \tag{1}$$

where z is the water depth (m), x is the distance from shore (m), and a is a grain size dependent parameter whose value is 0.1 for 200 µm sand. Figure 2b shows the initial bathymetry in the region around the river mouth.

We add random perturbations to the initial bed levels to simulate natural variability, which are drawn from a uniform distribution bounded by -0.01 and 0.01 m. To enable faster progradation and maintain the shallow water assumption, we limit initial depth to 10 m below sea level (which is beyond the inner depth of closure for the largest modeled waves, as defined by Hallermeier, 1981). The model results are insensitive to the bluff and beach dimensions, as well as the depth cutoff for the initial bathymetry.

Wave computations are solved on a separate grid covering an area of 572 km^2 (52 km in the longshore direction, 11 km in the cross-shore direction) (Figure 2a). Grid cell dimensions vary in the wave domain to speed up computations; areas overlapping the flow domain have a resolution of 50 x 50 m, while areas outside the flow domain have cells that are 400 m in the longshore direction and 50 m in the cross-shore direction. Initial bathymetry in the wave domain is identical to that of the flow domain, albeit expanded to fit the enlarged grid dimensions.

All simulations use a computational time step (Δt) of 15 seconds to obey numerical stability criteria. Flow and wave computations are fully coupled (bed levels, water levels, velocities) with a coupling interval (CI) of 30 minutes. We apply a morphological scaling factor (morfac) of 180 to speed up computations, assuming that bed relaxation is negligible at the modeled timescales. Each simulation is computed for 12 hours prior to the implementation of morphological changes. We assessed the sensitivity of our results to these choices, performing simulations with Δt as small as 5 seconds, CI as small as 5 minutes, and morfac as small as 45. We also tested our models sensitivity to the grain size and initial bed thickness of non-cohesive sediment. While these simulations indeed exhibit differences in details, the emergent processes and morphological trends discussed in this work do not change.

We model two sediment fractions, one non-cohesive (sand) and one with cohesion (mud). The sand fraction has a median grain size of 200 µm, a specific density of 2650 kg m^{-3}, and an initial bed thickness of 10 m that is constant throughout the domain. The mud fraction has a settling velocity of 0.00025 m s^{-1}, and critical shear stresses for erosion (τ_{ce}) and deposition (τ_{cd}) of 0.1 and 1000 N m^{-2}, respectively. Setting τ_{ce}<<τ_{cd} ensures constant mud deposition such that equilibrium depth is set by erosive shear stresses, rather than being dependent on initial sediment thickness (Edmonds & Slingerland, 2010). We chose a relatively low value for τ_{ce} to facilitate mud erosion and to avoid over representing the importance of cohesive sediment in delta dynamics.

The models initialize with no mud in the bed, a choice which notionally reflects the paucity of mud in wave-influenced nearshore settings prior to the introduction of fluvial

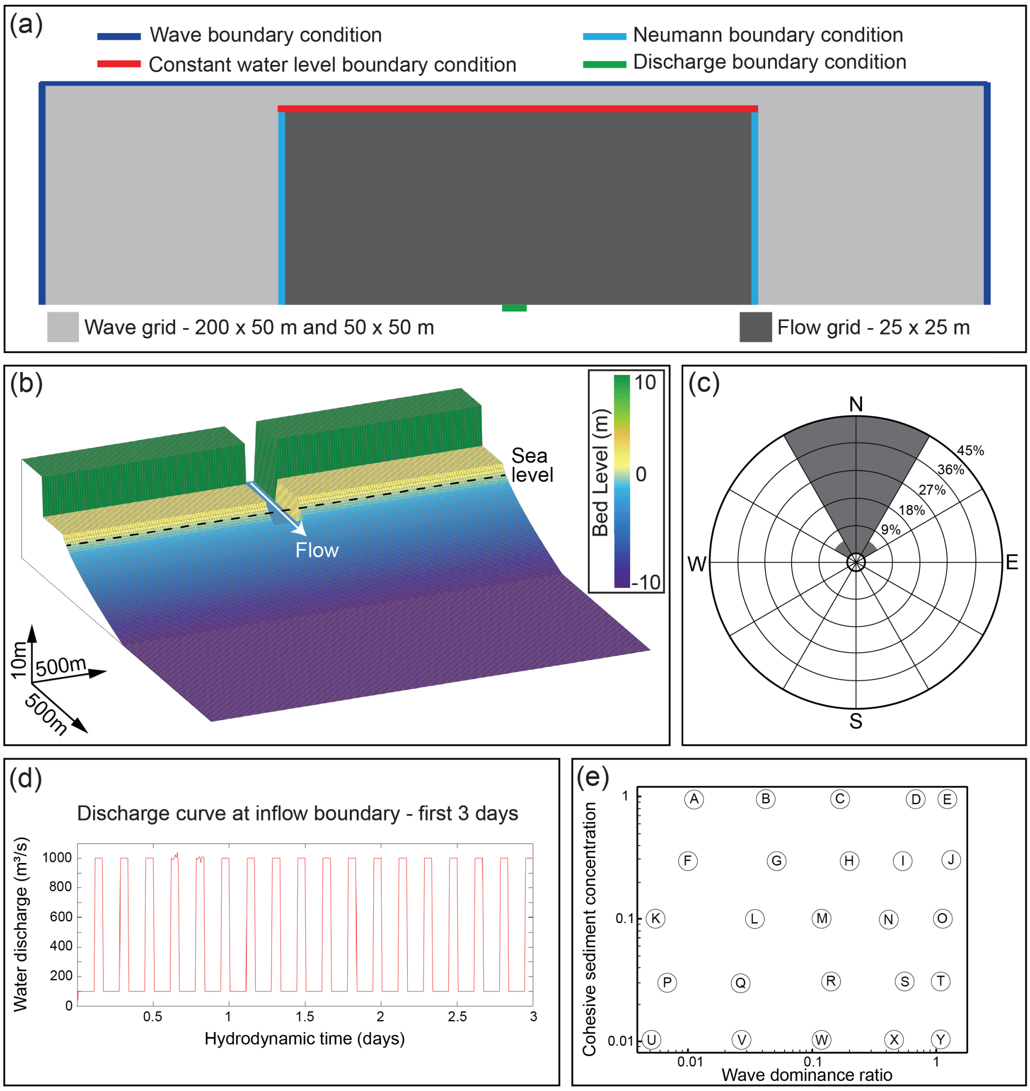

Figure 2. Model setup including domain and boundary locations (a), initial bathymetry (b), wave directional distribution (c), discharge curve (d) and simulation ensemble (e).

effluent. Non-cohesive sediment transport is computed using the Soulsby-Van Rijn relation as implemented in Delft3D, which requires the user to specify the calibration factor for sediment transport (1), the diameter ratio between 90th percentile and median grain sizes (1.5), and the roughness height used to compute the drag coefficient (0.006). We use the values recommended by Soulsby (1997). This formula predicts bed and suspended load transport based on the combined shear stress due to current velocity and root mean squared wave orbital velocity (neglecting transport by depth varying currents and wave asymmetry). Its simplicity makes it well suited to 2DH simulations of coastal morphodynamics. Cohesive sediment transport is computed using the well-known Partheniades-Krone relation. Each of these transport relations is described in detail in the Delft3D-FLOW User Manual.

Boundaries are placed along the North, East, and West edges of the wave domain, and impart significant wave heights that vary between runs but are constant for a given run. Wave direction changes at each coupling timestep, and for each simulation the sequence of wave directions are randomly drawn from a predefined wave energy density spectrum (which is constant across runs). The distribution of wave energy is such that 90% of the waves come from -30 and 30 degrees relative to shore normal, while 10% come from -45 and 45 degrees relative to shore normal (Figure 2c). Previous work has demonstrated that the most important spectral parameters in determining delta morphology are directional (a)symmetry and the fraction of waves that approach from high, unstable angles (45 degrees or greater) (Ashton & Giosan, 2011; Ratliff et al., 2018; Hu et al., 2022). We chose this spectrum for simplicity and to facilitate future comparison with one-line delta evolution models, in which it is commonly used.

Water and sediment enter the domain through a discharge boundary condition located at the upstream limit of the inflow channel (Figure 2a). We specify the cohesive sediment concentration at the inflow boundary (which varies between simulations but is constant throughout a given simulation) while allowing the non-cohesive sediment concentration to vary with the hydrodynamics (equilibrium concentration), which maintains a constant bed level and ensures stability. We specify a constant water level boundary along the Northern edge of the domain, and apply Neumann boundaries along the Eastern and Western edges to allow water and sediment to enter and exit freely. Turbulence closure in the x and y directions is achieved through subgrid horizontal large eddy simulations, using the default options suggested by Deltares (Delft3D-FLOW User Manual).

In order to represent the discharge variability inherent to most river systems, we defined the inflow hydrograph as an asymmetric quasi-square wave that oscillates between high (1000 m^3 s^{-1}) and low (100 m^3 s^{-1}) discharge values. For each oscillation period, the low and high flow duration is 160 and 70 minutes respectively, with a 10 minute "ramp" between low and high flows (Figure 2d). While most idealized delta modeling studies are performed with a constant discharge boundary condition, accurately representing the dynamics at work in wave-influenced deltas requires variable discharge, due to the higher recurrence intervals of significant wave events relative to significant discharge events. We also tested other wave forms and shapes for the hydrograph (sawtooth, sine wave, repeating beta distribution) and found that, for a given ratio of high to low flow duration, the morphology and processes that emerge are more or less constant.

We apply a spatially constant horizontal eddy viscosity (E_v) and horizontal eddy diffusivity (E_d) of 1 m^2 s^{-1}, and set the factor for erosion of adjacent dry cells (Θ_{sd}) to 0.5. We tested the model's sensitivity to these choices, varying E_v and E_d from 0.0001 to 1 m^2 $s^{-1}$and varying Θ_{sd} from 0.1 to 0.9. We found that varying these parameters did not significantly affect the morphological trends or emergent process described.

We apply a spatially constant Chezy roughness (C) value of 65 $m^{1/2}$ s^{-1} to our simulations, and tested values ranging from 45-75 $m^{1/2}$ s^{-1}. Changes to C impact jet spreading rates and longshore transport, and as a result impact the morphology of our simulations. In general, increasing C (lowering roughness) decreases jet spreading and increases longshore transport rates. Decreased jet spreading leads to more sediment being transported further from the river mouth, causing mouth bars to form less frequently, decreasing the number of outlets and deepening channels. Increased longshore transport rates lead to reduced delta progradation rates and smoother shorelines, which leads to lower values of the delta shape and shoreline roughness metrics. The opposite is true for decreases in C. We chose a value of 65 $m^{1/2}$ s^{-1} for our simulations because it is the default in Delft3D, produces realistic delta morphologies, and leads to emergent longshore transport rates similar to those predicted by empirical estimates (see section 3.3).

α_{bn} is a multiplicative factor applied to account for the effects of transverse bed slopes on sediment transport rates. Baar et al. (2019) demonstrated the importance of this parameter in controlling channel aspect ratios and total transport rates. Small values of α_{bn} favor channel deepening, narrowing, generally low transport rates, and accompanying lack of channel mobility. High values lead to increased transport rates, and shallow, wide channels that are highly mobile. We chose a value of 3 because it balances these effects to produce realistic channel aspect ratios and dynamics, with transport rates that fall within the range observed in rivers with similar discharge. This value is within the range suggested by both Deltares and Baar et al. (2019).

3.2 Simulated Parameter Space

To assess the roles of waves and fluvial sediment composition in controlling delta morphology and dynamics, we designed a suite of 25 simulations that vary the mud concentration and wave amplitudes at their respective boundaries while holding all other model parameters constant.

We vary mud concentration (C_{mud}) across two orders of magnitude, from 0.01 to 1 kg m^{-3}. We chose this quantity (rather than a non-dimensional descriptor, such as sand to mud ratio) because it is a measurable quantity in natural river systems, providing a basis for comparison between our simulations and reality.

To quantify differences in the degree of wave influence, we follow the sediment flux balance approach of Nienhuis et al. (2015) to define the wave dominance ratio (W) (equation 2) – the inverse of the river-dominance ratio (R) in Nienhuis et al. (2015). In essence, this approach defines a given delta's degree of "wave-influence" based on the river's ability to supply sediment, and the given wave climate's ability to transport sediment alongshore. This approach follows decades of work which collectively suggests that river delta formation and morphology depends on the fundamental balance between constructive (fluvial) and destructive (wave, tidal) forcings (L. D. Wright, 1973; Galloway, 1975; Komar, 1973; J. P. M. Syvitski & Saito, 2007; Caldwell et al., 2019).

Fluvial sediment flux (Q_{river}) is defined as the average non-cohesive sediment (sand) transport rate at the apex of a delta system (kg s^{-1}). Here we consider only the flux of sand to keep the role of mud isolated to a separate parameter and measure the time averaged sand flux values directly from simulation outputs.

For each simulation we estimate the maximum potential longshore transport rate (Q_{wave}) (kg s^{-1}) based on the method of Nienhuis et al. (2015). This method convolves the angular distribution of wave energy (equation 3) with an empirical estimate of longshore transport as a function of deep-water wave properties (equation 4) (P.D. Komar, 1998; Ashton & Murray, 2006) to yield a distribution of potential longshore transport rates as a function of shoreline orientation (equation 5) (see Nienhuis et al. (2015) for more details).

$$W = \frac{Q_{wave}}{Q_{river}} \tag{2}$$

$$E(\phi_0) = \frac{H_s^{12/5}(\phi_0) \cdot T^{1/5}(\phi_0)}{\sum_{\phi_0} H_s^{12/5}(\phi_0) \cdot T^{1/5}(\phi_0)} \tag{3}$$

$$Q_s = K \cdot \rho_s \cdot (1-p) \cdot H_s^{12/5} \cdot T^{1/5} \cdot cos^{6/5}(\phi_0 - \theta) \cdot sin(\phi_0 - \theta) \tag{4}$$

$$Q_{s,net}(\theta) = E(\phi_0) * Q_s(\phi_0 - \theta) \tag{5}$$

where $E(\phi_0)$ is the wave energy probability distribution for all possible deep water wave approach angles (ϕ_0). H_s is the significant wave height (m), T is the wave period (s), θ is a possible local shoreline orientation, ρ_s is the density of sediment (2650 kg m^{-3}), ρ is dry bed porosity (0.4), and K is an empirical constant equal to 0.06 m$^{3/5}$ s$^{-6/5}$ (Nienhuis et al., 2015).

We sum the maximum values for transport along the left and right delta flanks as our estimate for Q_{wave}, showing that a delta will continue growing its shoreline orientation until both flanks are at equilibrium with the rate of fluvial sediment delivery, or transport is maximized.

We hold the directional distribution of wave energy constant between simulations, varying H_s between 0.1 and 3 m, resulting in W values ranging from 0.005 to 1. We limit our investigation to this range of W values to focus on the transition from river to wave-dominance.

Figure 2e shows the locations of each simulation in the parameter space explored here (the basis for the contour plots in Figure 6). Each simulation is labeled with a letter, corresponding to the RunID listed in Table 1.

3.3 Validation – Longshore Transport Comparison

To assess our simulations' ability to correctly resolve the emergent dynamics of longshore sediment transport we compared the longshore transport fields produced by our simulations with empirical predictions of longshore transport based on the prescribed deep-water wave climates.

For a given timestep in a simulation we measured the longshore transport values by integrating then averaging sediment transport rates over shore-normal cross-sections that are manually defined at 6 locations (3 for each flank) along the active delta shoreline away from the river mouth (an interactive MATLAB code facilitates this process) (Figure 3a). Cross-sections had to be manually defined at each time step because the delta progrades through time, and because the output fields of Delft3D do not enable separation of currents or transport into fluvial versus wave-driven components. Although the cross sections are defined somewhat arbitrarily, having 6 for each timestep ensures we capture the variability inherent to a longshore transport field. Aggregating values from all cross-sections over the final 33% of the simulation period gives a distribution of single-flank longshore transport rates for a given simulation (Figure 3b). We use the 90$^{\text{th}}$ percentile value from this distribution (multiplied by a factor of two to represent the total littoral transport to the left and right of the river mouth) for comparison with an empirical estimate based on the above-described method of Nienhuis et al. (2015).

The comparison between predicted (empirical) and observed (modeled) longshore transport rates is shown in Figure 3c. The comparison includes simulations with intermediate fluvial mud concentration ($C_{mud} = 0.1$ kg m^{-3}) and $H_s > 1$ m. Note that this comparison considers only sand transport, which is the basis for most empirically-derived longshore transport relations (including the one used here).

Table 1. List of simulations used in contour plots. Run ID corresponds to the letters used in Figure 2e to denote positions in parameter space. C_{mud} = mud concentration (kg m^{-3}), H_s = significant wave height (m), W = wave dominance ratio, P_c = channel persistence (%), D_{sl} = fractional shoreline change (%), L_f = lagoon fraction (%), N_{out} = number of outlets, R^* = shoreline roughness, M_f = delta plain mud fraction (%).

RunID	C_{mud}	H_s	W	P_c	D_{sl}	L_f	N_{out}	R^*	M_f
A	1	0.1	1e-2	28.8	18.7	0.1	3	77	37.5
B	1	0.5	4e-2	36.7	26.5	0	2.2	53	36.7
C	1	1	1e-1	50.2	29	0.1	1.1	15	25.1
D	1	2	6e-1	72.6	47.4	1.3	1	4	20.8
E	1	3	1	75	57.1	1.7	1	4	19.1
F	0.3	0.1	1e-2	19	13.4	0.2	4.1	32	19.3
G	0.3	0.5	4e-2	21.6	17.8	0.1	1.8	28	14.6
H	0.3	1	2e-1	53.9	29.9	0.8	1.7	12	11
I	0.3	2	5e-1	63.1	47.8	3.7	1.2	4	9.3
J	0.3	3	1	67.1	55.8	1.8	1.7	4	8.5
K	0.1	0.1	6e-3	19.5	13.9	0	5.5	23	7.2
L	0.1	0.5	3e-2	26.6	18.9	0.1	2.6	20	6
M	0.1	1	1e-1	33.9	30.3	0.5	2	19	4.4
N	0.1	2	4e-1	51.8	54.9	6.1	2	5	3.4
O	0.1	3	1	61.1	56.8	2	1.7	4	3.4
P	0.03	0.1	7e-3	18	12.4	0	6.6	20	2.6
Q	0.03	0.5	2e-2	17.5	22.2	0	5.7	18	2.2
R	0.03	1	1e-1	24.5	31.6	0.1	3.5	14	1.9
S	0.03	2	5e-1	50.3	51.9	3.2	1.9	5	1.3
T	0.03	3	1	54.1	56.3	2.3	1.9	4	1.1
U	0.01	0.1	5e-3	14.1	11.4	0	6.8	20	0.8
V	0.01	0.5	3e-2	13.2	21	0	5.1	11	0.7
W	0.01	1	1e-1	14.3	39.6	0.1	3.7	10	0.6
X	0.01	2	5e-1	32.6	49.1	3.7	2	5	0.5
Y	0.01	3	1	44	56.8	2.9	1.9	4	0.4

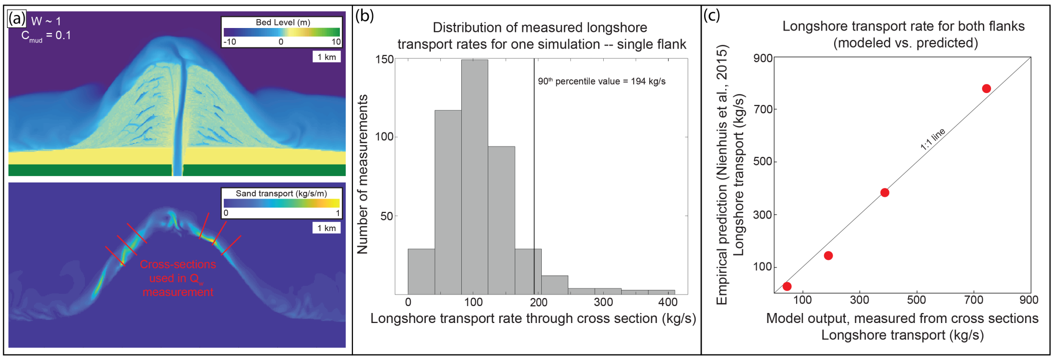

Figure 3. Comparison between empirically predicted and emergent longshore transport rates. (a) One time step of an example simulation showing bed levels (upper) and the sediment transport field (lower) at the same scale and resolution; red lines show the location of 6 example cross sections along which longshore transport is measured. This process is repeated for each low-flow time step over the final 33% of the simulation period. (b) Histogram showing the distribution of all measured longshore transport values for a single example simulation (note that these are values for a single flank). The 90$^{\text{th}}$ percentile value is multiplied by a factor of 2 to reflect transport on both flanks and used for comparison with empirical prediction for a given simulation. (c) Comparison between the measured longshore transport rates and empirically predicted maximum potential longshore transport rates for simulations with $C_{mud} = 0.1$ kg m^{-3} and $H_s \geq 1$ m. Each dot reflects these values for a given simulation.

3.4 Validation – Delta Shape Dynamics

To assess our simulations' ability to correctly resolve the delta-scale process interactions inherent to wave-influenced delta growth, we tracked the shape (ratio of maximum deposit length to maximum deposit width) of wave-influenced simulations through time. Previous work based on one-line models and observations of beach ridge orientations suggests that deltas exhibiting strong wave-influence or wave-dominance (in symmetrical wave climates) quickly obtain an equilibrium ratio of length to width and maintain this ratio throughout their growth (Komar, 1973; L. D. Wright, 1973; Ashton & Giosan, 2011). This fundamental characteristic of wave-influenced delta evolution reflects the interaction between fluvial and longshore transport process: fluvial sediment delivered to the shoreface causes seaward deflection of the shoreline, increasing the local wave approach angle and consequently the local longshore transport rate (which decreases toward the flanks as the delta flattens). When the fluvial sediment delivery rate matches the rate of longshore sediment transport away from the river mouth, an equilibrium shape is achieved, and further delta growth proceeds isometrically.

In our models, strongly wave-influenced simulations demonstrate exactly this process (Figure 4). All simulations with $W > 0.5$ eventually obtain an equilibrium shape, and simulations with more wave-influence achieve their equilibrium shape faster than those with less. Furthermore, simulations with greater wave-influence have equilibrium shapes that are flatter than those with less, paralleling observations of real-world wave-influenced deltas (Nienhuis et al., 2015). These observations build confidence in the ability of our simulations to resolve the delta-scale process interactions that control the evolution of wave-influenced deltas.

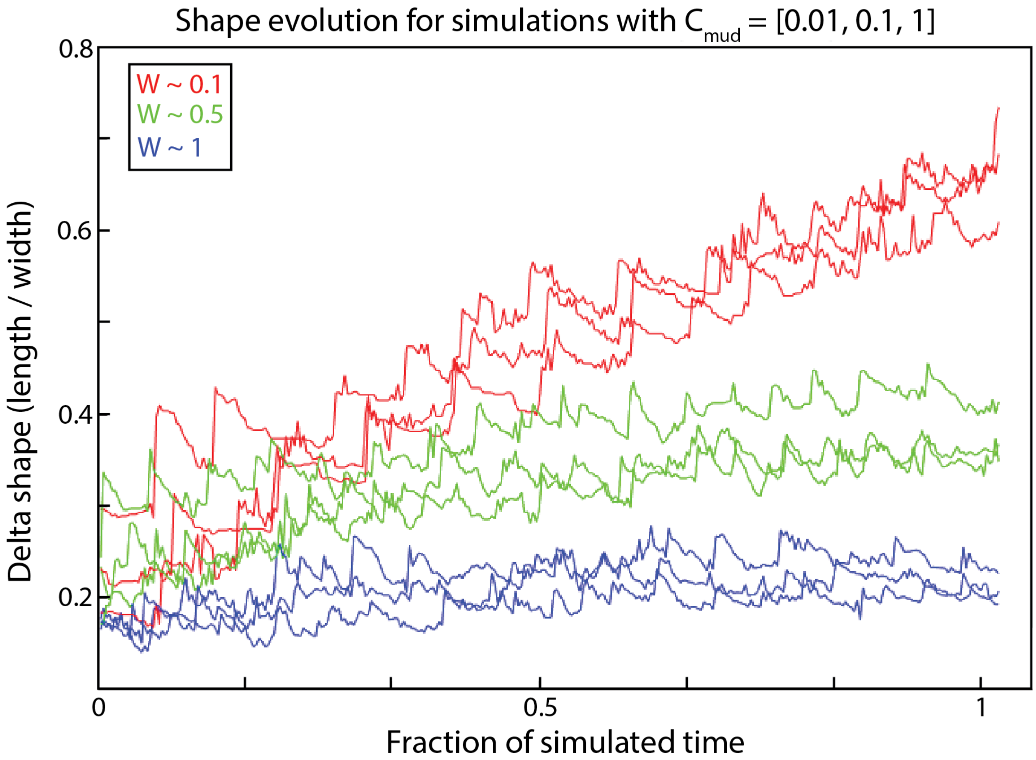

Figure 4. Evolution of delta shape through time. This plot includes simulations with 3 different mud concentrations (C_{mud} = 0.01, 0.1, 1 kg m^{-3}) and three different wave influences (W = 0.1, 0.5, 1) for nine total simulations. Note that simulations with $W < 0.5$ never reach an equilibrium shape, continuing a trend of elongation throughout the simulation period. By contrast, simulations with $W = 1$ obtain an equilibrium shape almost immediately.

3.5 Metrics

To quantify the morphology and dynamics of our simulations we developed MATLAB routines for automated extraction of various components of the delta system. Shorelines are defined using the opening angle method of Shaw et al. (2008) which permits objective definition of shorelines past openings, such as channels or inlets. Delta plains are defined as areas seaward of the initial shoreline and landward of the shoreline at a given timestep. Channelized areas are defined by thresholding maps of flow depth (threshold = 0.1 m) and velocity (threshold = 0.25 m s^{-1}) on the delta plain. We define lagoons as areas on the delta plain with depth greater than 0.5 m that are not part of the channel network. We quantify delta plain mud content (mud fraction, M_f) by the volume fraction of mud in delta deposits.

From our discretized representations of delta morphological attributes, we designed a suite of metrics that quantify their trends and dynamics through time. All time-dependent metrics are averaged over the final 50% of each run (90 flood cycles). The number of outlets (N_{out}) is defined as the number of contiguous overlapping regions of channelized areas and the shoreline. Shoreline roughness (R^*) is defined as the ratio between shoreline length and the length of the convex hull enclosing the delta plain. Lagoon area fraction (L_f) is defined as the ratio between total lagoon area and delta plain area. For each delta, these metrics are computed at the end of each flood cycle to characterize morphological tendencies for each. We quantify channel persistence (P_c) as the fraction of time a cell spent classified as channelized. We quantify the shoreline fractional change (D_{sl}) as the ratio of total length of new shoreline and length of the initial shoreline after each flood cycle.

4 Results

4.1 Controls of Mud and Waves on Gross Delta Morphology and Dynamics

Our simulations evolve through the same processes observed in natural delta systems and produce morphologies that strongly resemble real-world deltas across the spectrum of relative wave-influence (Figures 1 & 5). In the following sections we explore how these simulations vary with W and C_{mud}, in terms of the morphometrics defined in Section 3.5.

4.1.1 Distributary Channel Networks

Our simulations show that the number of distributary channel outlets decreases monotonically with increasing mud concentration (Figure 6a), and simulations with $C_{mud} =$ 1 kg m^{-3} have on average half as many outlets as those with $C_{mud} = 0.01$ kg m^{-3} for all values of W. Interestingly, we note that the proportion of cohesive sediment impacts the number of outlets even at high wave-influence.

Our simulations also show a monotonic decrease in the number of distributary outlets with increasing wave-influence, contrasting with previous work that suggests an increase in the propensity for mouth bars to form in the presence of small, short period waves (Nardin et al., 2013). At high wave-influence, channel networks are limited to one or two outlets throughout the lifespan of an evolving delta (Figure 6a).

Channel persistence increases monotonically with both mud concentration and wave-influence, demonstrating on average a two-fold increase across the simulated range of C_{mud} and a three-fold increase across the simulated range of W. Even at high wave-influence ($W > 1$) the stabilizing effect of mud is apparent, and the most persistent channels are observed in simulations with the highest mud concentration and wave-influence (Figure

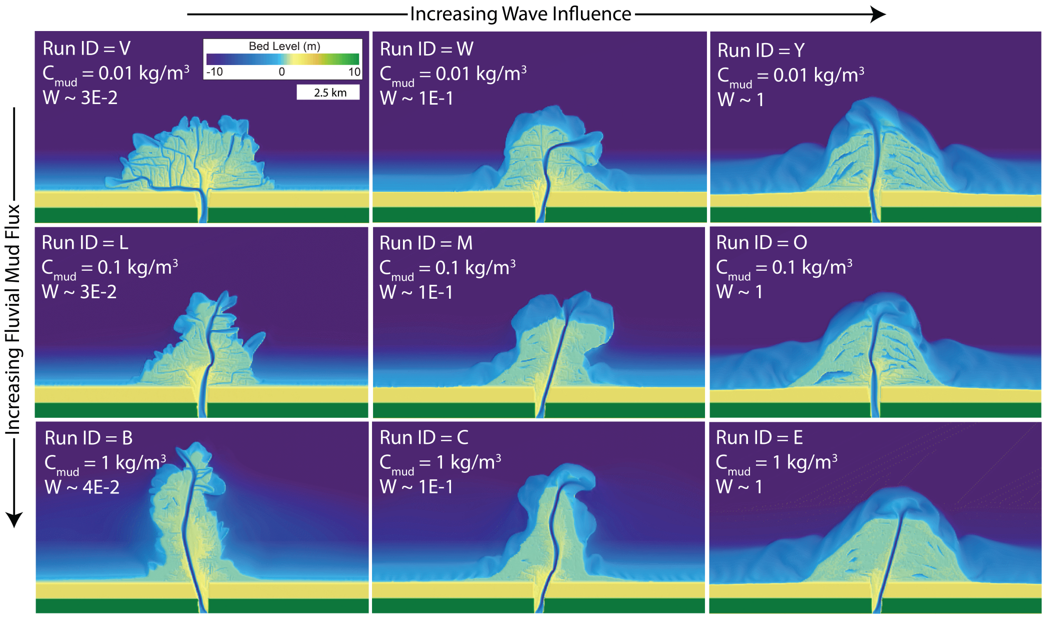

Figure 5. Simulated morphologies across a range of wave-influence and fluvial sediment compositions. Note the differences in channel networks and shorelines between simulations of different forcing, and the similarities with natural delta systems, in particular the presence of barrier-spits and lagoons in the most wave-influenced simulations

6b). These results demonstrate the important role of cohesive sediment in delta dynamics, even in the presence of large waves.

4.1.2 Delta shorelines

In river-dominated deltas, the shoreline morphology and dynamics are closely linked to those of the distributary channel network, with the creation of shoreline protuberances primarily driven by fluvial sediment deposition at channel mouths (W. Kim et al., 2006; Geleynse et al., 2012; Straub et al., 2015). The roughness of these shorelines is largely dependent on the length of distributary progradation, which in turn is influenced by fluvial sediment properties, particularly the concentration of cohesive sediments. This relationship is evident in our river-dominated simulations ($W < 0.1$), where we observe the highest shoreline roughness in scenarios with the greatest concentrations of cohesive sediment (Figure 6c).

As wave-influence increases, however, the role of cohesive sediment in determining shoreline roughness diminishes. At high wave influence ($W > 0.5$), fluvial sediment composition no longer significantly impacts shoreline roughness; the smoothest shorelines are found in simulations with the highest W values, regardless of sediment properties (Figure 6c). Several processes likely contribute to this shift. Beyond the well-known diffusional effect of low-angle waves and the role of longshore transport in smoothing shorelines (Swenson, 2005; Jerolmack & Swenson, 2007; Seybold et al., 2007), low-angle waves also act to dampen channel progradation, thereby reducing the length of deltaic protrusions near distributary outlets (Ashton & Giosan, 2011; Ratliff et al., 2018). Furthermore, our simulations show that waves limit the number of distributary outlets (Figure 6a) and stabilize channels (Figure 6b), limiting the number of new shoreline protrusions that are created.

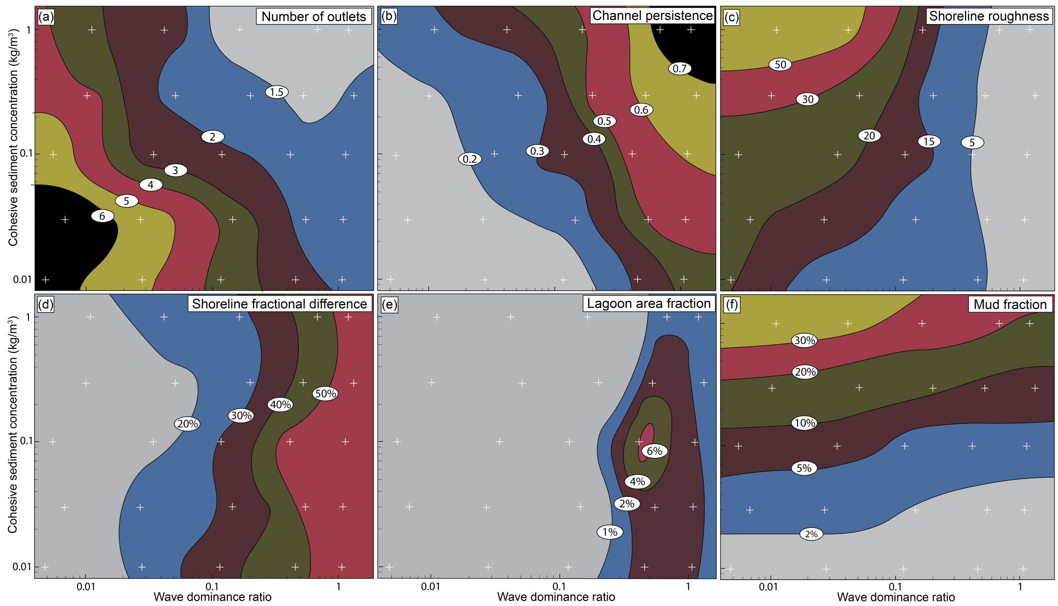

Figure 6. Contour plots for a variety of morphometrics across the simulated parameter space of wave dominance ratio and cohesive sediment concentration. White crosses denote positions of simulations (see Figure 2e for run IDs at each position). Numbers indicate metric value along a given contour line. Note the diagonal-directed gradients in the plots for number of outlets (a) and channel persistence (b), indicating dependence on both wave-influence and fluvial sediment composition. By contrast, shoreline roughness (c) shows a dependence transition at a wave-dominance ratio between 0.1-0.5, while shoreline fractional difference (d) is not overly sensitive to the cohesive sediment concentration. Lagoon area fraction (e) is maximized for $W = 0.5$ and $C_{mud} = 0.1$. Delta plain mud fraction (f) varies with W, but is more strongly dependent on C_{mud}

To determine which of these processes (wave-driven shoreline diffusion or progradation dampening and increased avulsion timescale) exerts a dominant role on shoreline morphology and dynamics, we compared the time-averaged fractional shoreline change between flood cycles across simulations (Figure 6d). Ignoring the effects of wave-driven shoreline diffusion, one would expect a decrease in the rates of shoreline change with increasing wave-influence, due to the progradation dampening and increased avulsion time scales associated with larger wave influence. Interestingly, our simulations show the opposite effect: fractional shoreline change increases monotonically with wave-influence (Figure 6d), demonstrating the dominance of shoreline diffusion over network suppression in wave-influenced delta shoreline dynamics.

These observations collectively indicate that the primary controls on local shoreline change (and consequently roughness) in deltas vary with wave-influence: in river-dominated deltas, local shoreline progradation depends on proximity to sediment sources (distributary outlets) and consequently on sediment composition. By contrast, shoreline change in wave-dominated deltas depends primarily on local shoreline geometry (specifically curvature) and how that geometry interacts with longshore transport and wave-driven erosion – which are independent of fluvial sediment properties.

4.1.3 Lagoons and Delta plains

Our simulations show that both waves and fluvial sediment composition play important roles in the sedimentary and environmental character of delta plains. Lagoons are common features on wave-influenced deltas (Figure 1); in our simulations they initially form in back-barrier settings and are incorporated into the delta plain during barrier-spit accretion (Figure 7, see section 4.2 for a more detailed discussion). For $0.1 < W < 0.7$, lagoon area fraction increases with wave influence (Figure 6e). As W approaches 1, there is an inflection point in this relationship, and lagoons become less prevalent with increasing W (Figure 6e).

Lagoon area fraction also exhibits a non-monotonic relationship with fluvial sediment composition; lagoons are most abundant in wave-influenced deltas with intermediate sediment composition (Figure 6e).

Finally, we quantified the abundance of mud in delta plain deposits to assess the importance of cohesive sediments from a sediment budget perspective. Unsurprisingly, delta plain mud fraction increases with increasing cohesive sediment concentration in the river, and decreases with increasing wave influence (Figure 6f). For the highest inflow concentrations, mud fraction in the delta plain decreases by a factor of 2 as W increases from 0.01 to 1. This decrease likely reflects transport of cohesive sediment to prodelta or offshore regions due to wave-enhanced shear stress near distributary outlets. This is augmented by the reduction in channel network complexity, since most of the delta plain mud is distributed within channels and associated levee deposits. However, despite this decrease, mud still constitutes a significant portion of the delta plain deposits in strongly wave-influenced simulations (15% in simulation E).

4.2 Barrier-Spit Accretion and the Growth of Wave-influenced Deltas

4.2.1 Qualitative Description

Our models demonstrate the essential processes by which wave-influenced deltas grow, which are distinct from those associated with the growth of river-dominated deltas. In simulations with limited wave influence, delta progradation is dominated by deposition of mouth bars and levees (see Movies S1-S4) in a fashion considered typical of river-dominated deltas (Edmonds & Slingerland, 2010). In more strongly wave-influenced simulations, however, deltas grow through a distinct multi-phase process involving jet deflection and wave-driven reworking of fluvial sediment that is initially deposited in the shoreface (Figure 7), which we refer to as the “barrier-spit accretion process”.

The process begins with deflection of the fluvial jet, either by locally high wave approach angles or by incipient mouth bar deposition (Figure 7a). Fluvial sediment is initially deposited on the landward side of the jet centerline as a set of scattered nearshore bars or incipient mouth bars (Figure 7a). Note that these bars do not emerge above water level at this stage, instead constructing a subaqueous platform of sediment. Over time, these bars amalgamate with each other and with levee deposits and coalesce through continued fluvial deposition and shoreward-directed reworking by waves until their elevation is high enough to inhibit through-flow (Figure 7b-d). Following initial emergence, continued fluvial deposition and sculpting by longshore currents leads to elongation of the barrier-spit and rotation to a shore-parallel orientation (Figure 7d-e). Continued elongation of the barrier-spit by longshore currents eventually welds it to the existing shoreline at its distal tip (Figure 7f), closing the associated back-barrier lagoon. This entire process repeats itself throughout the growth of the delta, creating multiple generations of barrier-spits that amalgamate to form the delta plain.

4.2.2 Temporal Characteristics

Despite widespread recognition as a key formative mechanism in wave-influenced deltas, several questions remain regarding the barrier-spit accretion process. These include the temporal characteristics of the process (time to emergence, time between events, cyclicity), and controls on spacing between successive generations of barrier-spits. To address these questions, we generated a long-running simulation with high temporal output resolution that facilitates quantitative frequency analysis. The simulation parameters match those of the ensemble simulation with the highest propensity for forming lagoons (run N).

It is impossible to objectively define barrier-spit extents in our simulations due to spatial and topographic overlap with adjacent areas of the delta plain. To circumvent this issue, we instead define a metric that tracks the evolution of the subaqueous platform near the delta front, noting that the growth and decay of this platform reflects the gradual accumulation of fluvial sediment followed by subsequent emergence of that sediment as subaerial barrier-spits (Figure 7). At the end of each flood cycle, we compute the "fill fraction" (F), which is defined as the volume of subaqueous sediment deposits normalized by the volume of accommodation space in the same area prior to delta growth.

The area over which F is computed changes as the delta advances. This area is bounded by the front third of the delta shoreline and extends 2.5 km offshore (more details in the supporting information). Normalizing by the initial accommodation volume minimizes sensitivity to the specific area boundaries over time. Growth in F reflects subaqueous sediment deposition, while decreases in F indicate sediment emergence above sea level and incorporation into the delta plain.

A time series of F throughout delta growth (F_t) shows a distinct oscillatory behavior against a background of gradual increase and eventual flattening (Figure 8a). The gradual increase is attributed to increases in total depth as the delta progrades into the basin, which eventually ceases once the delta front is located entirely within the flat portion of the basin. The oscillations are best characterized as "ramp-cliff" structures, where periods of relatively slow growth in F are followed by rapid decreases back to a background value. These oscillations reflect gradual buildup of subaqueous sediment deposited near the mouth followed by rapid reductions in F as the sediment coalesces (due to onshore transport as a result of wave asymmetry) and the barrier-spit emerges above sea-level.

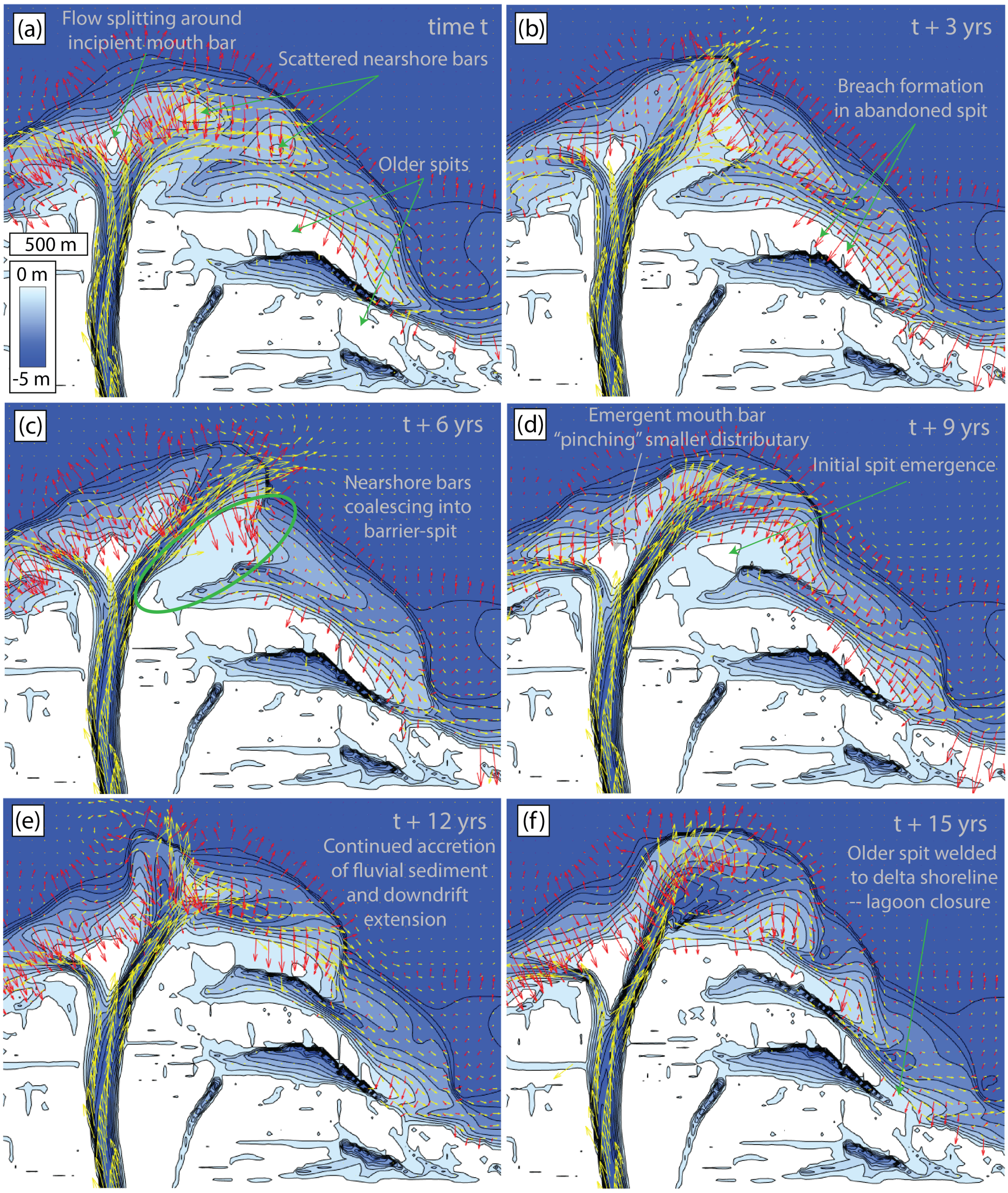

Figure 7. Example from a wave-dominated simulation demonstrating the processes by which wave-influenced deltas grow. Green arrows, circle highlight features of interest. Panels show the time evolution of bed level (filled contours at 0.5 m intervals), current velocity fields (yellow vectors) and wave forces (red vectors) during one cycle of shoreface fluvial deposition (a-c) barrier development (c-e) and accretion (e-f). At least two generations of older barrier-spits are visible here, highlighting the cyclical nature of this process.

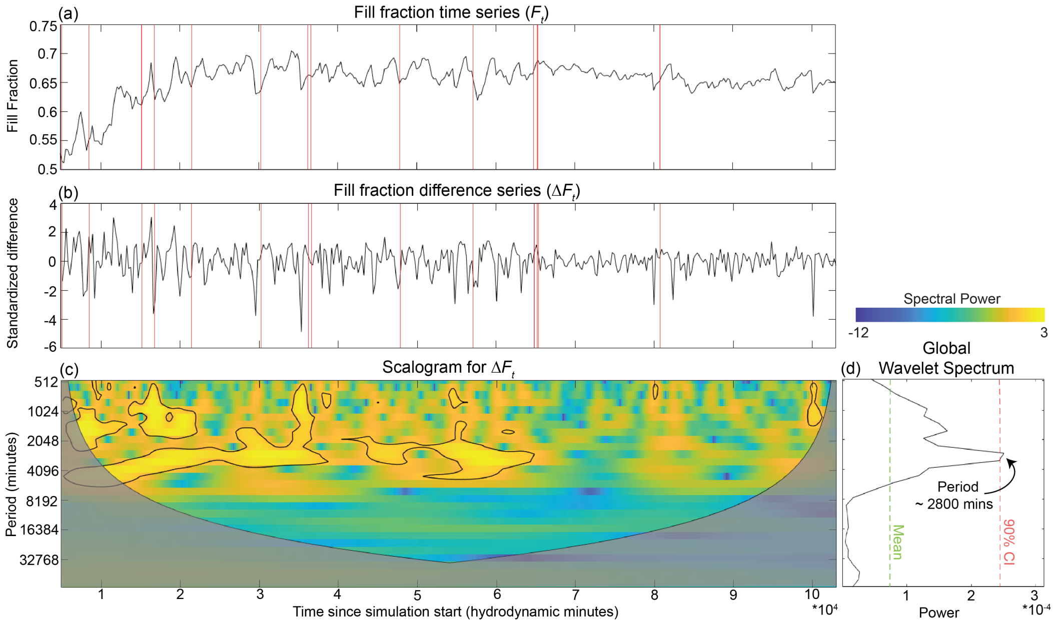

Figure 8. Cyclicity in the barrier-spit accretion process for a simulation with parameters matching run N. (a) Raw time series of the fill fraction (F_t) at the delta front, defined as the ratio of subaqueous sediment deposit volume to available accommodation space. (b) Difference time series of F (ΔF_t) used for wavelet analysis. (c) Local wavelet power spectrum (scalogram) showing the frequency distribution of signal variance over time. Gray areas indicate the cone of influence, where edge effects make power estimates unreliable. Thick black contours highlight regions where spectral power significantly exceeds the 90% confidence level against white noise, based on Torrence and Compo (1998). (d) Global wavelet spectrum, summing the power in (c) across time. Green and red lines in (d) represent the mean and 90% confidence spectra for white noise with identical signal length and degrees of freedom. Note the spike in spectral power around a period of 2800 minutes (∼15 flood cycles), exceeding the 90% confidence level. Vertical red lines in (a) and (b) indicate the formation times ("birthdays") of lagoons – discussed in section 5.2

To test whether barrier-spit accretion is a cyclical (rather than random) process, we analyze the frequency content of the F difference series ($\Delta F_t = F_t - F_{t-1}$) (Figure 8b) using a wavelet transform. As a spectral analysis tool, wavelets provide several advantages over the more commonly used Fourier transform, including better time-frequency localization and handling of non-stationary signals, reduced edge-effects, and improved detection of transients (Kumar & Foufoula-Georgiou, 1997). We operate on ΔF_t (rather than F_t) because we are interested in the time between barrier-spit emergence events, which are characterized by rapid reductions in F, manifesting as large negative spikes in ΔF_t. Operating on the difference series has the added benefit of reducing the spectral power at low frequencies associated with non-stationarity that can obfuscate features of interest at higher frequencies.

Figure 8c and 8d show the local and global wavelet spectra (respectively) of the ΔF_t computed using the Morlet wavelet (wavenumber = 6). The local wavelet spectrum (LWS, also known as the scalogram) shows the distribution of variance in the ΔF_t time series in the time and frequency domains. The global wavelet spectrum (GWS) is simply the time-sum of the LWS, and shows how signal variance is distributed in the frequency domain for the entire signal. Both the LWS and the GWS show a concentration of spectral power at an approximate scale of 2800 minutes (bright yellow regions in Figure 8c, large spike in Figure 8d), suggesting a periodic component in the ΔF_t time series at these scales.

We test the significance of peaks in the LWS and GWS against a background spectrum for a white-noise process with identical signal length and degrees of freedom to ΔF_t (Torrence & Compo, 1998) at an 90% confidence level. Several regions of the LWS exhibit spectral power surpassing this threshold (black contours in Figure 8c), and there is a statistically significant peak in the GWS at periods of approximately 2800 minutes (peak in Figure 8d). Although the spectra show additional peaks at lower frequencies (longer wavelengths) these are not considered significant against the assumed background spectra.

Analysis of the global wavelet spectra demonstrates that oscillations in F are indeed cyclical, with a periodicity equivalent to approximately 15 flood cycles. Depending on assumptions regarding recurrence intervals for geomorphically-significant flood events, these oscillations would have periods ranging from decades to centuries in real-world delta systems – similar to estimates from field examples such as the Danube, the Red and the Po river deltas (Vespremeanu-Stroe & Preoteasa, 2015; Preoteasa et al., 2016; Van Maren, 2005; Simeoni et al., 2007). This analysis suggests that barrier-spit accretion is a cyclical (rather than stochastic) autogenic process, which is driven by accumulation of nearshore subaqueous sediment, rather than being initiated by individual flood events. Simulations conducted during model development further support this finding; even with constant fluvial discharge, these simulations reproduce the delta growth processes described here (see Movie S5).

5 Discussion

5.1 Barrier-spit accretion process

Our simulations capture the transitions between river-dominated and wave-dominated delta growth processes and are able to reproduce the barrier-spit accretion process that has been documented in several natural wave-influenced delta systems (Bhattacharya & Giosan, 2003). Examples include the Tiber delta (Bellotti et al., 1995; Milli et al., 2013), the Vasishta lobe of the Godavari delta (Rao et al., 2005), the Rosetta lobe of the Nile delta (Sestini, 1989), the Sfantu Gheorge lobe of the Danube delta (Dan et al., 2011; Preoteasa et al., 2016), and the Ba Lat lobe of the Red River delta (Van Maren, 2005), among others.

Interestingly, barrier-spits emerge in the simulations in spite of relatively crude (or completely absent) parameterizations of processes that are considered important in their evolution, such as swash, overwash, and eolian transport. While these processes are certainly important for the longer-term evolution of these features (particularly in supply-limited environments, such as eroding headlands), their emergence in our simulations shows that the dominant factors controlling barrier-spit accretion in prograding deltas are the relative strengths of fluvial, longshore, and cross-shore sediment transport.

It has been suggested that the onset of barrier-spit growth in prograding deltas may be initiated by periods of rapid sediment delivery to the shoreface, such as during large river floods (Anthony, 2015; Bhattacharya and Giosan, 2003). However, recent work has demonstrated that spit emergence in both fluvial and non-fluvial settings may be preceded by a prolonged period of subaqueous nearshore sediment accumulation that constructs a platform onto which the spit can prograde (Preoteasa et al., 2016; van Kouwen et al., 2023). Futhermore, several case studies suggest that barrier-spit emergence in deltas exhibits some level of cyclicity (evidenced by abundant, regularly spaced inactive barriers preserved on the delta plain), with estimated recurrence intervals ranging from 10's to 100's of years – which is longer than typical recurrence intervals for bankfull floods (Van Maren, 2005; Vespremeanu-Stroe & Preoteasa, 2015; Preoteasa et al., 2016).

The time series and frequency analysis of fill fraction clearly show that there is a periodic component to barrier-spit accretion on timescales of about 15 floods, far exceeding the frequency of "bankfull" discharge events. This emergent cyclicity suggests that the role of gradual sediment buildup in the subaqueous portions of the delta front may be more important in determining when barrier-spits form than periods of pulsed sediment supply, though this likely depends on system-specific variables in real-world deltas.

5.2 Lagoon optimization, birthdays and life expectancy

Our analysis shows that intermediate fluvial mud concentrations ($C_{mud} = 0.1$) optimize the conditions for barrier growth and lagoon formation, with lagoon area fraction decreasing for $C_{mud} < 0.1$ and $C_{mud} > 0.1$. We attribute this to different processes; at high fluvial mud concentrations, back-barrier deposition of fine-grained sediments "erases" lagoons as quickly as they form. At low mud concentrations, channels are less stable and change positions frequently, limiting sediment supply to (and consequently size of) individual barrier features. Our simulations also show that lagoon area fraction is optimized for $W = 0.5$, and decreases with increasing or decreasing W. We attribute this to the mechanisms involved in lagoon formation; barrier-spits (and consequently lagoons) only form in settings with significant wave influence, but large waves favor the accretion of sediment directly onto the existing shoreline due to strong onshore-directed transport.

Barrier-spits are common features in real-world wave-influenced deltas, but not all systems preserve lagoons on the delta plain. Likewise, our simulations indicate that even under "optimal" conditions, not every barrier-spit leads to the formation of a lagoon that is ultimately preserved. In Figure 8b, the "birthdays" of lagoons that persist until the end of the simulation are shown, overlaid on the time series of ΔF_f (see the supporting information for details on how lagoon birthdays are calculated). This simulation uses parameters that optimize the conditions for lagoon preservation. Lagoon birthdays are typically preceded by significant negative spikes in ΔF_f, associated with the emergence of subaqueous sediment as barrier-spits develop. However, not every negative spike in ΔF_f results in a lagoon, and several barrier-spit emergence events—particularly later in the simulation—do not correspond with lagoon preservation.

This analysis, though somewhat ad-hoc, highlights the complexity of the barrier-spit accretion process and the factors that determine whether or not a lagoon becomes incorporated into the delta plain. Even in our simplified models, we speculate that multiple factors may control the preservation of individual lagoons, including the lagoon's initial geometry (namely width), the shoreline's initial orientation and bathymetry, and the balance between longshore and cross-shore sediment transport during evolution of the enclosing barrier-spit. Furthermore, lagoon preservation in real-world delta systems also depends on processes which are not represented in the model, including overwash and eolian transport. The interplay of these dynamic and time-varying factors suggests that predicting whether an individual lagoon will be preserved on the delta plain may be impossible.

Nevertheless, our simulations show that, at a broad scale, the proportion of the delta plain covered by lagoons is influenced by both the characteristics of fluvial sediment and the balance between fluvial and longshore sediment transport. Lagoon preservation tends to be maximized under intermediate conditions of fluvial mud concentration and relative wave influence. This finding is significant for paleoenvironmental interpretation, as the presence of abundant back-barrier lagoonal deposits may indicate a specific set of environmental conditions.

5.3 Role of mud in wave-influenced delta morphodynamics

Our simulations show that mud plays important roles in delta evolution, even in wave-dominated environments. In river-dominated deltas, higher mud concentrations in fluvial effluent are thought to enhance the stability of distributary channels and inhibit the bifurcation process, resulting in a decrease in the overall number of outlets and an increase in the persistence of individual distributaries (Hoyal & Sheets, 2009; Martin et al., 2009; Edmonds & Slingerland, 2010; Caldwell & Edmonds, 2014; Straub et al., 2015; Liang et al., 2015). Waves are also thought to decrease the number of channel outlets (by inhibiting bifurcation) (J. P. M. Syvitski & Saito, 2007; Jerolmack & Swenson, 2007; Geleynse et al., 2011; Nardin & Fagherazzi, 2012; Nardin et al., 2013; Anthony, 2015; Gao et al., 2018), and have stabilizing effects on distributary channels (Swenson, 2005; Ratliff et al., 2018; Gao et al., 2018; Liu et al., 2020; Hu et al., 2022; Zăinescu et al., 2024). Our simulations not only confirm these previous results, but show the effects of mud and waves in simplifying and stabilizing distributary networks actually work in concert: the simplest networks and most stable channels are found in simulations where W and C_{mud} are both maximized.

By controlling network morphology and dynamics, fluvial sediment composition controls how sediment is distributed at the shoreline. However, despite this, shoreline geometry (as quantified by rugosity) in wave-dominated deltas does not depend on fluvial sediment composition. This highlights the dominance of wave-driven processes (erosion and longshore transport) over fluvial processes (bifurcation, levee progradation and avulsion) in controlling the shoreline dynamics of these systems.

Mud also affects the barrier-spit accretion process by preferentially filling back-barrier lagoons and inhibiting their preservation as open water on the delta plain, impacting the character of delta deposits. Anthony (2015) highlighted a knowledge gap concerning the controls on beach-ridge spacing in wave-influenced deltas, suggesting sediment supply as a possible controlling variable. Our simulations suggest that the abundance of mud in fluvial effluent may explain the distinction between deltas with systems of welded beach ridges (and the occasional lagoon) and deltas where beach ridges are interspersed with fine-grained back-barrier deposits.

Finally, there are several other ways in which mud could influence the growth of wave-influenced deltas beyond those modeled and described here. Mud can settle in the subaqueous platform or prodelta of wave-influenced systems as a result of density currents or during periods of relative wave quiescence (Steel et al., 2024), facilitating progradation and helping to stave off delta autoretreat (M. Kim et al., 2024). In very large delta systems, mud can be transported by longshore currents to areas with less wave energy, wherein it may be the dominant constructional material, such as the downdrift flanks of the Mekong and Amazon deltas (Anthony, 2015).

5.4 Limitations

It is important to note that our simulations are a highly schematized and simplified representation of reality, and as such ignore several processes common to wave-influenced deltas. For instance, phase differences between periods of high river discharge and intense wave-action are the norm in strongly wave-influenced systems, and may significantly impact the barrier formation and accretion process. Strong, onshore directed wind fields are also common in wave-dominated delta systems, creating important features such as coastal dunes and potentially contributing to barrier rollover and accretion. Ignoring these important processes may lead to our simulations overestimating the prevalence of lagoons on the delta plain, especially in environments dominated by sand. Still, our models are among the first to recreate the processes by which symmetrical wave-influenced systems grow and evolve, and are useful for assessing how those processes vary in response to wave forcing and fluvial sediment composition.

6 Conclusions

Our study offers new insights into the complex roles of wave-influence and fine-grained cohesive sediment on the morphodynamics of river deltas. By leveraging physics-based numerical models, we have elucidated key processes and morphological characteristics that differentiate wave-influenced deltas from their river-dominated counterparts. Waves influence delta morphology through processes such as jet deflection, barrier formation, and longshore sediment transport. Wave-driven reworking of fluvial sediments results in distinctive features relative to river-dominated deltas: shorelines are smoother and reworked more frequently, channel networks exhibit limited complexity and are more persistent, and deltas grow through a cyclical process of barrier-spit formation and accretion, producing delta plains with sedimentary facies that are distinct from their river-dominated counterparts. These processes and features parallel those observed in natural deltas, such as the Red, Sinu, and Coco river deltas, among others.

Our results highlight the important role of cohesive sediment in the accretion of wave-influenced deltas. Mud affects network properties and in turn affects how sediment is distributed at the delta shoreline. Mud is preserved on the delta plain in levees and behind barrier-spits, and thus is an important component in the mass balance of these systems. Finally, mud also affects the barrier-spit accretion process, and determines barrier-spit spacing for a given degree of wave-influence. These results have implications for delta sediment budgets and resultant management actions, as well as for sedimentary facies models in wave-influenced deltas and resultant paleoenvironmental interpretations.

Finally, our simulations show that deltas near the transition of fluvial and wave-dominance may be particularly sensitive to changes in sedimentary or hydrodynamic forcing conditions, as the dominant processes controlling local shoreline variability and the creation of new land change near $W = 1$. Furthermore, the creation and preservation of back-barrier lagoons is optimized within a narrow range of W and C_{mud} values, and an abundance of these features or their deposits in a natural delta system may be indicative of a specific set of formative conditions.

Open Research Section

As open source software, build 69179 of Delft3D is available from Deltares at the following URL: https://svn.oss.deltares.nl/repos/delft3d/tags/delft3d4/69179/. Simulation input files and MATLAB code used to process and analyze simulation outputs are available through a Zenodo repository: https://zenodo.org/records/14166672 (Broaddus, 2024).

Acknowledgments

CB acknowledges support by a NASA FINESST grant (Grant 80NSSC24K0033). EF-G acknowledges support by the Samueli endowed chair and by NSF (Grant EAR 2342937, RISE 2425748).

References

Anderson, A. M., Allen, D. M., & Venditti, J. G. (2023, 11). Sensitivity of Subsurface Permeability in Coastal Deltas to Their Morphodynamic and Geomorphic Characteristics. *Water Resources Research*, *59*(11), e2022WR034136. https://doi.org/10.1029/2022WR034136

Anthony, E. J. (2015, 3). Wave influence in the construction, shaping and destruction of river deltas: A review. *Marine Geology*, *361*, 53–78. https://doi.org/10.1016/J.MARGEO.2014.12.004

Ashton, A. D., & Giosan, L. (2011, 7). Wave-angle control of delta evolution. *Geophysical Research Letters*, *38*(13). https://doi.org/10.1029/2011GL047630

Ashton, A. D., & Murray, A. B. (2006, 11). High-angle wave instability and emergent shoreline shapes: 2. Wave climate analysis and comparisons to nature. *Journal of Geophysical Research: Earth Surface*, *111*(F4). https://doi.org/10.1029/2005JF000423

Baar, A. W., Boechat Albernaz, M., van Dijk, W. M., & Kleinhans, M. G. (2019, 10). Critical dependence of morphodynamic models of fluvial and tidal systems on empirical downslope sediment transport. *Nature Communications 2019 10:1*, *10*(1), 1–12. https://doi.org/10.1038/s41467-019-12753-x

Bellotti, P., Milli, S., Tortora, P., & Valeri, P. (1995, 8). Physical stratigraphy and sedimentology of the Late Pleistocene-Holocene Tiber Delta depositional sequence. *Sedimentology*, *42*(4), 617–634. https://doi.org/10.1111/j.1365-3091.1995.tb00396.x

Bhattacharya, J. P., & Giosan, L. (2003, 2). Wave-influenced deltas: geomorphological implications for facies reconstruction. *Sedimentology*, *50*(1), 187–210. https://doi.org/10.1046/J.1365-3091.2003.00545.X

Broaddus, C. M. (2024). *Wave-influenced deltas grow through cyclical accretion of barrier-spits: Software and data.* Zenodo. https://doi.org/10.5281/zenodo.14166672

Broaddus, C. M., Brown, J., Edmonds, D. A., Vulis, L. M., Tejedor, A., Nienhuis, J. H., ... Foufoula-Georgiou, E. (2022). First-Order River Delta Morphology is Explained by the Sediment Flux Balance from Rivers, Waves, and Tides. *Geophysical Research Letters*. https://doi.org/10.1029/2022GL100355

Burpee, A. P., Slingerland, R. L., Edmonds, D. A., Parsons, D., Best, J., Cederberg, J., ... Royce, J. (2015, 6). Grain-Size Controls On the Morphology and Internal Geometry of River-Dominated Deltas. *Journal of Sedimentary Research*, *85*(6), 699–714. https://doi.org/10.2110/JSR.2015.39

Caldwell, R. L., & Edmonds, D. A. (2014, 11). The effects of sediment properties on deltaic processes and morphologies: A numerical modeling study. *Journal of Geophysical Research: Earth Surface*, *119*(5), 961–982. https://doi.org/10.1002/2013JF002965

Caldwell, R. L., Edmonds, D. A., Baumgardner, S., Paola, C., Roy, S., & Nienhuis, J. H. (2019, 11). A global delta dataset and the environmental variables that predict delta formation on marine coastlines. *Earth Surface Dynamics*, *7*(3), 773–787. Retrieved from `https://esurf.copernicus.org/articles/7/773/2019/http://files/73/Caldwelletal.-2019`

-Aglobaldeltadatasetandtheenvironmentalvaria.pdfhttp://files/74/2019.html 10.5194/esurf-7-773-2019
Dan, S., Walstra, D. J. R., Stive, M. J., & Panin, N. (2011, 2). Processes controlling the development of a river mouth spit. *Marine Geology*, *280*(1-4), 116–129. https://doi.org/10.1016/j.margeo.2010.12.005
Dominguez, J. M. (1996). The São Francisco strandplain: A paradigm for wave-dominated deltas? *Geological Society Special Publication*, *117*, 217–231. https://doi.org/10.1144/GSL.SP.1996.117.01.13
Edmonds, D. A., & Slingerland, R. L. (2007, 11). Mechanics of river mouth bar formation: Implications for the morphodynamics of delta distributary networks. *Journal of Geophysical Research: Earth Surface*, *112*(F2). https://doi.org/10.1029/2006JF000574
Edmonds, D. A., & Slingerland, R. L. (2010, 11). Significant effect of sediment cohesion on delta morphology. *Nature Geoscience*, *3*(2), 105–109. https://doi.org/10.1038/ngeo730
Ericson, J. P., Vörösmarty, C. J., Dingman, S. L., Ward, L. G., & Meybeck, M. (2006). Effective sea-level rise and deltas: Causes of change and human dimension implications. *Global and Planetary Change*, *50*, 63–82. Retrieved from www.elsevier.com/locate/gloplacha 10.1016/j.gloplacha.2005.07.004
Esposito, C. R., Georgiou, I. Y., & Kolker, A. S. (2013, 4). Hydrodynamic and geomorphic controls on mouth bar evolution. *Geophysical Research Letters*, *40*(8), 1540–1545. https://doi.org/10.1002/GRL.50333
Fagherazzi, S., Edmonds, D. A., Nardin, W., Leonardi, N., Canestrelli, A., Falcini, F., ... Slingerland, R. L. (2015, 9). Dynamics of river mouth deposits. *Reviews of Geophysics*, *53*(3), 642–672. https://doi.org/10.1002/2014RG000451
Galloway, W. E. (1975). Process Framework for Describing the Morphologic and Stratigraphic Evolution of Deltaic Depositional Systems. *Deltas, Models for Exploration*, 86–98. Retrieved from http://files/5/Galloway-ProcessFrameworkforDescribingtheMorphologica.pdf
Gao, W., Nienhuis, J., Nardin, W., Wang, Z. B., Shao, D., Sun, T., & Cui, B. (2020, 9). Wave Controls on Deltaic Shoreline-Channel Morphodynamics: Insights From a Coupled Model. *Water Resources Research*, *56*(9), e2020WR027298. https://doi.org/10.1029/2020WR027298
Gao, W., Shao, D., Wang, Z. B., Nardin, W., Yang, W., Sun, T., & Cui, B. (2018, 12). Combined Effects of Unsteady River Discharges and Wave Conditions on River Mouth Bar Morphodynamics. *Geophysical Research Letters*, *45*(23), 903–12. https://doi.org/10.1029/2018GL080447
Geleynse, N., Storms, J. E. A., Walstra, D.-J. R., Jagers, H. R. A., Wang, Z. B., & Stive, M. J. F. (2011, 11). Controls on river delta formation; insights from numerical modelling. *Earth and Planetary Science Letters*, *302*(1), 217–226. https://doi.org/10.1016/j.epsl.2010.12.013
Geleynse, N., Voller, V. R., Paola, C., & Ganti, V. (2012, 11). Characterization of river delta shorelines. *Geophysical Research Letters*, *39*(17). https://doi.org/10.1029/2012GL052845
Giosan, L., Syvitski, J., Constantinescu, S., & Day, J. (2014, 12). Climate change: Protect the world's deltas. *Nature 2014 516:7529*, *516*(7529), 31–33. https://doi.org/10.1038/516031a
Hoitink, A. J. F., Nittrouer, J. A., Passalacqua, P., Shaw, J. B., Langendoen, E. J., Huismans, Y., & van Maren, D. S. (2020, 11). Resilience of River Deltas in the Anthropocene. *Journal of Geophysical Research: Earth Surface*, *125*(3), e2019JF005201. https://doi.org/10.1029/2019JF005201
Hoyal, D. C. J. D., & Sheets, B. A. (2009, 11). Morphodynamic evolution of experimental cohesive deltas. *Journal of Geophysical Research: Earth Surface*, *114*(F2). https://doi.org/10.1029/2007JF000882
Hu, N., Murray, A. B., Ratliff, K. M., Little, Z., & Hutton, E. W. (2022, 5). Wave-

Climate Asymmetry Influence on Delta Evolution and River Dynamics. *Geophysical Research Letters*, *49*(9), e2021GL096315. https://doi.org/10.1029/2021GL096315

Ibàñez, C., Canicio, A., Day, J. W., & Curcó, A. (1997, 1). Morphologic development, relative sea level rise and sustainable management of water and sediment in the Ebre Delta, Spain. *Journal of Coastal Conservation*, *3*(1), 191–202. https://doi.org/10.1007/BF02908194

Ibáñez, C., Day, J. W., & Reyes, E. (2014, 4). The response of deltas to sea-level rise: Natural mechanisms and management options to adapt to high-end scenarios. *Ecological Engineering*, *65*, 122–130. https://doi.org/10.1016/J.ECOLENG.2013.08.002

Jerolmack, D. J., & Swenson, J. B. (2007, 11). Scaling relationships and evolution of distributary networks on wave-influenced deltas. *Geophysical Research Letters*, *34*(23). https://doi.org/10.1029/2007GL031823

Kim, M., Chun, B., Chamberlain, E., & Kim, W. (2024). Enhanced mud retention as an autogenic mechanism for sustained delta growth: Insight from records of the Lafourche subdelta of the Mississippi River. *Sedimentology*. https://doi.org/10.1111/SED.13230

Kim, W., Paola, C., Swenson, J. B., & Voller, V. R. (2006, 12). Shoreline response to autogenic processes of sediment storage and release in the fluvial system. *Journal of Geophysical Research: Earth Surface*, *111*(F4), 4013. https://doi.org/10.1029/2006JF000470

Komar, P. D. (1973). *Computer Models of Delta Growth due to Sediment Input from Rivers and Longshore Transport — GSA Bulletin — GeoScienceWorld.* https://doi.org/10.1130/0016-7606(1973)84⟨2217:CMODGD⟩2.0.CO;2

Korus, J. T., & Fielding, C. R. (2015, 11). Asymmetry in Holocene river deltas: Patterns, controls, and stratigraphic effects. *Earth-Science Reviews*, *150*, 219–242. https://doi.org/10.1016/j.earscirev.2015.07.013

Kumar, P., & Foufoula-Georgiou, E. (1997, 11). Wavelet analysis for geophysical applications. *Reviews of Geophysics*, *35*(4), 385–412. https://doi.org/10.1029/97RG00427

L. D. Wright, J. M. C. (1973). Variations in Morphology of Major River Deltas as Functions of Ocean Wave and River Discharge Regimes. *AAPG Bulletin*, *57*(2), 370–398. Retrieved from `https://archives.datapages.com/data/bulletns/1971-73/data/pg/0057/0002/0350/0370.htm`

Li, Q., Matthew Benson, W., Harlan, M., Robichaux, P., Sha, X., Xu, K., & Straub, K. M. (2017, 10). Influence of Sediment Cohesion on Deltaic Morphodynamics and Stratigraphy Over Basin-Filling Time Scales. *Journal of Geophysical Research: Earth Surface*, *122*(10), 1808–1826. https://doi.org/10.1002/2017JF004216

Liang, M., Voller, V. R., & Paola, C. (2015, 12). A reduced-complexity model for river delta formation – Part 1: Modeling deltas with channel dynamics. *Earth Surface Dynamics*, *3*(1), 67–86. https://doi.org/10.5194/esurf-3-67-2015

Liu, Y., Chen, H., Wang, J., Yang, S., & Chen, A. (2020, 1). Numerical simulation for the effects of waves and grain size on deltaic processes and morphologies. *Open Geosciences*, *12*(1), 1286–1301. https://doi.org/10.1515/geo-2020-0196

Martin, J., Sheets, B., Paola, C., & Hoyal, D. (2009, 9). Influence of steady base-level rise on channel mobility, shoreline migration, and scaling properties of a cohesive experimental delta. *Journal of Geophysical Research: Earth Surface*, *114*(F3), 3017. https://doi.org/10.1029/2008JF001142

Milli, S., D'Ambrogi, C., Bellotti, P., Calderoni, G., Carboni, M. G., Celant, A., ... Ricci, V. (2013, 2). The transition from wave-dominated estuary to wave-dominated delta: The Late Quaternary stratigraphic architecture of Tiber River deltaic succession (Italy). *Sedimentary Geology*, *284-285*, 159–180.

https://doi.org/10.1016/J.SEDGEO.2012.12.003

Nardin, W., & Fagherazzi, S. (2012, 11). The effect of wind waves on the development of river mouth bars. *Geophysical Research Letters*, *39*(12). https://doi.org/10.1029/2012GL051788

Nardin, W., Mariotti, G., Edmonds, D. A., Guercio, R., & Fagherazzi, S. (2013, 6). Growth of river mouth bars in sheltered bays in the presence of frontal waves. *Journal of Geophysical Research: Earth Surface*, *118*(2), 872–886. https://doi.org/10.1002/JGRF.20057

Nienhuis, J. H., Ashton, A. D., Edmonds, D. A., Hoitink, A. J. F., Kettner, A. J., Rowland, J. C., & Törnqvist, T. E. (2020, 10). Global-scale human impact on delta morphology has led to net land area gain. *Nature*, *577*(7791), 514–518. https://doi.org/10.1038/s41586-019-1905-9

Nienhuis, J. H., Ashton, A. D., & Giosan, L. (2015, 11). What makes a delta wave-dominated? *Geology*, *43*(6), 511–514. https://doi.org/10.1130/G36518.1

Nienhuis, J. H., Ashton, A. D., & Giosan, L. (2016, 11). Littoral steering of deltaic channels. *Earth and Planetary Science Letters*, *453*, 204–214. https://doi.org/10.1016/J.EPSL.2016.08.018

Nienhuis, J. H., Ashton, A. D., Kettner, A. J., & Giosan, L. (2017, 9). Large-scale coastal and fluvial models constrain the late Holocene evolution of the Ebro Delta. *Earth Surface Dynamics*, *5*(3), 585–603. https://doi.org/10.5194/ESURF-5-585-2017

Nienhuis, J. H., Ashton, A. D., Nardin, W., Fagherazzi, S., & Giosan, L. (2016, 4). Alongshore sediment bypassing as a control on river mouth morphodynamics. *Journal of Geophysical Research: Earth Surface*, *121*(4), 664–683. https://doi.org/10.1002/2015JF003780

Nota, P. J., Zhang, X., Liu, H., Mubikirwa, H., & Majid, A. (2024, 9). Effects of upstream and downstream boundary conditions on lacustrine shallow-water delta morphologies: A numerical modeling approach. *Marine and Petroleum Geology*, *167*, 106966. https://doi.org/10.1016/J.MARPETGEO.2024.106966

Olariu, C., & Bhattacharya, J. P. (2006, 2). Terminal Distributary Channels and Delta Front Architecture of River-Dominated Delta Systems. *Journal of Sedimentary Research*, *76*(2), 212–233. https://doi.org/10.2110/jsr.2006.026

Orton, G. J., & Reading, H. G. (1993, 6). Variability of deltaic processes in terms of sediment supply, with particular emphasis on grain size. *Sedimentology*, *40*(3), 475–512. https://doi.org/10.1111/J.1365-3091.1993.TB01347.X

Otvos, E. G. (2000, 2). Beach ridges — definitions and significance. *Geomorphology*, *32*(1-2), 83–108. https://doi.org/10.1016/S0169-555X(99)00075-6

P.D. Komar. (1998). *Beach processes and sedimentation* . Prentice Hall.

Penland, S., Boyd, R., & Suter, J. R. (1988, 11). Transgressive depositional systems of the Mississippi Delta plain; a model for barrier shoreline and shelf sand development. *Journal of Sedimentary Research*, *58*(6), 932–949. https://doi.org/10.1306/212F8EC2-2B24-11D7-8648000102C1865D

Preoteasa, L., Vespremeanu-Stroe, A., Tătui, F., Zăinescu, F., Timar-Gabor, A., & Cîrdan, I. (2016, 1). The evolution of an asymmetric deltaic lobe (Sf. Gheorghe, Danube) in association with cyclic development of the river-mouth bar: Long-term pattern and present adaptations to human-induced sediment depletion. *Geomorphology*, *253*, 59–73. https://doi.org/10.1016/J.GEOMORPH.2015.09.023

Rao, K. N., Sadakata, N., Malini, B. H., & Takayasu, K. (2005, 8). Sedimentation Processes and Asymmetric Development of the Godavari Delta, India. *River Deltas-Concepts, Models, and Examples*, 435–451. https://doi.org/10.2110/PEC.05.83.0435

Ratliff, K. M., Hutton, E. H., & Murray, A. B. (2018, 11). Exploring Wave and Sea-Level Rise Effects on Delta Morphodynamics With a Coupled River-Ocean Model. *Journal of Geophysical Research: Earth Surface*, *123*(11), 2887–2900.

https://doi.org/10.1029/2018JF004757
Rodriguez, A. B., Hamilton, M. D., & Anderson, J. B. (2000, 3). Facies and Evolution of the Modern Brazos Delta, Texas: Wave Versus Flood Influence. *Journal of Sedimentary Research*, *70*(2), 283–295. https://doi.org/10.1306/2DC40911-0E47-11D7-8643000102C1865D
Rossi, V. M., Kim, W., Leva López, J., Edmonds, D., Geleynse, N., Olariu, C., ... Passalacqua, P. (2016, 11). Impact of tidal currents on delta-channel deepening, stratigraphic architecture, and sediment bypass beyond the shoreline. *Geology*, *44*(11), 927–930. https://doi.org/10.1130/G38334.1
Sestini, G. (1989). Nile Delta: A review of depositional environments and geological history. *Geological Society Special Publication*, *41*, 99–127. https://doi.org/10.1144/GSL.SP.1989.041.01.09
Seybold, H., Andrade, J. S., & Herrmann, H. J. (2007, 12). Modeling river delta formation. *Proceedings of the National Academy of Sciences*, *104*(43), 16804–16809. https://doi.org/10.1073/pnas.0705265104
Shaw, J. B., Wolinsky, M. A., Paola, C., & Voller, V. R. (2008, 11). An image-based method for shoreline mapping on complex coasts. *Geophysical Research Letters*, *35*(12). https://doi.org/10.1029/2008GL033963
Simeoni, U., Fontolan, G., Tessari, U., & Corbau, C. (2007, 5). Domains of spit evolution in the Goro area, Po Delta, Italy. *Geomorphology*, *86*(3-4), 332–348. https://doi.org/10.1016/J.GEOMORPH.2006.09.006
Sloan, E., Dodd, N., & Briganti, R. (2024, 9). Effects of Tidal Range and Significant Wave Height on Delta Development. *Journal of Geophysical Research: Earth Surface*, *129*(9), e2024JF007688. https://doi.org/10.1029/2024JF007688
Soulsby, R. L. (1997). Dynamics of marine sands: a manual for practical applications. *Oceanographic Literature Review*, *44*(9), 947.
Stapor, F. W., & Stone, G. W. (2004, 2). A new depositional model for the buried 4000 yr BP New Orleans barrier: implications for sea-level fluctuations and onshore transport from a nearshore shelf source. *Marine Geology*, *204*(1-2), 215–234. 10.1016/S0025-3227(03)00350-5
Steel, R., Osman, A., Rossi, V. M., Alabdullatif, J., Olariu, C., Peng, Y., & Rey, F. (2024, 9). Subaqueous deltas in the stratigraphic record: Catching up with the marine geologists. *Earth-Science Reviews*, *256*, 104879. https://doi.org/10.1016/J.EARSCIREV.2024.104879
Storms, J. E., Stive, M. J., Roelvink, D. J., & Walstra, D. J. (2007). Initial morphologic and stratigraphic delta evolution related to buoyant river plumes. *Coastal Sediments '07 - Proceedings of 6th International Symposium on Coastal Engineering and Science of Coastal Sediment Processes*. https://doi.org/10.1061/40926(239)56
Straub, K. M., Li, Q., & Benson, W. M. (2015, 11). Influence of sediment cohesion on deltaic shoreline dynamics and bulk sediment retention: A laboratory study. *Geophysical Research Letters*, *42*(22), 9808–9815. https://doi.org/10.1002/2015GL066131
Stutz, M. L., & Pilkey, O. H. (2002, 11). Global Distribution and Morphology of Deltaic Barrier Island Systems. *Journal of Coastal Research*, 694–707. https://doi.org/10.2112/1551-5036-36.sp1.694
Swenson, J. B. (2005, 12). Relative importance of fluvial input and wave energy in controlling the timescale for distributary-channel avulsion. *Geophysical Research Letters*, *32*(23), 1–5. https://doi.org/10.1029/2005GL024758
Syvitski, J. P., Kettner, A. J., Overeem, I., Hutton, E. W., Hannon, M. T., Brakenridge, G. R., ... Nicholls, R. J. (2009, 9). Sinking deltas due to human activities. *Nature Geoscience 2009 2:10*, *2*(10), 681–686. Retrieved from `https://www.nature.com/articles/ngeo629` 10.1038/ngeo629
Syvitski, J. P. M., & Saito, Y. (2007, 11). Morphodynamics of deltas under the influence of humans. *Global and Planetary Change*, *57*(3), 261–282. https://doi

.org/10.1016/j.gloplacha.2006.12.001
Tamura, T. (2012, 9). Beach ridges and prograded beach deposits as palaeoenvironment records. *Earth-Science Reviews*, *114*(3-4), 279–297. https://doi.org/10.1016/J.EARSCIREV.2012.06.004
Tessler, Z. D., Vörösmarty, C. J., Grossberg, M., Gladkova, I., Aizenman, H., Syvitski, J. P., & Foufoula-Georgiou, E. (2015, 8). Profiling risk and sustainability in coastal deltas of the world. *Science*, *349*(6248), 638–643. https://doi.org/10.1126/SCIENCE.AAB3574
Tessler, Z. D., Vörösmarty, C. J., Overeem, I., & Syvitski, J. P. (2018, 3). A model of water and sediment balance as determinants of relative sea level rise in contemporary and future deltas. *Geomorphology*, *305*, 209–220. https://doi.org/10.1016/J.GEOMORPH.2017.09.040
Todd, T. W. (1968, 9). Dynamic diversion; influence of longshore current-tidal flow interaction on chenier and barrier island plains. *Journal of Sedimentary Research*, *38*(3), 734–746. https://doi.org/10.1306/74D71A5A-2B21-11D7-8648000102C1865D
Torrence, C., & Compo, G. P. (1998). A practical guide to wavelet analysis. *Bulletin of the American Meteorological Society*, *79*, 61–78. https://doi.org/10.1175/1520-0477(1998)079⟨0061:APGTWA⟩2.0.CO;2
van Kouwen, N. C., Ton, A. M., Vos, S. E., Vijverberg, T., Reniers, A. J., & Aarninkhof, S. G. (2023, 9). Quantifying spit growth and its hydrodynamic drivers in wind-dominated lake environments. *Geomorphology*, *437*, 108799. https://doi.org/10.1175/1520-0477(1998)079⟨0061:APGTWA⟩2.0.CO;210.1016/J.GEOMORPH.2023.108799
Van Maren, D. S. (2005). Barrier formation on an actively prograding delta system: The Red River Delta, Vietnam. *Marine Geology*, *224*, 123–143. https://doi.org/10.1016/j.margeo.2005.07.008
van Maren, D. S. (2007, 2). Water and sediment dynamics in the Red River mouth and adjacent coastal zone. *Journal of Asian Earth Sciences*, *29*(4), 508–522. https://doi.org/10.1016/J.JSEAES.2006.03.012
Vespremeanu-Stroe, A., & Preoteasa, L. (2015). Morphology and the Cyclic Evolution of Danube Delta Spits. *Coastal Research Library*, *12*, 327–339. Retrieved from `https://link.springer.com/chapter/10.1007/978-3-319-13716-2_18`
Vespremeanu-Stroe, A., Preoteasa, L., Zăinescu, F., Rotaru, S., Croitoru, L., & Timar-Gabor, A. (2016, 9). Formation of Danube delta beach ridge plains and signatures in morphology. *Quaternary International*, *415*, 268–285. https://doi.org/10.1016/J.QUAINT.2015.12.060
Vulis, L., Tejedor, A., Ma, H., Nienhuis, J. H., Broaddus, C., Brown, J., ... Foufoula-Georgiou, E. (2023). River delta morphotypes emerge from multiscale characterization of shorelines. *Geophysical Research Letters*. https://doi.org/10.1029/2022GL102684
Willis, B. J., Sun, T., & Ainsworth, R. B. (2021, 3). Contrasting facies patterns between river-dominated and symmetrical wave-dominated delta deposits. *Journal of Sedimentary Research*, *91*(3), 262–295. https://doi.org/10.2110/JSR.2020.131
Willis, B. J., Sun, T., & Ainsworth, R. B. (2022, 6). Sharp-based shoreface successions reconsidered in three-dimensions: A forward stratigraphic modelling perspective. *The Depositional Record*, *8*(2), 685–717. https://doi.org/10.1002/DEP2.177
Xu, Z., & Plink-Björklund, P. (2023, 10). Quantifying Formative Processes in River- and Tide-Dominated Deltas for Accurate Prediction of Future Change. *Geophysical Research Letters*, *50*(20), e2023GL104434. https://doi.org/10.1029/2023GL104434
Zăinescu, F., Anthony, E., & Vespremeanu-Stroe, A. (2021, 8). River Jets Versus

Wave-Driven Longshore Currents at River Mouths. *Frontiers in Marine Science*, *8*, 708258. https://doi.org/10.3389/fmars.2021.708258

Zăinescu, F., Storms, J. E. A., Vespremeanu-Stroe, A., Vegt, H. V. D., Schuster, M., & Anthony, E. (2024, 10). Wave-Influenced Delta Morphodynamics, Long-Term Sediment Bypass and Trapping Controlled by Relative Magnitudes of Riverine and Wave-Driven Sediment Transport. *Geophysical Research Letters*, *51*(19), e2024GL111069. https://doi.org/10.1029/2024GL111069

Zainescu, F., Vespremeanu-Stroe, A., & Tatui, F. (2016, 3). Comparative spit dynamics. the case of deltaic river mouth spits. *Journal of Coastal Research*, *1*(75), 800–804. https://doi.org/10.2112/SI75-161.1

Wave-influenced deltas grow through cyclical accretion of barrier-spits

Connor Broaddus[1], Jaap H. Nienhuis[2], Douglas A. Edmonds[3], Efi Foufoula-Georgiou[1,4]

[1]Department of Civil and Environmental Engineering, University of California Irvine, USA
[2]Department of Physical Geography, Utrecht University, NL
[3]Department of Earth and Atmospheric Sciences, Indiana University, USA
[4]Department of Earth System Science, University of California Irvine, USA

Key Points:

- Barrier-spits are the primary constructional elements of wave-dominated deltas and leave distinct signatures (lagoons) on the delta plain.
- Accretion of barrier-spits is a cyclical autogenic process controlled by accumulation of fluvial sediment near the delta front.
- Mud exerts important controls barrier-spit accretion and distributary channel network morphodynamics, even in wave-dominated deltas.

Corresponding author: Connor Broaddus, cbroaddu@uci.edu

Abstract

Wave-influenced deltas are the most abundant delta type and are also potentially the most at-risk to human-caused changes, owing to the effects of wave-driven sediment transport processes and the short timescales on which they operate. Despite this, the processes controlling wave-influenced growth are poorly understood, and the role of fine-grained cohesive sediment (mud) is typically neglected. Here we simulate idealized river deltas in Delft3D across a range of conditions to interrogate how relative wave-influence and fluvial sediment composition impact delta evolution on decadal-millennial timescales. Our simulations capture the barrier-spit formation and accretion process characteristic of prograding wave-influenced deltas, such as those of the Red (Vietnam), Sinu (Colombia), and Coco (Nicaragua) rivers. Barrier-spit accretion exhibits multi-decadal cyclicity driven by subaqueous accumulation of fluvial sediment near river mouths. Using a range of metrics, we quantify how waves and mud influence delta morphology and dynamics. Results show that waves stabilize and simplify channel networks, smooth shorelines, increase shoreline reworking rates, reduce mud retention in the delta plain, and rework mouth bar sediments to form barrier-spits. Higher fluvial mud concentrations produce simpler and more stable distributary networks, rougher shorelines, and limit back-barrier lagoon preservation without altering shoreline reworking rates. Our findings reveal distinct controls on shoreline change between river-dominated and wave-influenced deltas and demonstrate that mud plays a critical role in delta evolution, even under strong wave influence. These insights could enhance paleoenvironmental reconstructions and inform predictions of delta responses to climate and land-use changes.

Plain Language Summary

Humans have disrupted sediment delivery to river deltas globally, and deltas with strong wave climates (wave-influenced deltas) may be the most vulnerable to these disruptions. However, wave-influenced deltas are poorly understood. To address this, we developed computer models of wave-influenced delta growth and used them to investigate how the processes involved in delta formation are affected by waves and by the type of sediment delivered by the river. Our models show that wave-influenced delta growth is fundamentally different from deltas with weak wave-climates; wave-influenced deltas are made up of shore-parallel sand bodies, which we call "barrier-spits". Each barrier-spit takes multiple decades to form, and they are added to the delta at regular intervals. Our models also show that mud affects the way in which deltas form, even when waves are large. Mud is deposited between barrier-spits, affecting delta deposits. Mud also impacts the way that river channels grow and move around the delta, where more mud leads to fewer and more stable channels. Overall, our models are useful for understanding how waves and mud impact the growth of river deltas, which may help us to predict how deltas will respond to changes in sediment delivery caused by humans.

1 Introduction

In the absence of tides, river deltas exhibit a spectrum of processes and forms thought to be the result of varying degrees of fluvial and wave influence. At one end of this spectrum are fully "river-dominated" deltas with complex distributary networks and large, lobate shoreline protrusions (L. D. Wright, 1973; Galloway, 1975; Broaddus et al., 2022; ?, ?). These systems grow through a combination of avulsion and mouth-bar driven bifurcation, both of which can be driven by channel elongation and resultant reductions in local sediment transport capacity (Jerolmack & Swenson, 2007; Edmonds & Slingerland, 2007, 2010; Fagherazzi et al., 2015). At the other end of this spectrum are "wave-dominated" deltas, which lack distributary networks and have smooth, cuspate shorelines with limited protrusions (L. D. Wright, 1973; Galloway, 1975; Anthony, 2015; Broaddus et al., 2022; Vulis et al., 2023). Wave-dominated deltas grow through onshore-directed

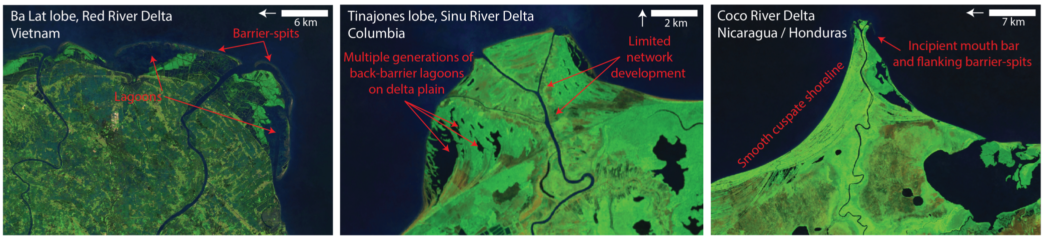

Figure 1. Examples of real-world wave-influenced deltas. Note the ubiquitous presence of shore-parallel barriers and associated lagoons, which are unique to wave-influenced systems. Other diagnostic features include simple distributary networks and smooth shorelines ranging from lobate to cuspate.

wave-driven reworking of fluvial sediment deposited in the shoreface and through impoundment of non-deltaic littoral sediment carried from updrift locations by longshore currents (Komar, 1973; L. D. Wright, 1973; Galloway, 1975; Dominguez, 1996; Ashton & Giosan, 2011; Anthony, 2015).

While the processes governing the evolution of the above-described end-members are well understood, intermediate, "wave-influenced" deltas have received considerably less attention, despite being the most abundant category of deltas (Nienhuis et al., 2020). These deltas have morphologies that vary between river and wave-dominance, but also include unique features such as barriers, spits and lagoons (Figure 1). Questions remain concerning the morphological transitions between river and wave-dominated deltas, and especially the role of mud. Do deltaic processes and morphology vary monotonically with wave-influence? And are the transitions gradual, or abrupt?

Addressing these questions is of urgent importance, as the driving forces that control delta morphology and dynamics are changing rapidly (Giosan et al., 2014; Tessler et al., 2015; Hoitink et al., 2020). Changes in land use and climate are affecting the volumes of water and sediment that reach deltas (Nienhuis et al., 2020; Tessler et al., 2018), while sea level rise and land subsidence threaten to drown existing delta deposits (J. P. Syvitski et al., 2009; Ericson et al., 2006; Ibáñez et al., 2014). Understanding how delta morphology and dynamics vary across a range of environmental forcing conditions is the first step toward predicting how deltas will respond to the plethora of anthropogenic pressures which they currently face.

2 Background

2.1 Physics-based modeling of wave influenced delta growth across scales

Physics-based numerical models provide a promising path toward predicting how wave-influenced deltas will respond to change by facilitating investigation into the interactions between river flow, wave-action, and longshore currents which govern sediment transport across a range of scales. Models such as Delft3D and MIKE (coupled with spectral wave models) provide an avenue for exploring the development and modification of river mouth bars in the presence of waves on timescales relevant to engineering (years to decades). Nardin and Fagherazzi (2012) used an idealized Delft3D model of a river mouth to show that waves impact mouth bar development by enhancing bed shear stress, changing the direction of the river jet (in the case of non-frontal waves), and increasing jet spreading. They showed that bar morphology is modulated by these processes, and bar formation is inhibited in the presence of large waves that approach from high angles. Nardin et al. (2013) used a similar model to demonstrate that the jet spreading effect dominates over increased bed shear stress in the presence of small frontal waves, which actually increases the propensity of bars to form closer to the river mouth. They suggested that a non-monotonic relation exists between wave energy and mouth bar formation; small waves enhance mouth bar formation over cases with no waves, while larger waves inhibit mouth bar formation. More recently Zăinescu et al. (2021) developed idealized river mouth models in MIKE21 FM to simulate interactions between longshore currents, mouth bars, and fluvial jets, finding that jet behavior and flow circulation patterns near the river mouth can be predicted by the momentum or discharge balances between the fluvial jet and longshore currents. A detailed review of the controls on river mouth morphodynamics is presented in Fagherazzi et al. (2015).

Physics-based numerical models are also capable of simulating the growth and evolution of wave-influenced river deltas over longer timescales (decades to centuries). Historically, wave-dominated deltas have been simulated primarily using so called "1-line" shoreline models (Komar, 1973; Ashton & Giosan, 2011; Gao et al., 2018). These models work well to simulate shoreline evolution but cannot capture the transition to river dominance due to their inability to simulate mouth bars. In this transition, mouth bars are expected to appear as fluvial sediment supply outpaces potential longshore transport (Nienhuis et al., 2015). Geleynse et al. (2011) developed idealized delta-scale simulations in Delft3D to show that waves act to limit sequestration of fine-grained sediment on the delta plain, and reduce the number of active distributaries, leading to smoother (less rugose) delta shorelines. In a similar effort, Liu et al. (2020) showed that deltas subject to wave-action produced shallower topset gradients and reduced distributary avulsion frequency, leading to smoother shorelines. Willis et al. (2021, 2022) used the Chevron CompStrat model (which, similar to Delft3D and MIKE, is governed by the shallow water equations) to explore wave-influenced delta deposit stratigraphy under conditions of changing sea level. Their simulations develop morphologies that are remarkably similar to real-world wave-influenced delta systems, including dual clinoform delta fronts with large subaqueous platforms. Sloan et al. (2024) used idealized Delft3D models to explore the conditions under which waves completely inhibit delta accretion. Recently, Zăinescu et al. (2024) used idealized delta-scale simulations in Delft3D to investigate morphodynamics in asymmetrical wave-influenced deltas. They found that increasing degrees of wave-influence lead to channel stabilization and a reduction in avulsion frequency compared to river-dominated deltas, paralleling results from Liu et al. (2020) and morphodynamic models (Swenson, 2005; Ratliff et al., 2018; Gao et al., 2018; Hu et al., 2022). They also demonstrate that the trade-off between trapping and bypassing of updrift sediment around the river mouth is highly sensitive to the relative strengths of fluvial and longshore sediment transport, and that this relationship determines the morphology of asymmetric wave-influenced deltas.

These efforts collectively demonstrate the efficacy and utility of using physics-based numerical models to reproduce the dynamics and morphologic features common to wave-influenced deltas. Despite these advances, substantial knowledge gaps remain, particularly on the role of mud and the morphologic transition from mouth bars to barrier-spits as the dominant delta constructional element.

2.2 Barrier-spits

Among the most characteristic features of wave-influenced and wave-dominated deltas are barriers and spits (Anthony, 2015). Both barriers and spits form through a combination of cross-shore and longshore sediment transport processes, and differ primarily in that barriers are true islands while spits are connected to an adjacent landmass at one end. These features were historically associated with phases of delta abandonment, and their deposits interpreted to represent an allogenic response to changes in sedimentary (upstream) or marine (downstream) forcing. The best known example is the Chandeleur Islands of the Mississippi River delta, a set of barriers which formed by headland erosion of delta lobes (Penland et al., 1988) or onshore transport of shelf deposits (Stapor & Stone, 2004) following abandonment during large scale avulsions. Another example is the visually striking system of paired spits that flank the Ebro River delta, which have been shown through historical reconstructions and numerical modeling to be a result of decreases in fluvial sediment flux following a river avulsion (Ibàñez et al., 1997; Nienhuis et al., 2017).

More recently, a separate category of deltaic barriers and spits have been recognized which are genetically distinct from those formed as a result of marine transgression or delta lobe abandonment. This category is associated with punctuated progradation in wave-influenced environments, and may be the most common genetic mode for these features on river deltas (Stutz & Pilkey, 2002; Bhattacharya & Giosan, 2003). Furthermore, progradational barrier-spit accretion may be the dominate process by which wave-influenced deltas build new land (Vespremeanu-Stroe & Preoteasa, 2015), as evidenced by the unique geometry and sedimentary character of their deposits. While river-dominated deltas have deposits characterized by systems of mouth bars, crevasses and abandoned distributary channels (Olariu & Bhattacharya, 2006; Edmonds & Slingerland, 2010; Esposito et al., 2013; Willis et al., 2021; Nota et al., 2024), wave-influenced delta deposits are typically composed of series of regularly-spaced, elongate, shore-parallel sand bodies. These sand bodies may amalgamate to form "beach-ridge plains", or may be separated by back-barrier deposits of fine-grained sediment, forming "cheniers" (Otvos, 2000; Tamura, 2012).

The mechanisms and sediment sources responsible for the formation of barrier-spits (and their subsequent incorporation into the delta plain) are thought to vary between symmetric and asymmetric wave-influenced deltas. Asymmetric deltas form under wave climates that exhibit a dominant angle of approach, setting up unidirectional longshore currents that impart distinct processes and sedimentary facies on the updrift and downdrift flanks of the delta (Bhattacharya & Giosan, 2003; Korus & Fielding, 2015; Vespremeanu-Stroe et al., 2016; Preoteasa et al., 2016). Barrier-spits can develop on the updrift flank and morphologically "deflect" distributary outlets due to blocking of longshore currents by the fluvial jet (Todd, 1968; Komar, 1973; Nienhuis, Ashton, & Giosan, 2016; Gao et al., 2020). Barrier-spits can also develop on the downdrift flank of asymmetric deltas as a result of several different processes, including high wave approach angles that cause instabilities in the longshore transport field (Ashton & Giosan, 2011), or by gradual development of a subaqueous sediment platform followed by wave-driven onshore transport (Vespremeanu-Stroe & Preoteasa, 2015; Preoteasa et al., 2016; Zainescu et al., 2016).

Barrier-spits and their associated deposits (beach-ridges / cheniers) are also prevalent in symmetric wave-influenced deltas. The mechanisms involved in the formation and evolution of these features, however, as well as their overall role in the progradation of symmetric deltas, have received less attention than those on asymmetric systems, and are still poorly understood (Zainescu et al., 2016). One well studied example is the Red River Delta of Vietnam, where cyclical barrier-spit development is characterized by a multi-phase process consisting of subaqueous fluvial sediment accumulation, onshore transport due to wave asymmetry, and reworking by longshore currents (Van Maren, 2005; van Maren, 2007). The process is similar to that described for the downdrift flank of the asymmetric Sfantu Gheorge lobe of the Danube delta (Vespremeanu-Stroe & Preoteasa, 2015; Preoteasa et al., 2016). A similar process is thought to describe the development of the Goro spit system in the Po River delta of Italy (Simeoni et al., 2007).

Despite a likely similar origin of mouth bars (on river dominated deltas) and barrier-spits (on wave dominated deltas), they have historically been considered separately. Perhaps the conditions under which barrier-spit formation dominates over mouth bar accretion would determine the resulting morphology, and thereby also affect beach ridge spacing, and the timescales of barrier-spit formation.

2.3 Role of fine-grained cohesive sediment

There is also significant uncertainty surrounding the role of fluvial sediment composition in the formation of wave-influenced deltas. Several studies have highlighted the crucial role of fine-grained cohesive sediment (mud) in shaping the morphology and dynamics of river-dominated deltas. Higher proportions of mud in fluvial effluent reduces channel mobility, enhances the formation of levees, deepens channels and inhibits bifurcations and avulsions, limiting the total number of active distributaries on a delta (Edmonds & Slingerland, 2010; Martin et al., 2009; Li et al., 2017). The effects of mud on the channel network propagate to the overall shape of the delta and its shoreline; fluvial sediment flux is distributed less evenly across the delta shoreline, leading to enhanced growth of local shoreline protrusions and producing more elongate delta plains with rougher shorelines (Geleynse et al., 2011; Caldwell & Edmonds, 2014).

By contrast, the role of fine-grained cohesive sediment (mud) in wave-influenced delta evolution has received significantly less attention and is commonly ignored in numerical modeling efforts due to long settling timescales and the high degree of turbulence associated with surf-zone environments (Geleynse et al., 2011; Nardin et al., 2013; Nienhuis, Ashton, Nardin, et al., 2016; Broaddus et al., 2022; Sloan et al., 2024; Zăinescu et al., 2024). However, large portions of the delta front can be sheltered from wave action by barriers and spits, permitting deposition of fine-grained sediment in these locations (Rodriguez et al., 2000; Bhattacharya & Giosan, 2003; Stutz & Pilkey, 2002; Van Maren, 2005). Both channel geometry and network dynamics are strongly dependent on the character of fluvial sediment (Orton & Reading, 1993; Hoyal & Sheets, 2009; Martin et al., 2009; Edmonds & Slingerland, 2010; Caldwell & Edmonds, 2014). Furthermore, phase differences between periods of peak discharge and significant wave events are common in deltas with large drainage basins (Anthony, 2015), which could allow fluvial mud to be incorporated in the shoreface regardless of the long-term average wave conditions.

To address the knowledge gaps outlined above we developed physics-based numerical simulations capable of resolving the complex interactions between fluvial and wave processes that control morphodynamics in wave-influenced deltas. Our simulations reproduce emergent features considered to be characteristic of wave-influenced deltas, such as mouth bars, barriers, and spits (which we refer to collectively as barrier-spits), at the timescales on which deltas grow and evolve. They differ from previous efforts (Geleynse et al., 2011; Liu et al., 2020; Willis et al., 2021; Sloan et al., 2024; Zăinescu et al., 2024) by focusing on the role of mud. We characterize the barrier-spit accretion process and its temporal characteristics using quantitative frequency analysis. We present metrics to quantify delta morphology and dynamics and show how the processes controlling delta evolution vary with wave-influence and the proportion of cohesive sediment in fluvial effluent. Finally, we discuss the implications of our findings for management actions, paleoenvironmental interpretation, and general knowledge of wave-influenced delta morphodynamics.

3 Methods

3.1 Model Setup

Delft3D is a hydro-morphodynamic modeling package capable of simulating fluid flow (Reynolds-averaged Navier-Stokes equations), wave action (SWAN model), sediment transport, and morphological change. It has been validated for a wide range of hydrodynamic conditions and has been shown to be capable of simulating idealized delta development (Storms et al., 2007; Edmonds & Slingerland, 2010; Geleynse et al., 2011; Burpee et al., 2015; Caldwell & Edmonds, 2014; Rossi et al., 2016; Liu et al., 2020; Broaddus et al., 2022; Xu & Plink-Björklund, 2023; Anderson et al., 2023; Nota et al., 2024; Sloan et al., 2024; Zăinescu et al., 2024), as well as the morphodynamics at wave-influenced river mouths (Edmonds & Slingerland, 2007; Nardin & Fagherazzi, 2012; Nardin et al., 2013; Nienhuis, Ashton, & Giosan, 2016; Gao et al., 2018; Zăinescu et al., 2021).

Using Delft3D we set up an idealized model of river delta growth and evolution in the presence of waves. For simplicity we ignore the effects of tides, wind, density gradients, Coriolis forces, and other factors that may impact delta morphodynamics. The flow equations are solved on a rectilinear grid of 25 m square cells covering an area of 189 km^2 (21 km in the cross-shore direction, 9 km in the long shore direction) (Figure 2a). Initial bed levels in all simulations consist of a river with a trapezoidal geometry (width = 300 m, depth = 3 m) that cuts through a bluff-backed beach (bluff height = 10 m, bluff width = 500 m, beach height = 2 m, beach width = 500 m) and terminates into a sloping basin (Figure 2b). The basin slope follows an equilibrium shoreface profile for 200 µm sand (Equation 1), as defined by Dean (1991).

$$z(x) = ax^{2/3} \tag{1}$$

where z is the water depth (m), x is the distance from shore (m), and a is a grain size dependent parameter whose value is 0.1 for 200 µm sand. Figure 2b shows the initial bathymetry in the region around the river mouth.

We add random perturbations to the initial bed levels to simulate natural variability, which are drawn from a uniform distribution bounded by -0.01 and 0.01 m. To enable faster progradation and maintain the shallow water assumption, we limit initial depth to 10 m below sea level (which is beyond the inner depth of closure for the largest modeled waves, as defined by Hallermeier, 1981). The model results are insensitive to the bluff and beach dimensions, as well as the depth cutoff for the initial bathymetry.

Wave computations are solved on a separate grid covering an area of 572 km^2 (52 km in the longshore direction, 11 km in the cross-shore direction) (Figure 2a). Grid cell dimensions vary in the wave domain to speed up computations; areas overlapping the flow domain have a resolution of 50 x 50 m, while areas outside the flow domain have cells that are 400 m in the longshore direction and 50 m in the cross-shore direction. Initial bathymetry in the wave domain is identical to that of the flow domain, albeit expanded to fit the enlarged grid dimensions.

All simulations use a computational time step (Δt) of 15 seconds to obey numerical stability criteria. Flow and wave computations are fully coupled (bed levels, water levels, velocities) with a coupling interval (CI) of 30 minutes. We apply a morphological scaling factor (morfac) of 180 to speed up computations, assuming that bed relaxation is negligible at the modeled timescales. Each simulation is computed for 12 hours prior to the implementation of morphological changes. We assessed the sensitivity of our results to these choices, performing simulations with Δt as small as 5 seconds, CI as small as 5 minutes, and morfac as small as 45. We also tested our models sensitivity to the grain size and initial bed thickness of non-cohesive sediment. While these simulations indeed exhibit differences in details, the emergent processes and morphological trends discussed in this work do not change.

We model two sediment fractions, one non-cohesive (sand) and one with cohesion (mud). The sand fraction has a median grain size of 200 µm, a specific density of 2650 kg m^{-3}, and an initial bed thickness of 10 m that is constant throughout the domain. The mud fraction has a settling velocity of 0.00025 m s^{-1}, and critical shear stresses for erosion (τ_{ce}) and deposition (τ_{cd}) of 0.1 and 1000 N m^{-2}, respectively. Setting $\tau_{ce} << \tau_{cd}$ ensures constant mud deposition such that equilibrium depth is set by erosive shear stresses, rather than being dependent on initial sediment thickness (Edmonds & Slingerland, 2010). We chose a relatively low value for τ_{ce} to facilitate mud erosion and to avoid over representing the importance of cohesive sediment in delta dynamics.

The models initialize with no mud in the bed, a choice which notionally reflects the paucity of mud in wave-influenced nearshore settings prior to the introduction of fluvial

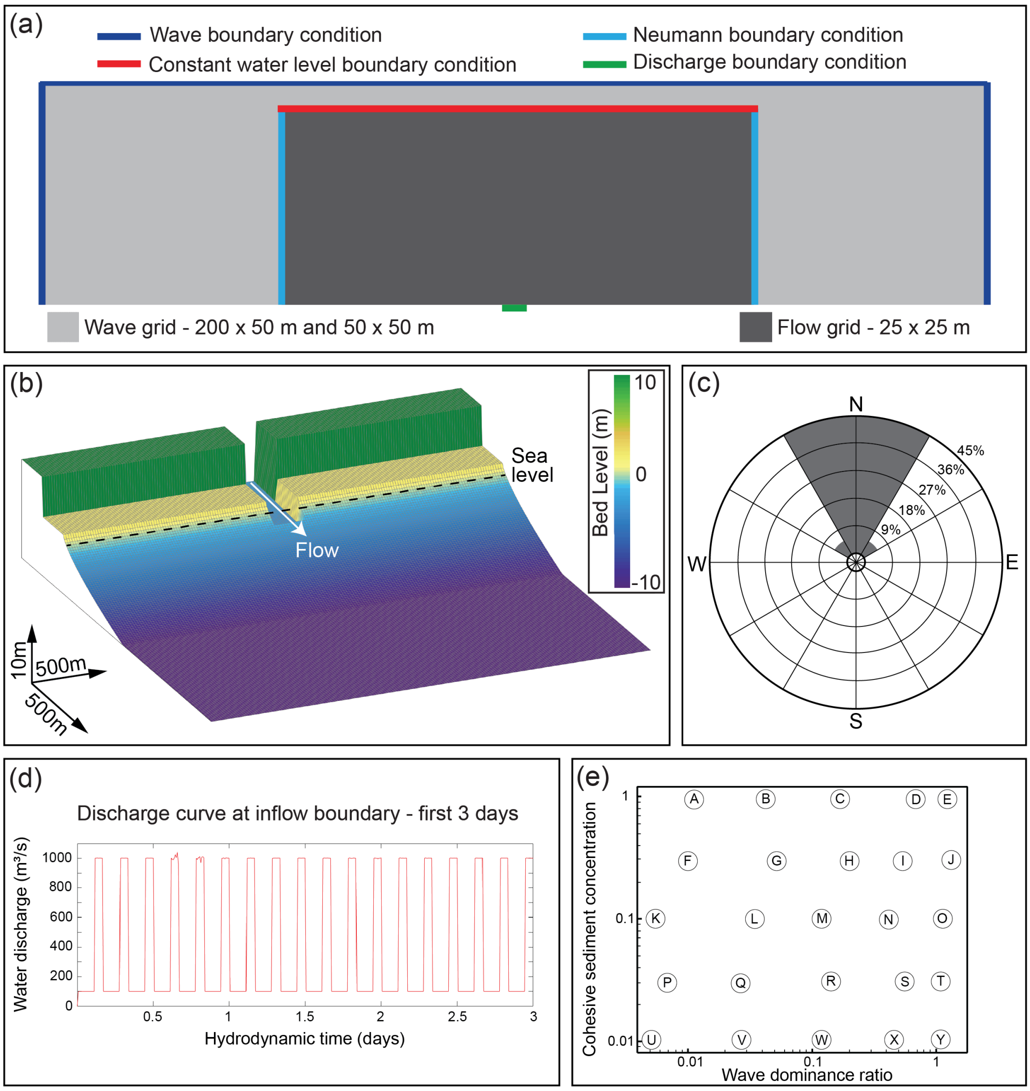

Figure 2. Model setup including domain and boundary locations (a), initial bathymetry (b), wave directional distribution (c), discharge curve (d) and simulation ensemble (e).

effluent. Non-cohesive sediment transport is computed using the Soulsby-Van Rijn relation as implemented in Delft3D, which requires the user to specify the calibration factor for sediment transport (1), the diameter ratio between 90th percentile and median grain sizes (1.5), and the roughness height used to compute the drag coefficient (0.006). We use the values recommended by Soulsby (1997). This formula predicts bed and suspended load transport based on the combined shear stress due to current velocity and root mean squared wave orbital velocity (neglecting transport by depth varying currents and wave asymmetry). Its simplicity makes it well suited to 2DH simulations of coastal morphodynamics. Cohesive sediment transport is computed using the well-known Partheniades-Krone relation. Each of these transport relations is described in detail in the Delft3D-FLOW User Manual.

Boundaries are placed along the North, East, and West edges of the wave domain, and impart significant wave heights that vary between runs but are constant for a given run. Wave direction changes at each coupling timestep, and for each simulation the sequence of wave directions are randomly drawn from a predefined wave energy density spectrum (which is constant across runs). The distribution of wave energy is such that 90% of the waves come from -30 and 30 degrees relative to shore normal, while 10% come from -45 and 45 degrees relative to shore normal (Figure 2c). Previous work has demonstrated that the most important spectral parameters in determining delta morphology are directional (a)symmetry and the fraction of waves that approach from high, unstable angles (45 degrees or greater) (Ashton & Giosan, 2011; Ratliff et al., 2018; Hu et al., 2022). We chose this spectrum for simplicity and to facilitate future comparison with one-line delta evolution models, in which it is commonly used.

Water and sediment enter the domain through a discharge boundary condition located at the upstream limit of the inflow channel (Figure 2a). We specify the cohesive sediment concentration at the inflow boundary (which varies between simulations but is constant throughout a given simulation) while allowing the non-cohesive sediment concentration to vary with the hydrodynamics (equilibrium concentration), which maintains a constant bed level and ensures stability. We specify a constant water level boundary along the Northern edge of the domain, and apply Neumann boundaries along the Eastern and Western edges to allow water and sediment to enter and exit freely. Turbulence closure in the x and y directions is achieved through subgrid horizontal large eddy simulations, using the default options suggested by Deltares (Delft3D-FLOW User Manual).

In order to represent the discharge variability inherent to most river systems, we defined the inflow hydrograph as an asymmetric quasi-square wave that oscillates between high (1000 m^3 s^{-1}) and low (100 m^3 s^{-1}) discharge values. For each oscillation period, the low and high flow duration is 160 and 70 minutes respectively, with a 10 minute "ramp" between low and high flows (Figure 2d). While most idealized delta modeling studies are performed with a constant discharge boundary condition, accurately representing the dynamics at work in wave-influenced deltas requires variable discharge, due to the higher recurrence intervals of significant wave events relative to significant discharge events. We also tested other wave forms and shapes for the hydrograph (sawtooth, sine wave, repeating beta distribution) and found that, for a given ratio of high to low flow duration, the morphology and processes that emerge are more or less constant.

We apply a spatially constant horizontal eddy viscosity (E_v) and horizontal eddy diffusivity (E_d) of 1 m^2 s^{-1}, and set the factor for erosion of adjacent dry cells (Θ_{sd}) to 0.5. We tested the model's sensitivity to these choices, varying E$_v$ and E$_d$ from 0.0001 to 1 m^2 s^{-1}and varying Θ_{sd} from 0.1 to 0.9. We found that varying these parameters did not significantly affect the morphological trends or emergent process described.

We apply a spatially constant Chezy roughness (C) value of 65 m$^{1/2}$ s^{-1} to our simulations, and tested values ranging from 45-75 m$^{1/2}$ s^{-1}. Changes to C impact jet spreading rates and longshore transport, and as a result impact the morphology of our simulations. In general, increasing C (lowering roughness) decreases jet spreading and increases longshore transport rates. Decreased jet spreading leads to more sediment being transported further from the river mouth, causing mouth bars to form less frequently, decreasing the number of outlets and deepening channels. Increased longshore transport rates lead to reduced delta progradation rates and smoother shorelines, which leads to lower values of the delta shape and shoreline roughness metrics. The opposite is true for decreases in C. We chose a value of 65 $\mathrm{m}^{1/2}\ \mathrm{s}^{-1}$ for our simulations because it is the default in Delft3D, produces realistic delta morphologies, and leads to emergent longshore transport rates similar to those predicted by empirical estimates (see section 3.3).

α_{bn} is a multiplicative factor applied to account for the effects of transverse bed slopes on sediment transport rates. Baar et al. (2019) demonstrated the importance of this parameter in controlling channel aspect ratios and total transport rates. Small values of α_{bn} favor channel deepening, narrowing, generally low transport rates, and accompanying lack of channel mobility. High values lead to increased transport rates, and shallow, wide channels that are highly mobile. We chose a value of 3 because it balances these effects to produce realistic channel aspect ratios and dynamics, with transport rates that fall within the range observed in rivers with similar discharge. This value is within the range suggested by both Deltares and Baar et al. (2019).

3.2 Simulated Parameter Space

To assess the roles of waves and fluvial sediment composition in controlling delta morphology and dynamics, we designed a suite of 25 simulations that vary the mud concentration and wave amplitudes at their respective boundaries while holding all other model parameters constant.

We vary mud concentration (C_{mud}) across two orders of magnitude, from 0.01 to 1 kg m^{-3}. We chose this quantity (rather than a non-dimensional descriptor, such as sand to mud ratio) because it is a measurable quantity in natural river systems, providing a basis for comparison between our simulations and reality.

To quantify differences in the degree of wave influence, we follow the sediment flux balance approach of Nienhuis et al. (2015) to define the wave dominance ratio (W) (equation 2) – the inverse of the river-dominance ratio (R) in Nienhuis et al. (2015). In essence, this approach defines a given delta's degree of "wave-influence" based on the river's ability to supply sediment, and the given wave climate's ability to transport sediment alongshore. This approach follows decades of work which collectively suggests that river delta formation and morphology depends on the fundamental balance between constructive (fluvial) and destructive (wave, tidal) forcings (L. D. Wright, 1973; Galloway, 1975; Komar, 1973; J. P. M. Syvitski & Saito, 2007; Caldwell et al., 2019).

Fluvial sediment flux (Q_{river}) is defined as the average non-cohesive sediment (sand) transport rate at the apex of a delta system (kg s^{-1}). Here we consider only the flux of sand to keep the role of mud isolated to a separate parameter and measure the time averaged sand flux values directly from simulation outputs.

For each simulation we estimate the maximum potential longshore transport rate (Q_{wave}) (kg s^{-1}) based on the method of Nienhuis et al. (2015). This method convolves the angular distribution of wave energy (equation 3) with an empirical estimate of longshore transport as a function of deep-water wave properties (equation 4) (P.D. Komar, 1998; Ashton & Murray, 2006) to yield a distribution of potential longshore transport rates as a function of shoreline orientation (equation 5) (see Nienhuis et al. (2015) for more details).

$$W = \frac{Q_{wave}}{Q_{river}} \tag{2}$$

$$E(\phi_0) = \frac{H_s^{12/5}(\phi_0) \cdot T^{1/5}(\phi_0)}{\sum_{\phi_0} H_s^{12/5}(\phi_0) \cdot T^{1/5}(\phi_0)} \tag{3}$$

$$Q_s = K \cdot \rho_s \cdot (1-p) \cdot H_s^{12/5} \cdot T^{1/5} \cdot cos^{6/5}(\phi_0 - \theta) \cdot sin(\phi_0 - \theta) \tag{4}$$

$$Q_{s,net}(\theta) = E(\phi_0) * Q_s(\phi_0 - \theta) \tag{5}$$

where $E(\phi_0)$ is the wave energy probability distribution for all possible deep water wave approach angles (ϕ_0). H_s is the significant wave height (m), T is the wave period (s), θ is a possible local shoreline orientation, ρ_s is the density of sediment (2650 kg m^{-3}), ρ is dry bed porosity (0.4), and K is an empirical constant equal to 0.06 m$^{3/5}$ s$^{-6/5}$ (Nienhuis et al., 2015).

We sum the maximum values for transport along the left and right delta flanks as our estimate for Q_{wave}, showing that a delta will continue growing its shoreline orientation until both flanks are at equilibrium with the rate of fluvial sediment delivery, or transport is maximized.

We hold the directional distribution of wave energy constant between simulations, varying H_s between 0.1 and 3 m, resulting in W values ranging from 0.005 to 1. We limit our investigation to this range of W values to focus on the transition from river to wave-dominance.

Figure 2e shows the locations of each simulation in the parameter space explored here (the basis for the contour plots in Figure 6). Each simulation is labeled with a letter, corresponding to the RunID listed in Table 1.

3.3 Validation – Longshore Transport Comparison

To assess our simulations' ability to correctly resolve the emergent dynamics of longshore sediment transport we compared the longshore transport fields produced by our simulations with empirical predictions of longshore transport based on the prescribed deep-water wave climates.

For a given timestep in a simulation we measured the longshore transport values by integrating then averaging sediment transport rates over shore-normal cross-sections that are manually defined at 6 locations (3 for each flank) along the active delta shoreline away from the river mouth (an interactive MATLAB code facilitates this process) (Figure 3a). Cross-sections had to be manually defined at each time step because the delta progrades through time, and because the output fields of Delft3D do not enable separation of currents or transport into fluvial versus wave-driven components. Although the cross sections are defined somewhat arbitrarily, having 6 for each timestep ensures we capture the variability inherent to a longshore transport field. Aggregating values from all cross-sections over the final 33% of the simulation period gives a distribution of single-flank longshore transport rates for a given simulation (Figure 3b). We use the 90$^{\text{th}}$ percentile value from this distribution (multiplied by a factor of two to represent the total littoral transport to the left and right of the river mouth) for comparison with an empirical estimate based on the above-described method of Nienhuis et al. (2015).

The comparison between predicted (empirical) and observed (modeled) longshore transport rates is shown in Figure 3c. The comparison includes simulations with intermediate fluvial mud concentration (C_{mud} = 0.1 kg m^{-3}) and H_s > 1 m. Note that this comparison considers only sand transport, which is the basis for most empirically-derived longshore transport relations (including the one used here).

Table 1. List of simulations used in contour plots. Run ID corresponds to the letters used in Figure 2e to denote positions in parameter space. C_{mud} = mud concentration (kg m^{-3}), H_s = significant wave height (m), W = wave dominance ratio, P_c = channel persistence (%), D_{sl} = fractional shoreline change (%), L_f = lagoon fraction (%), N_{out} = number of outlets, R^* = shoreline roughness, M_f = delta plain mud fraction (%).

RunID	C_{mud}	H_s	W	P_c	D_{sl}	L_f	N_{out}	R^*	M_f
A	1	0.1	1e-2	28.8	18.7	0.1	3	77	37.5
B	1	0.5	4e-2	36.7	26.5	0	2.2	53	36.7
C	1	1	1e-1	50.2	29	0.1	1.1	15	25.1
D	1	2	6e-1	72.6	47.4	1.3	1	4	20.8
E	1	3	1	75	57.1	1.7	1	4	19.1
F	0.3	0.1	1e-2	19	13.4	0.2	4.1	32	19.3
G	0.3	0.5	4e-2	21.6	17.8	0.1	1.8	28	14.6
H	0.3	1	2e-1	53.9	29.9	0.8	1.7	12	11
I	0.3	2	5e-1	63.1	47.8	3.7	1.2	4	9.3
J	0.3	3	1	67.1	55.8	1.8	1.7	4	8.5
K	0.1	0.1	6e-3	19.5	13.9	0	5.5	23	7.2
L	0.1	0.5	3e-2	26.6	18.9	0.1	2.6	20	6
M	0.1	1	1e-1	33.9	30.3	0.5	2	19	4.4
N	0.1	2	4e-1	51.8	54.9	6.1	2	5	3.4
O	0.1	3	1	61.1	56.8	2	1.7	4	3.4
P	0.03	0.1	7e-3	18	12.4	0	6.6	20	2.6
Q	0.03	0.5	2e-2	17.5	22.2	0	5.7	18	2.2
R	0.03	1	1e-1	24.5	31.6	0.1	3.5	14	1.9
S	0.03	2	5e-1	50.3	51.9	3.2	1.9	5	1.3
T	0.03	3	1	54.1	56.3	2.3	1.9	4	1.1
U	0.01	0.1	5e-3	14.1	11.4	0	6.8	20	0.8
V	0.01	0.5	3e-2	13.2	21	0	5.1	11	0.7
W	0.01	1	1e-1	14.3	39.6	0.1	3.7	10	0.6
X	0.01	2	5e-1	32.6	49.1	3.7	2	5	0.5
Y	0.01	3	1	44	56.8	2.9	1.9	4	0.4

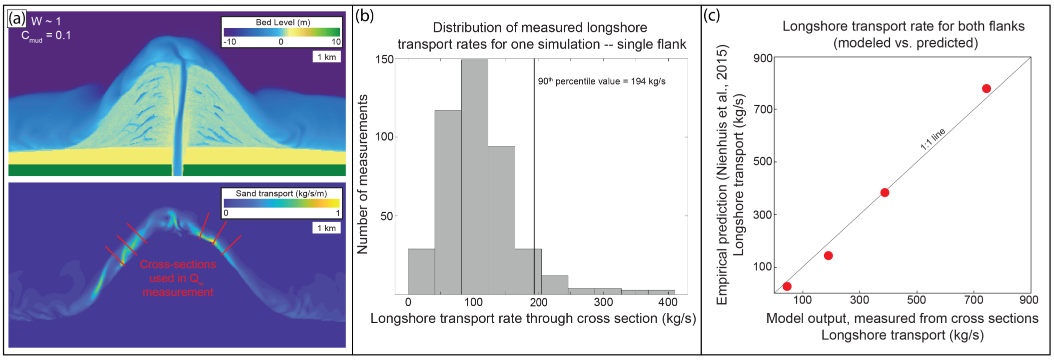

Figure 3. Comparison between empirically predicted and emergent longshore transport rates. (a) One time step of an example simulation showing bed levels (upper) and the sediment transport field (lower) at the same scale and resolution; red lines show the location of 6 example cross sections along which longshore transport is measured. This process is repeated for each low-flow time step over the final 33% of the simulation period. (b) Histogram showing the distribution of all measured longshore transport values for a single example simulation (note that these are values for a single flank). The 90$^{\text{th}}$ percentile value is multiplied by a factor of 2 to reflect transport on both flanks and used for comparison with empirical prediction for a given simulation. (c) Comparison between the measured longshore transport rates and empirically predicted maximum potential longshore transport rates for simulations with $C_{mud} = 0.1$ kg m^{-3} and $H_s \geq 1$ m. Each dot reflects these values for a given simulation.

3.4 Validation – Delta Shape Dynamics

To assess our simulations' ability to correctly resolve the delta-scale process interactions inherent to wave-influenced delta growth, we tracked the shape (ratio of maximum deposit length to maximum deposit width) of wave-influenced simulations through time. Previous work based on one-line models and observations of beach ridge orientations suggests that deltas exhibiting strong wave-influence or wave-dominance (in symmetrical wave climates) quickly obtain an equilibrium ratio of length to width and maintain this ratio throughout their growth (Komar, 1973; L. D. Wright, 1973; Ashton & Giosan, 2011). This fundamental characteristic of wave-influenced delta evolution reflects the interaction between fluvial and longshore transport process: fluvial sediment delivered to the shoreface causes seaward deflection of the shoreline, increasing the local wave approach angle and consequently the local longshore transport rate (which decreases toward the flanks as the delta flattens). When the fluvial sediment delivery rate matches the rate of longshore sediment transport away from the river mouth, an equilibrium shape is achieved, and further delta growth proceeds isometrically.

In our models, strongly wave-influenced simulations demonstrate exactly this process (Figure 4). All simulations with $W > 0.5$ eventually obtain an equilibrium shape, and simulations with more wave-influence achieve their equilibrium shape faster than those with less. Furthermore, simulations with greater wave-influence have equilibrium shapes that are flatter than those with less, paralleling observations of real-world wave-influenced deltas (Nienhuis et al., 2015). These observations build confidence in the ability of our simulations to resolve the delta-scale process interactions that control the evolution of wave-influenced deltas.

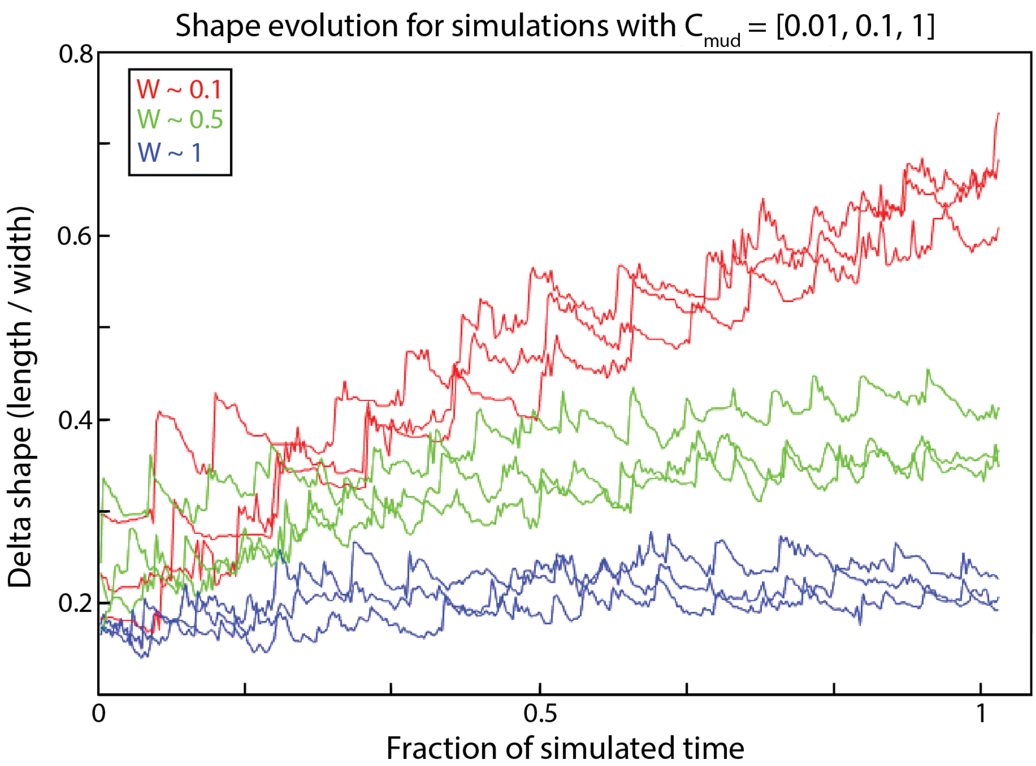

Figure 4. Evolution of delta shape through time. This plot includes simulations with 3 different mud concentrations ($C_{mud} = 0.01, 0.1, 1$ kg m^{-3}) and three different wave influences ($W = 0.1, 0.5, 1$) for nine total simulations. Note that simulations with $W < 0.5$ never reach an equilibrium shape, continuing a trend of elongation throughout the simulation period. By contrast, simulations with $W = 1$ obtain an equilibrium shape almost immediately.

3.5 Metrics

To quantify the morphology and dynamics of our simulations we developed MATLAB routines for automated extraction of various components of the delta system. Shorelines are defined using the opening angle method of Shaw et al. (2008) which permits objective definition of shorelines past openings, such as channels or inlets. Delta plains are defined as areas seaward of the initial shoreline and landward of the shoreline at a given timestep. Channelized areas are defined by thresholding maps of flow depth (threshold = 0.1 m) and velocity (threshold = 0.25 m s^{-1}) on the delta plain. We define lagoons as areas on the delta plain with depth greater than 0.5 m that are not part of the channel network. We quantify delta plain mud content (mud fraction, M_f) by the volume fraction of mud in delta deposits.

From our discretized representations of delta morphological attributes, we designed a suite of metrics that quantify their trends and dynamics through time. All time-dependent metrics are averaged over the final 50% of each run (90 flood cycles). The number of outlets (N_{out}) is defined as the number of contiguous overlapping regions of channelized areas and the shoreline. Shoreline roughness (R^*) is defined as the ratio between shoreline length and the length of the convex hull enclosing the delta plain. Lagoon area fraction (L_f) is defined as the ratio between total lagoon area and delta plain area. For each delta, these metrics are computed at the end of each flood cycle to characterize morphological tendencies for each. We quantify channel persistence (P_c) as the fraction of time a cell spent classified as channelized. We quantify the shoreline fractional change (D_{sl}) as the ratio of total length of new shoreline and length of the initial shoreline after each flood cycle.

4 Results

4.1 Controls of Mud and Waves on Gross Delta Morphology and Dynamics

Our simulations evolve through the same processes observed in natural delta systems and produce morphologies that strongly resemble real-world deltas across the spectrum of relative wave-influence (Figures 1 & 5). In the following sections we explore how these simulations vary with W and C_{mud}, in terms of the morphometrics defined in Section 3.5.

4.1.1 Distributary Channel Networks

Our simulations show that the number of distributary channel outlets decreases monotonically with increasing mud concentration (Figure 6a), and simulations with C_{mud} = 1 kg m^{-3} have on average half as many outlets as those with C_{mud} = 0.01 kg m^{-3} for all values of W. Interestingly, we note that the proportion of cohesive sediment impacts the number of outlets even at high wave-influence.

Our simulations also show a monotonic decrease in the number of distributary outlets with increasing wave-influence, contrasting with previous work that suggests an increase in the propensity for mouth bars to form in the presence of small, short period waves (Nardin et al., 2013). At high wave-influence, channel networks are limited to one or two outlets throughout the lifespan of an evolving delta (Figure 6a).

Channel persistence increases monotonically with both mud concentration and wave-influence, demonstrating on average a two-fold increase across the simulated range of C_{mud} and a three-fold increase across the simulated range of W. Even at high wave-influence ($W > 1$) the stabilizing effect of mud is apparent, and the most persistent channels are observed in simulations with the highest mud concentration and wave-influence (Figure

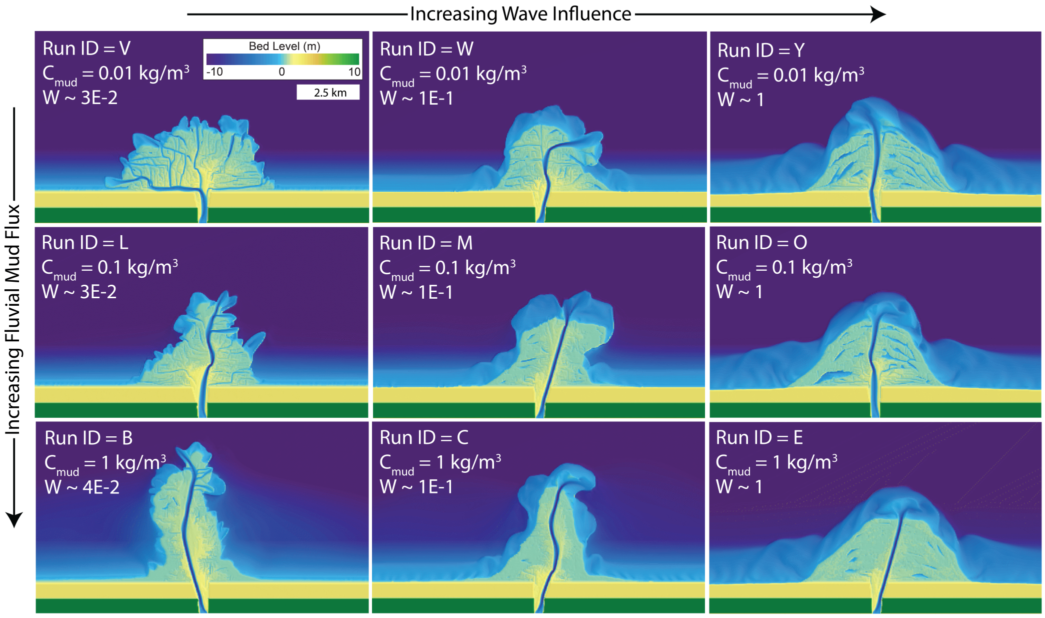

Figure 5. Simulated morphologies across a range of wave-influence and fluvial sediment compositions. Note the differences in channel networks and shorelines between simulations of different forcing, and the similarities with natural delta systems, in particular the presence of barrier-spits and lagoons in the most wave-influenced simulations

6b). These results demonstrate the important role of cohesive sediment in delta dynamics, even in the presence of large waves.

4.1.2 Delta shorelines

In river-dominated deltas, the shoreline morphology and dynamics are closely linked to those of the distributary channel network, with the creation of shoreline protuberances primarily driven by fluvial sediment deposition at channel mouths (W. Kim et al., 2006; Geleynse et al., 2012; Straub et al., 2015). The roughness of these shorelines is largely dependent on the length of distributary progradation, which in turn is influenced by fluvial sediment properties, particularly the concentration of cohesive sediments. This relationship is evident in our river-dominated simulations ($W < 0.1$), where we observe the highest shoreline roughness in scenarios with the greatest concentrations of cohesive sediment (Figure 6c).

As wave-influence increases, however, the role of cohesive sediment in determining shoreline roughness diminishes. At high wave influence ($W > 0.5$), fluvial sediment composition no longer significantly impacts shoreline roughness; the smoothest shorelines are found in simulations with the highest W values, regardless of sediment properties (Figure 6c). Several processes likely contribute to this shift. Beyond the well-known diffusional effect of low-angle waves and the role of longshore transport in smoothing shorelines (Swenson, 2005; Jerolmack & Swenson, 2007; Seybold et al., 2007), low-angle waves also act to dampen channel progradation, thereby reducing the length of deltaic protrusions near distributary outlets (Ashton & Giosan, 2011; Ratliff et al., 2018). Furthermore, our simulations show that waves limit the number of distributary outlets (Figure 6a) and stabilize channels (Figure 6b), limiting the number of new shoreline protrusions that are created.

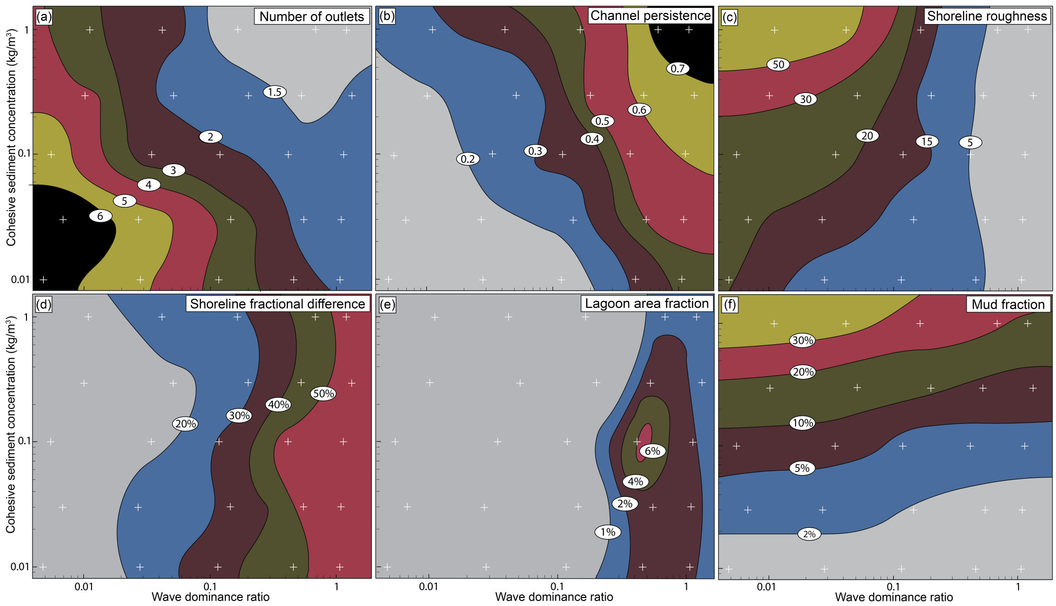

Figure 6. Contour plots for a variety of morphometrics across the simulated parameter space of wave dominance ratio and cohesive sediment concentration. White crosses denote positions of simulations (see Figure 2e for run IDs at each position). Numbers indicate metric value along a given contour line. Note the diagonal-directed gradients in the plots for number of outlets (a) and channel persistence (b), indicating dependence on both wave-influence and fluvial sediment composition. By contrast, shoreline roughness (c) shows a dependence transition at a wave-dominance ratio between 0.1-0.5, while shoreline fractional difference (d) is not overly sensitive to the cohesive sediment concentration. Lagoon area fraction (e) is maximized for $W = 0.5$ and $C_{mud} = 0.1$. Delta plain mud fraction (f) varies with W, but is more strongly dependent on C_{mud}

To determine which of these processes (wave-driven shoreline diffusion or progradation dampening and increased avulsion timescale) exerts a dominant role on shoreline morphology and dynamics, we compared the time-averaged fractional shoreline change between flood cycles across simulations (Figure 6d). Ignoring the effects of wave-driven shoreline diffusion, one would expect a decrease in the rates of shoreline change with increasing wave-influence, due to the progradation dampening and increased avulsion time scales associated with larger wave influence. Interestingly, our simulations show the opposite effect: fractional shoreline change increases monotonically with wave-influence (Figure 6d), demonstrating the dominance of shoreline diffusion over network suppression in wave-influenced delta shoreline dynamics.

These observations collectively indicate that the primary controls on local shoreline change (and consequently roughness) in deltas vary with wave-influence: in river-dominated deltas, local shoreline progradation depends on proximity to sediment sources (distributary outlets) and consequently on sediment composition. By contrast, shoreline change in wave-dominated deltas depends primarily on local shoreline geometry (specifically curvature) and how that geometry interacts with longshore transport and wave-driven erosion – which are independent of fluvial sediment properties.

4.1.3 Lagoons and Delta plains

Our simulations show that both waves and fluvial sediment composition play important roles in the sedimentary and environmental character of delta plains. Lagoons are common features on wave-influenced deltas (Figure 1); in our simulations they initially form in back-barrier settings and are incorporated into the delta plain during barrier-spit accretion (Figure 7, see section 4.2 for a more detailed discussion). For $0.1 < W < 0.7$, lagoon area fraction increases with wave influence (Figure 6e). As W approaches 1, there is an inflection point in this relationship, and lagoons become less prevalent with increasing W (Figure 6e).

Lagoon area fraction also exhibits a non-monotonic relationship with fluvial sediment composition; lagoons are most abundant in wave-influenced deltas with intermediate sediment composition (Figure 6e).

Finally, we quantified the abundance of mud in delta plain deposits to assess the importance of cohesive sediments from a sediment budget perspective. Unsurprisingly, delta plain mud fraction increases with increasing cohesive sediment concentration in the river, and decreases with increasing wave influence (Figure 6f). For the highest inflow concentrations, mud fraction in the delta plain decreases by a factor of 2 as W increases from 0.01 to 1. This decrease likely reflects transport of cohesive sediment to prodelta or offshore regions due to wave-enhanced shear stress near distributary outlets. This is augmented by the reduction in channel network complexity, since most of the delta plain mud is distributed within channels and associated levee deposits. However, despite this decrease, mud still constitutes a significant portion of the delta plain deposits in strongly wave-influenced simulations (15% in simulation E).

4.2 Barrier-Spit Accretion and the Growth of Wave-influenced Deltas

4.2.1 Qualitative Description

Our models demonstrate the essential processes by which wave-influenced deltas grow, which are distinct from those associated with the growth of river-dominated deltas. In simulations with limited wave influence, delta progradation is dominated by deposition of mouth bars and levees (see Movies S1-S4) in a fashion considered typical of river-dominated deltas (Edmonds & Slingerland, 2010). In more strongly wave-influenced simulations, however, deltas grow through a distinct multi-phase process involving jet deflection and wave-driven reworking of fluvial sediment that is initially deposited in the shoreface (Figure 7), which we refer to as the "barrier-spit accretion process".

The process begins with deflection of the fluvial jet, either by locally high wave approach angles or by incipient mouth bar deposition (Figure 7a). Fluvial sediment is initially deposited on the landward side of the jet centerline as a set of scattered nearshore bars or incipient mouth bars (Figure 7a). Note that these bars do not emerge above water level at this stage, instead constructing a subaqueous platform of sediment. Over time, these bars amalgamate with each other and with levee deposits and coalesce through continued fluvial deposition and shoreward-directed reworking by waves until their elevation is high enough to inhibit through-flow (Figure 7b-d). Following initial emergence, continued fluvial deposition and sculpting by longshore currents leads to elongation of the barrier-spit and rotation to a shore-parallel orientation (Figure 7d-e). Continued elongation of the barrier-spit by longshore currents eventually welds it to the existing shoreline at its distal tip (Figure 7f), closing the associated back-barrier lagoon. This entire process repeats itself throughout the growth of the delta, creating multiple generations of barrier-spits that amalgamate to form the delta plain.

4.2.2 Temporal Characteristics

Despite widespread recognition as a key formative mechanism in wave-influenced deltas, several questions remain regarding the barrier-spit accretion process. These include the temporal characteristics of the process (time to emergence, time between events, cyclicity), and controls on spacing between successive generations of barrier-spits. To address these questions, we generated a long-running simulation with high temporal output resolution that facilitates quantitative frequency analysis. The simulation parameters match those of the ensemble simulation with the highest propensity for forming lagoons (run N).

It is impossible to objectively define barrier-spit extents in our simulations due to spatial and topographic overlap with adjacent areas of the delta plain. To circumvent this issue, we instead define a metric that tracks the evolution of the subaqueous platform near the delta front, noting that the growth and decay of this platform reflects the gradual accumulation of fluvial sediment followed by subsequent emergence of that sediment as subaerial barrier-spits (Figure 7). At the end of each flood cycle, we compute the "fill fraction" (F), which is defined as the volume of subaqueous sediment deposits normalized by the volume of accommodation space in the same area prior to delta growth.

The area over which F is computed changes as the delta advances. This area is bounded by the front third of the delta shoreline and extends 2.5 km offshore (more details in the supporting information). Normalizing by the initial accommodation volume minimizes sensitivity to the specific area boundaries over time. Growth in F reflects subaqueous sediment deposition, while decreases in F indicate sediment emergence above sea level and incorporation into the delta plain.

A time series of F throughout delta growth (F_t) shows a distinct oscillatory behavior against a background of gradual increase and eventual flattening (Figure 8a). The gradual increase is attributed to increases in total depth as the delta progrades into the basin, which eventually ceases once the delta front is located entirely within the flat portion of the basin. The oscillations are best characterized as "ramp-cliff" structures, where periods of relatively slow growth in F are followed by rapid decreases back to a background value. These oscillations reflect gradual buildup of subaqueous sediment deposited near the mouth followed by rapid reductions in F as the sediment coalesces (due to onshore transport as a result of wave asymmetry) and the barrier-spit emerges above sealevel.

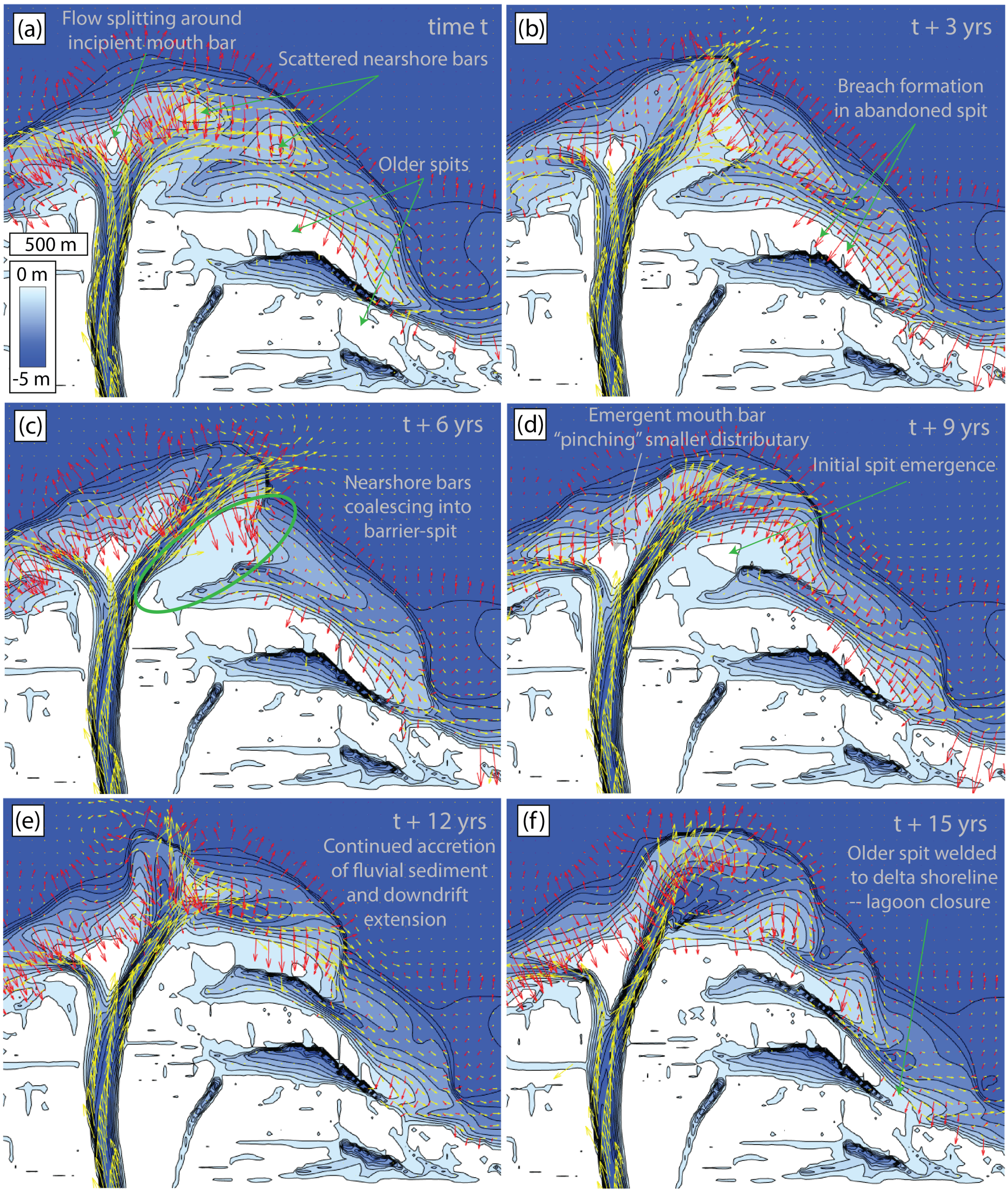

Figure 7. Example from a wave-dominated simulation demonstrating the processes by which wave-influenced deltas grow. Green arrows, circle highlight features of interest. Panels show the time evolution of bed level (filled contours at 0.5 m intervals), current velocity fields (yellow vectors) and wave forces (red vectors) during one cycle of shoreface fluvial deposition (a-c) barrier development (c-e) and accretion (e-f). At least two generations of older barrier-spits are visible here, highlighting the cyclical nature of this process.

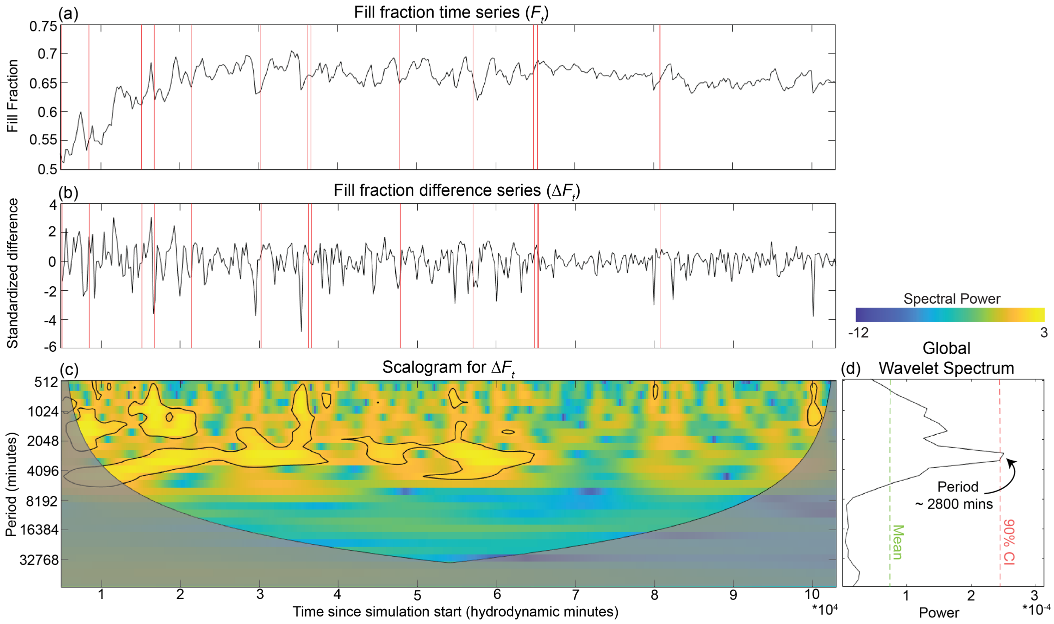

Figure 8. Cyclicity in the barrier-spit accretion process for a simulation with parameters matching run N. (a) Raw time series of the fill fraction (F_t) at the delta front, defined as the ratio of subaqueous sediment deposit volume to available accommodation space. (b) Difference time series of F (ΔF_t) used for wavelet analysis. (c) Local wavelet power spectrum (scalogram) showing the frequency distribution of signal variance over time. Gray areas indicate the cone of influence, where edge effects make power estimates unreliable. Thick black contours highlight regions where spectral power significantly exceeds the 90% confidence level against white noise, based on Torrence and Compo (1998). (d) Global wavelet spectrum, summing the power in (c) across time. Green and red lines in (d) represent the mean and 90% confidence spectra for white noise with identical signal length and degrees of freedom. Note the spike in spectral power around a period of 2800 minutes (∼15 flood cycles), exceeding the 90% confidence level. Vertical red lines in (a) and (b) indicate the formation times ("birthdays") of lagoons – discussed in section 5.2

To test whether barrier-spit accretion is a cyclical (rather than random) process, we analyze the frequency content of the F difference series ($\Delta F_t = F_t - F_{t-1}$) (Figure 8b) using a wavelet transform. As a spectral analysis tool, wavelets provide several advantages over the more commonly used Fourier transform, including better time-frequency localization and handling of non-stationary signals, reduced edge-effects, and improved detection of transients (Kumar & Foufoula-Georgiou, 1997). We operate on ΔF_t (rather than F_t) because we are interested in the time between barrier-spit emergence events, which are characterized by rapid reductions in F, manifesting as large negative spikes in ΔF_t. Operating on the difference series has the added benefit of reducing the spectral power at low frequencies associated with non-stationarity that can obfuscate features of interest at higher frequencies.

Figure 8c and 8d show the local and global wavelet spectra (respectively) of the ΔF_t computed using the Morlet wavelet (wavenumber = 6). The local wavelet spectrum (LWS, also known as the scalogram) shows the distribution of variance in the ΔF_t time series in the time and frequency domains. The global wavelet spectrum (GWS) is simply the time-sum of the LWS, and shows how signal variance is distributed in the frequency domain for the entire signal. Both the LWS and the GWS show a concentration of spectral power at an approximate scale of 2800 minutes (bright yellow regions in Figure 8c, large spike in Figure 8d), suggesting a periodic component in the ΔF_t time series at these scales.

We test the significance of peaks in the LWS and GWS against a background spectrum for a white-noise process with identical signal length and degrees of freedom to ΔF_t (Torrence & Compo, 1998) at an 90% confidence level. Several regions of the LWS exhibit spectral power surpassing this threshold (black contours in Figure 8c), and there is a statistically significant peak in the GWS at periods of approximately 2800 minutes (peak in Figure 8d). Although the spectra show additional peaks at lower frequencies (longer wavelengths) these are not considered significant against the assumed background spectra.

Analysis of the global wavelet spectra demonstrates that oscillations in F are indeed cyclical, with a periodicity equivalent to approximately 15 flood cycles. Depending on assumptions regarding recurrence intervals for geomorphically-significant flood events, these oscillations would have periods ranging from decades to centuries in real-world delta systems – similar to estimates from field examples such as the Danube, the Red and the Po river deltas (Vespremeanu-Stroe & Preoteasa, 2015; Preoteasa et al., 2016; Van Maren, 2005; Simeoni et al., 2007). This analysis suggests that barrier-spit accretion is a cyclical (rather than stochastic) autogenic process, which is driven by accumulation of nearshore subaqueous sediment, rather than being initiated by individual flood events. Simulations conducted during model development further support this finding; even with constant fluvial discharge, these simulations reproduce the delta growth processes described here (see Movie S5).

5 Discussion

5.1 Barrier-spit accretion process

Our simulations capture the transitions between river-dominated and wave-dominated delta growth processes and are able to reproduce the barrier-spit accretion process that has been documented in several natural wave-influenced delta systems (Bhattacharya & Giosan, 2003). Examples include the Tiber delta (Bellotti et al., 1995; Milli et al., 2013), the Vasishta lobe of the Godavari delta (Rao et al., 2005), the Rosetta lobe of the Nile delta (Sestini, 1989), the Sfantu Gheorge lobe of the Danube delta (Dan et al., 2011; Preoteasa et al., 2016), and the Ba Lat lobe of the Red River delta (Van Maren, 2005), among others.

Interestingly, barrier-spits emerge in the simulations in spite of relatively crude (or completely absent) parameterizations of processes that are considered important in their evolution, such as swash, overwash, and eolian transport. While these processes are certainly important for the longer-term evolution of these features (particularly in supply-limited environments, such as eroding headlands), their emergence in our simulations shows that the dominant factors controlling barrier-spit accretion in prograding deltas are the relative strengths of fluvial, longshore, and cross-shore sediment transport.

It has been suggested that the onset of barrier-spit growth in prograding deltas may be initiated by periods of rapid sediment delivery to the shoreface, such as during large river floods (Anthony, 2015; Bhattacharya and Giosan, 2003). However, recent work has demonstrated that spit emergence in both fluvial and non-fluvial settings may be preceded by a prolonged period of subaqueous nearshore sediment accumulation that constructs a platform onto which the spit can prograde (Preoteasa et al., 2016; van Kouwen et al., 2023). Futhermore, several case studies suggest that barrier-spit emergence in deltas exhibits some level of cyclicity (evidenced by abundant, regularly spaced inactive barriers preserved on the delta plain), with estimated recurrence intervals ranging from 10's to 100's of years – which is longer than typical recurrence intervals for bankfull floods (Van Maren, 2005; Vespremeanu-Stroe & Preoteasa, 2015; Preoteasa et al., 2016).

The time series and frequency analysis of fill fraction clearly show that there is a periodic component to barrier-spit accretion on timescales of about 15 floods, far exceeding the frequency of "bankfull" discharge events. This emergent cyclicity suggests that the role of gradual sediment buildup in the subaqueous portions of the delta front may be more important in determining when barrier-spits form than periods of pulsed sediment supply, though this likely depends on system-specific variables in real-world deltas.

5.2 Lagoon optimization, birthdays and life expectancy

Our analysis shows that intermediate fluvial mud concentrations ($C_{mud} = 0.1$) optimize the conditions for barrier growth and lagoon formation, with lagoon area fraction decreasing for $C_{mud} < 0.1$ and $C_{mud} > 0.1$. We attribute this to different processes; at high fluvial mud concentrations, back-barrier deposition of fine-grained sediments "erases" lagoons as quickly as they form. At low mud concentrations, channels are less stable and change positions frequently, limiting sediment supply to (and consequently size of) individual barrier features. Our simulations also show that lagoon area fraction is optimized for $W = 0.5$, and decreases with increasing or decreasing W. We attribute this to the mechanisms involved in lagoon formation; barrier-spits (and consequently lagoons) only form in settings with significant wave influence, but large waves favor the accretion of sediment directly onto the existing shoreline due to strong onshore-directed transport.

Barrier-spits are common features in real-world wave-influenced deltas, but not all systems preserve lagoons on the delta plain. Likewise, our simulations indicate that even under "optimal" conditions, not every barrier-spit leads to the formation of a lagoon that is ultimately preserved. In Figure 8b, the "birthdays" of lagoons that persist until the end of the simulation are shown, overlaid on the time series of ΔF_f (see the supporting information for details on how lagoon birthdays are calculated). This simulation uses parameters that optimize the conditions for lagoon preservation. Lagoon birthdays are typically preceded by significant negative spikes in ΔF_f, associated with the emergence of subaqueous sediment as barrier-spits develop. However, not every negative spike in ΔF_f results in a lagoon, and several barrier-spit emergence events—particularly later in the simulation—do not correspond with lagoon preservation.

This analysis, though somewhat ad-hoc, highlights the complexity of the barrier-spit accretion process and the factors that determine whether or not a lagoon becomes incorporated into the delta plain. Even in our simplified models, we speculate that multiple factors may control the preservation of individual lagoons, including the lagoon's initial geometry (namely width), the shoreline's initial orientation and bathymetry, and the balance between longshore and cross-shore sediment transport during evolution of the enclosing barrier-spit. Furthermore, lagoon preservation in real-world delta systems also depends on processes which are not represented in the model, including overwash and eolian transport. The interplay of these dynamic and time-varying factors suggests that predicting whether an individual lagoon will be preserved on the delta plain may be impossible.

Nevertheless, our simulations show that, at a broad scale, the proportion of the delta plain covered by lagoons is influenced by both the characteristics of fluvial sediment and the balance between fluvial and longshore sediment transport. Lagoon preservation tends to be maximized under intermediate conditions of fluvial mud concentration and relative wave influence. This finding is significant for paleoenvironmental interpretation, as the presence of abundant back-barrier lagoonal deposits may indicate a specific set of environmental conditions.

5.3 Role of mud in wave-influenced delta morphodynamics

Our simulations show that mud plays important roles in delta evolution, even in wave-dominated environments. In river-dominated deltas, higher mud concentrations in fluvial effluent are thought to enhance the stability of distributary channels and inhibit the bifurcation process, resulting in a decrease in the overall number of outlets and an increase in the persistence of individual distributaries (Hoyal & Sheets, 2009; Martin et al., 2009; Edmonds & Slingerland, 2010; Caldwell & Edmonds, 2014; Straub et al., 2015; Liang et al., 2015). Waves are also thought to decrease the number of channel outlets (by inhibiting bifurcation) (J. P. M. Syvitski & Saito, 2007; Jerolmack & Swenson, 2007; Geleynse et al., 2011; Nardin & Fagherazzi, 2012; Nardin et al., 2013; Anthony, 2015; Gao et al., 2018), and have stabilizing effects on distributary channels (Swenson, 2005; Ratliff et al., 2018; Gao et al., 2018; Liu et al., 2020; Hu et al., 2022; Zăinescu et al., 2024). Our simulations not only confirm these previous results, but show the effects of mud and waves in simplifying and stabilizing distributary networks actually work in concert: the simplest networks and most stable channels are found in simulations where W and C_{mud} are both maximized.

By controlling network morphology and dynamics, fluvial sediment composition controls how sediment is distributed at the shoreline. However, despite this, shoreline geometry (as quantified by rugosity) in wave-dominated deltas does not depend on fluvial sediment composition. This highlights the dominance of wave-driven processes (erosion and longshore transport) over fluvial processes (bifurcation, levee progradation and avulsion) in controlling the shoreline dynamics of these systems.

Mud also affects the barrier-spit accretion process by preferentially filling back-barrier lagoons and inhibiting their preservation as open water on the delta plain, impacting the character of delta deposits. Anthony (2015) highlighted a knowledge gap concerning the controls on beach-ridge spacing in wave-influenced deltas, suggesting sediment supply as a possible controlling variable. Our simulations suggest that the abundance of mud in fluvial effluent may explain the distinction between deltas with systems of welded beach ridges (and the occasional lagoon) and deltas where beach ridges are interspersed with fine-grained back-barrier deposits.

Finally, there are several other ways in which mud could influence the growth of wave-influenced deltas beyond those modeled and described here. Mud can settle in the subaqueous platform or prodelta of wave-influenced systems as a result of density currents or during periods of relative wave quiescence (Steel et al., 2024), facilitating progradation and helping to stave off delta autoretreat (M. Kim et al., 2024). In very large delta systems, mud can be transported by longshore currents to areas with less wave energy, wherein it may be the dominant constructional material, such as the downdrift flanks of the Mekong and Amazon deltas (Anthony, 2015).

5.4 Limitations

It is important to note that our simulations are a highly schematized and simplified representation of reality, and as such ignore several processes common to wave-influenced deltas. For instance, phase differences between periods of high river discharge and intense wave-action are the norm in strongly wave-influenced systems, and may significantly impact the barrier formation and accretion process. Strong, onshore directed wind fields are also common in wave-dominated delta systems, creating important features such as coastal dunes and potentially contributing to barrier rollover and accretion. Ignoring these important processes may lead to our simulations overestimating the prevalence of lagoons on the delta plain, especially in environments dominated by sand. Still, our models are among the first to recreate the processes by which symmetrical wave-influenced systems grow and evolve, and are useful for assessing how those processes vary in response to wave forcing and fluvial sediment composition.

6 Conclusions

Our study offers new insights into the complex roles of wave-influence and fine-grained cohesive sediment on the morphodynamics of river deltas. By leveraging physics-based numerical models, we have elucidated key processes and morphological characteristics that differentiate wave-influenced deltas from their river-dominated counterparts. Waves influence delta morphology through processes such as jet deflection, barrier formation, and longshore sediment transport. Wave-driven reworking of fluvial sediments results in distinctive features relative to river-dominated deltas: shorelines are smoother and reworked more frequently, channel networks exhibit limited complexity and are more persistent, and deltas grow through a cyclical process of barrier-spit formation and accretion, producing delta plains with sedimentary facies that are distinct from their river-dominated counterparts. These processes and features parallel those observed in natural deltas, such as the Red, Sinu, and Coco river deltas, among others.

Our results highlight the important role of cohesive sediment in the accretion of wave-influenced deltas. Mud affects network properties and in turn affects how sediment is distributed at the delta shoreline. Mud is preserved on the delta plain in levees and behind barrier-spits, and thus is an important component in the mass balance of these systems. Finally, mud also affects the barrier-spit accretion process, and determines barrier-spit spacing for a given degree of wave-influence. These results have implications for delta sediment budgets and resultant management actions, as well as for sedimentary facies models in wave-influenced deltas and resultant paleoenvironmental interpretations.

Finally, our simulations show that deltas near the transition of fluvial and wave-dominance may be particularly sensitive to changes in sedimentary or hydrodynamic forcing conditions, as the dominant processes controlling local shoreline variability and the creation of new land change near $W = 1$. Furthermore, the creation and preservation of back-barrier lagoons is optimized within a narrow range of W and C_{mud} values, and an abundance of these features or their deposits in a natural delta system may be indicative of a specific set of formative conditions.

Open Research Section

As open source software, build 69179 of Delft3D is available from Deltares at the following URL: https://svn.oss.deltares.nl/repos/delft3d/tags/delft3d4/69179/. Simulation input files and MATLAB code used to process and analyze simulation outputs are available through a Zenodo repository: https://zenodo.org/records/14166672 (Broaddus, 2024).

Acknowledgments

CB acknowledges support by a NASA FINESST grant (Grant 80NSSC24K0033). EF-G acknowledges support by the Samueli endowed chair and by NSF (Grant EAR 2342937, RISE 2425748).

References

Anderson, A. M., Allen, D. M., & Venditti, J. G. (2023, 11). Sensitivity of Subsurface Permeability in Coastal Deltas to Their Morphodynamic and Geomorphic Characteristics. *Water Resources Research*, *59*(11), e2022WR034136. https://doi.org/10.1029/2022WR034136

Anthony, E. J. (2015, 3). Wave influence in the construction, shaping and destruction of river deltas: A review. *Marine Geology*, *361*, 53–78. https://doi.org/10.1016/J.MARGEO.2014.12.004

Ashton, A. D., & Giosan, L. (2011, 7). Wave-angle control of delta evolution. *Geophysical Research Letters*, *38*(13). https://doi.org/10.1029/2011GL047630

Ashton, A. D., & Murray, A. B. (2006, 11). High-angle wave instability and emergent shoreline shapes: 2. Wave climate analysis and comparisons to nature. *Journal of Geophysical Research: Earth Surface*, *111*(F4). https://doi.org/10.1029/2005JF000423

Baar, A. W., Boechat Albernaz, M., van Dijk, W. M., & Kleinhans, M. G. (2019, 10). Critical dependence of morphodynamic models of fluvial and tidal systems on empirical downslope sediment transport. *Nature Communications 2019 10:1*, *10*(1), 1–12. https://doi.org/10.1038/s41467-019-12753-x

Bellotti, P., Milli, S., Tortora, P., & Valeri, P. (1995, 8). Physical stratigraphy and sedimentology of the Late Pleistocene-Holocene Tiber Delta depositional sequence. *Sedimentology*, *42*(4), 617–634. https://doi.org/10.1111/j.1365-3091.1995.tb00396.x

Bhattacharya, J. P., & Giosan, L. (2003, 2). Wave-influenced deltas: geomorphological implications for facies reconstruction. *Sedimentology*, *50*(1), 187–210. https://doi.org/10.1046/J.1365-3091.2003.00545.X

Broaddus, C. M. (2024). *Wave-influenced deltas grow through cyclical accretion of barrier-spits: Software and data.* Zenodo. https://doi.org/10.5281/zenodo.14166672

Broaddus, C. M., Brown, J., Edmonds, D. A., Vulis, L. M., Tejedor, A., Nienhuis, J. H., . . . Foufoula-Georgiou, E. (2022). First-Order River Delta Morphology is Explained by the Sediment Flux Balance from Rivers, Waves, and Tides. *Geophysical Research Letters*. https://doi.org/10.1029/2022GL100355

Burpee, A. P., Slingerland, R. L., Edmonds, D. A., Parsons, D., Best, J., Cederberg, J., . . . Royce, J. (2015, 6). Grain-Size Controls On the Morphology and Internal Geometry of River-Dominated Deltas. *Journal of Sedimentary Research*, *85*(6), 699–714. https://doi.org/10.2110/JSR.2015.39

Caldwell, R. L., & Edmonds, D. A. (2014, 11). The effects of sediment properties on deltaic processes and morphologies: A numerical modeling study. *Journal of Geophysical Research: Earth Surface*, *119*(5), 961–982. https://doi.org/10.1002/2013JF002965

Caldwell, R. L., Edmonds, D. A., Baumgardner, S., Paola, C., Roy, S., & Nienhuis, J. H. (2019, 11). A global delta dataset and the environmental variables that predict delta formation on marine coastlines. *Earth Surface Dynamics*, *7*(3), 773–787. Retrieved from `https://esurf.copernicus.org/articles/7/773/2019/http://files/73/Caldwelletal.-2019`

-Aglobaldeltadatasetandtheenvironmentalvaria.pdfhttp://files/74/2019.html 10.5194/esurf-7-773-2019

Dan, S., Walstra, D. J. R., Stive, M. J., & Panin, N. (2011, 2). Processes controlling the development of a river mouth spit. *Marine Geology*, *280*(1-4), 116–129. https://doi.org/10.1016/j.margeo.2010.12.005

Dominguez, J. M. (1996). The São Francisco strandplain: A paradigm for wave-dominated deltas? *Geological Society Special Publication*, *117*, 217–231. https://doi.org/10.1144/GSL.SP.1996.117.01.13

Edmonds, D. A., & Slingerland, R. L. (2007, 11). Mechanics of river mouth bar formation: Implications for the morphodynamics of delta distributary networks. *Journal of Geophysical Research: Earth Surface*, *112*(F2). https://doi.org/10.1029/2006JF000574

Edmonds, D. A., & Slingerland, R. L. (2010, 11). Significant effect of sediment cohesion on delta morphology. *Nature Geoscience*, *3*(2), 105–109. https://doi.org/10.1038/ngeo730

Ericson, J. P., Vörösmarty, C. J., Dingman, S. L., Ward, L. G., & Meybeck, M. (2006). Effective sea-level rise and deltas: Causes of change and human dimension implications. *Global and Planetary Change*, *50*, 63–82. Retrieved from www.elsevier.com/locate/gloplacha 10.1016/j.gloplacha.2005.07.004

Esposito, C. R., Georgiou, I. Y., & Kolker, A. S. (2013, 4). Hydrodynamic and geomorphic controls on mouth bar evolution. *Geophysical Research Letters*, *40*(8), 1540–1545. https://doi.org/10.1002/GRL.50333

Fagherazzi, S., Edmonds, D. A., Nardin, W., Leonardi, N., Canestrelli, A., Falcini, F., ... Slingerland, R. L. (2015, 9). Dynamics of river mouth deposits. *Reviews of Geophysics*, *53*(3), 642–672. https://doi.org/10.1002/2014RG000451

Galloway, W. E. (1975). Process Framework for Describing the Morphologic and Stratigraphic Evolution of Deltaic Depositional Systems. *Deltas, Models for Exploration*, 86–98. Retrieved from http://files/5/Galloway-ProcessFrameworkforDescribingtheMorphologica.pdf

Gao, W., Nienhuis, J., Nardin, W., Wang, Z. B., Shao, D., Sun, T., & Cui, B. (2020, 9). Wave Controls on Deltaic Shoreline-Channel Morphodynamics: Insights From a Coupled Model. *Water Resources Research*, *56*(9), e2020WR027298. https://doi.org/10.1029/2020WR027298

Gao, W., Shao, D., Wang, Z. B., Nardin, W., Yang, W., Sun, T., & Cui, B. (2018, 12). Combined Effects of Unsteady River Discharges and Wave Conditions on River Mouth Bar Morphodynamics. *Geophysical Research Letters*, *45*(23), 903–12. https://doi.org/10.1029/2018GL080447

Geleynse, N., Storms, J. E. A., Walstra, D.-J. R., Jagers, H. R. A., Wang, Z. B., & Stive, M. J. F. (2011, 11). Controls on river delta formation; insights from numerical modelling. *Earth and Planetary Science Letters*, *302*(1), 217–226. https://doi.org/10.1016/j.epsl.2010.12.013

Geleynse, N., Voller, V. R., Paola, C., & Ganti, V. (2012, 11). Characterization of river delta shorelines. *Geophysical Research Letters*, *39*(17). https://doi.org/10.1029/2012GL052845

Giosan, L., Syvitski, J., Constantinescu, S., & Day, J. (2014, 12). Climate change: Protect the world's deltas. *Nature 2014 516:7529*, *516*(7529), 31–33. https://doi.org/10.1038/516031a

Hoitink, A. J. F., Nittrouer, J. A., Passalacqua, P., Shaw, J. B., Langendoen, E. J., Huismans, Y., & van Maren, D. S. (2020, 11). Resilience of River Deltas in the Anthropocene. *Journal of Geophysical Research: Earth Surface*, *125*(3), e2019JF005201. https://doi.org/10.1029/2019JF005201

Hoyal, D. C. J. D., & Sheets, B. A. (2009, 11). Morphodynamic evolution of experimental cohesive deltas. *Journal of Geophysical Research: Earth Surface*, *114*(F2). https://doi.org/10.1029/2007JF000882

Hu, N., Murray, A. B., Ratliff, K. M., Little, Z., & Hutton, E. W. (2022, 5). Wave-

Climate Asymmetry Influence on Delta Evolution and River Dynamics. *Geophysical Research Letters*, *49*(9), e2021GL096315. https://doi.org/10.1029/2021GL096315

Ibàñez, C., Canicio, A., Day, J. W., & Curcó, A. (1997, 1). Morphologic development, relative sea level rise and sustainable management of water and sediment in the Ebre Delta, Spain. *Journal of Coastal Conservation*, *3*(1), 191–202. https://doi.org/10.1007/BF02908194

Ibáñez, C., Day, J. W., & Reyes, E. (2014, 4). The response of deltas to sea-level rise: Natural mechanisms and management options to adapt to high-end scenarios. *Ecological Engineering*, *65*, 122–130. https://doi.org/10.1016/J.ECOLENG.2013.08.002

Jerolmack, D. J., & Swenson, J. B. (2007, 11). Scaling relationships and evolution of distributary networks on wave-influenced deltas. *Geophysical Research Letters*, *34*(23). https://doi.org/10.1029/2007GL031823

Kim, M., Chun, B., Chamberlain, E., & Kim, W. (2024). Enhanced mud retention as an autogenic mechanism for sustained delta growth: Insight from records of the Lafourche subdelta of the Mississippi River. *Sedimentology*. https://doi.org/10.1111/SED.13230

Kim, W., Paola, C., Swenson, J. B., & Voller, V. R. (2006, 12). Shoreline response to autogenic processes of sediment storage and release in the fluvial system. *Journal of Geophysical Research: Earth Surface*, *111*(F4), 4013. https://doi.org/10.1029/2006JF000470

Komar, P. D. (1973). *Computer Models of Delta Growth due to Sediment Input from Rivers and Longshore Transport — GSA Bulletin — GeoScienceWorld.* https://doi.org/10.1130/0016-7606(1973)84⟨2217:CMODGD⟩2.0.CO;2

Korus, J. T., & Fielding, C. R. (2015, 11). Asymmetry in Holocene river deltas: Patterns, controls, and stratigraphic effects. *Earth-Science Reviews*, *150*, 219–242. https://doi.org/10.1016/j.earscirev.2015.07.013

Kumar, P., & Foufoula-Georgiou, E. (1997, 11). Wavelet analysis for geophysical applications. *Reviews of Geophysics*, *35*(4), 385–412. https://doi.org/10.1029/97RG00427

L. D. Wright, J. M. C. (1973). Variations in Morphology of Major River Deltas as Functions of Ocean Wave and River Discharge Regimes. *AAPG Bulletin*, *57*(2), 370–398. Retrieved from `https://archives.datapages.com/data/bulletns/1971-73/data/pg/0057/0002/0350/0370.htm`

Li, Q., Matthew Benson, W., Harlan, M., Robichaux, P., Sha, X., Xu, K., & Straub, K. M. (2017, 10). Influence of Sediment Cohesion on Deltaic Morphodynamics and Stratigraphy Over Basin-Filling Time Scales. *Journal of Geophysical Research: Earth Surface*, *122*(10), 1808–1826. https://doi.org/10.1002/2017JF004216

Liang, M., Voller, V. R., & Paola, C. (2015, 12). A reduced-complexity model for river delta formation – Part 1: Modeling deltas with channel dynamics. *Earth Surface Dynamics*, *3*(1), 67–86. https://doi.org/10.5194/esurf-3-67-2015

Liu, Y., Chen, H., Wang, J., Yang, S., & Chen, A. (2020, 1). Numerical simulation for the effects of waves and grain size on deltaic processes and morphologies. *Open Geosciences*, *12*(1), 1286–1301. https://doi.org/10.1515/geo-2020-0196

Martin, J., Sheets, B., Paola, C., & Hoyal, D. (2009, 9). Influence of steady base-level rise on channel mobility, shoreline migration, and scaling properties of a cohesive experimental delta. *Journal of Geophysical Research: Earth Surface*, *114*(F3), 3017. https://doi.org/10.1029/2008JF001142

Milli, S., D'Ambrogi, C., Bellotti, P., Calderoni, G., Carboni, M. G., Celant, A., ... Ricci, V. (2013, 2). The transition from wave-dominated estuary to wave-dominated delta: The Late Quaternary stratigraphic architecture of Tiber River deltaic succession (Italy). *Sedimentary Geology*, *284-285*, 159–180.

https://doi.org/10.1016/J.SEDGEO.2012.12.003

Nardin, W., & Fagherazzi, S. (2012, 11). The effect of wind waves on the development of river mouth bars. *Geophysical Research Letters*, *39*(12). https://doi.org/10.1029/2012GL051788

Nardin, W., Mariotti, G., Edmonds, D. A., Guercio, R., & Fagherazzi, S. (2013, 6). Growth of river mouth bars in sheltered bays in the presence of frontal waves. *Journal of Geophysical Research: Earth Surface*, *118*(2), 872–886. https://doi.org/10.1002/JGRF.20057

Nienhuis, J. H., Ashton, A. D., Edmonds, D. A., Hoitink, A. J. F., Kettner, A. J., Rowland, J. C., & Törnqvist, T. E. (2020, 10). Global-scale human impact on delta morphology has led to net land area gain. *Nature*, *577*(7791), 514–518. https://doi.org/10.1038/s41586-019-1905-9

Nienhuis, J. H., Ashton, A. D., & Giosan, L. (2015, 11). What makes a delta wave-dominated? *Geology*, *43*(6), 511–514. https://doi.org/10.1130/G36518.1

Nienhuis, J. H., Ashton, A. D., & Giosan, L. (2016, 11). Littoral steering of deltaic channels. *Earth and Planetary Science Letters*, *453*, 204–214. https://doi.org/10.1016/J.EPSL.2016.08.018

Nienhuis, J. H., Ashton, A. D., Kettner, A. J., & Giosan, L. (2017, 9). Large-scale coastal and fluvial models constrain the late Holocene evolution of the Ebro Delta. *Earth Surface Dynamics*, *5*(3), 585–603. https://doi.org/10.5194/ESURF-5-585-2017

Nienhuis, J. H., Ashton, A. D., Nardin, W., Fagherazzi, S., & Giosan, L. (2016, 4). Alongshore sediment bypassing as a control on river mouth morphodynamics. *Journal of Geophysical Research: Earth Surface*, *121*(4), 664–683. https://doi.org/10.1002/2015JF003780

Nota, P. J., Zhang, X., Liu, H., Mubikirwa, H., & Majid, A. (2024, 9). Effects of upstream and downstream boundary conditions on lacustrine shallow-water delta morphologies: A numerical modeling approach. *Marine and Petroleum Geology*, *167*, 106966. https://doi.org/10.1016/J.MARPETGEO.2024.106966

Olariu, C., & Bhattacharya, J. P. (2006, 2). Terminal Distributary Channels and Delta Front Architecture of River-Dominated Delta Systems. *Journal of Sedimentary Research*, *76*(2), 212–233. https://doi.org/10.2110/jsr.2006.026

Orton, G. J., & Reading, H. G. (1993, 6). Variability of deltaic processes in terms of sediment supply, with particular emphasis on grain size. *Sedimentology*, *40*(3), 475–512. https://doi.org/10.1111/J.1365-3091.1993.TB01347.X

Otvos, E. G. (2000, 2). Beach ridges — definitions and significance. *Geomorphology*, *32*(1-2), 83–108. https://doi.org/10.1016/S0169-555X(99)00075-6

P.D. Komar. (1998). *Beach processes and sedimentation* . Prentice Hall.

Penland, S., Boyd, R., & Suter, J. R. (1988, 11). Transgressive depositional systems of the Mississippi Delta plain; a model for barrier shoreline and shelf sand development. *Journal of Sedimentary Research*, *58*(6), 932–949. https://doi.org/10.1306/212F8EC2-2B24-11D7-8648000102C1865D

Preoteasa, L., Vespremeanu-Stroe, A., Tătui, F., Zăinescu, F., Timar-Gabor, A., & Cîrdan, I. (2016, 1). The evolution of an asymmetric deltaic lobe (Sf. Gheorghe, Danube) in association with cyclic development of the river-mouth bar: Long-term pattern and present adaptations to human-induced sediment depletion. *Geomorphology*, *253*, 59–73. https://doi.org/10.1016/J.GEOMORPH.2015.09.023

Rao, K. N., Sadakata, N., Malini, B. H., & Takayasu, K. (2005, 8). Sedimentation Processes and Asymmetric Development of the Godavari Delta, India. *River Deltas-Concepts, Models, and Examples*, 435–451. https://doi.org/10.2110/PEC.05.83.0435

Ratliff, K. M., Hutton, E. H., & Murray, A. B. (2018, 11). Exploring Wave and Sea-Level Rise Effects on Delta Morphodynamics With a Coupled River-Ocean Model. *Journal of Geophysical Research: Earth Surface*, *123*(11), 2887–2900.

https://doi.org/10.1029/2018JF004757

Rodriguez, A. B., Hamilton, M. D., & Anderson, J. B. (2000, 3). Facies and Evolution of the Modern Brazos Delta, Texas: Wave Versus Flood Influence. *Journal of Sedimentary Research*, *70*(2), 283–295. https://doi.org/10.1306/2DC40911-0E47-11D7-8643000102C1865D

Rossi, V. M., Kim, W., Leva López, J., Edmonds, D., Geleynse, N., Olariu, C., ... Passalacqua, P. (2016, 11). Impact of tidal currents on delta-channel deepening, stratigraphic architecture, and sediment bypass beyond the shoreline. *Geology*, *44*(11), 927–930. https://doi.org/10.1130/G38334.1

Sestini, G. (1989). Nile Delta: A review of depositional environments and geological history. *Geological Society Special Publication*, *41*, 99–127. https://doi.org/10.1144/GSL.SP.1989.041.01.09

Seybold, H., Andrade, J. S., & Herrmann, H. J. (2007, 12). Modeling river delta formation. *Proceedings of the National Academy of Sciences*, *104*(43), 16804–16809. https://doi.org/10.1073/pnas.0705265104

Shaw, J. B., Wolinsky, M. A., Paola, C., & Voller, V. R. (2008, 11). An image-based method for shoreline mapping on complex coasts. *Geophysical Research Letters*, *35*(12). https://doi.org/10.1029/2008GL033963

Simeoni, U., Fontolan, G., Tessari, U., & Corbau, C. (2007, 5). Domains of spit evolution in the Goro area, Po Delta, Italy. *Geomorphology*, *86*(3-4), 332–348. https://doi.org/10.1016/J.GEOMORPH.2006.09.006

Sloan, E., Dodd, N., & Briganti, R. (2024, 9). Effects of Tidal Range and Significant Wave Height on Delta Development. *Journal of Geophysical Research: Earth Surface*, *129*(9), e2024JF007688. https://doi.org/10.1029/2024JF007688

Soulsby, R. L. (1997). Dynamics of marine sands: a manual for practical applications. *Oceanographic Literature Review*, *44*(9), 947.

Stapor, F. W., & Stone, G. W. (2004, 2). A new depositional model for the buried 4000 yr BP New Orleans barrier: implications for sea-level fluctuations and onshore transport from a nearshore shelf source. *Marine Geology*, *204*(1-2), 215–234. 10.1016/S0025-3227(03)00350-5

Steel, R., Osman, A., Rossi, V. M., Alabdullatif, J., Olariu, C., Peng, Y., & Rey, F. (2024, 9). Subaqueous deltas in the stratigraphic record: Catching up with the marine geologists. *Earth-Science Reviews*, *256*, 104879. https://doi.org/10.1016/J.EARSCIREV.2024.104879

Storms, J. E., Stive, M. J., Roelvink, D. J., & Walstra, D. J. (2007). Initial morphologic and stratigraphic delta evolution related to buoyant river plumes. *Coastal Sediments '07 - Proceedings of 6th International Symposium on Coastal Engineering and Science of Coastal Sediment Processes*. https://doi.org/10.1061/40926(239)56

Straub, K. M., Li, Q., & Benson, W. M. (2015, 11). Influence of sediment cohesion on deltaic shoreline dynamics and bulk sediment retention: A laboratory study. *Geophysical Research Letters*, *42*(22), 9808–9815. https://doi.org/10.1002/2015GL066131

Stutz, M. L., & Pilkey, O. H. (2002, 11). Global Distribution and Morphology of Deltaic Barrier Island Systems. *Journal of Coastal Research*, 694–707. https://doi.org/10.2112/1551-5036-36.sp1.694

Swenson, J. B. (2005, 12). Relative importance of fluvial input and wave energy in controlling the timescale for distributary-channel avulsion. *Geophysical Research Letters*, *32*(23), 1–5. https://doi.org/10.1029/2005GL024758

Syvitski, J. P., Kettner, A. J., Overeem, I., Hutton, E. W., Hannon, M. T., Brakenridge, G. R., ... Nicholls, R. J. (2009, 9). Sinking deltas due to human activities. *Nature Geoscience 2009 2:10*, *2*(10), 681–686. Retrieved from `https://www.nature.com/articles/ngeo629` 10.1038/ngeo629

Syvitski, J. P. M., & Saito, Y. (2007, 11). Morphodynamics of deltas under the influence of humans. *Global and Planetary Change*, *57*(3), 261–282. https://doi

.org/10.1016/j.gloplacha.2006.12.001

Tamura, T. (2012, 9). Beach ridges and prograded beach deposits as palaeoenvironment records. *Earth-Science Reviews*, *114*(3-4), 279–297. https://doi.org/10.1016/J.EARSCIREV.2012.06.004

Tessler, Z. D., Vörösmarty, C. J., Grossberg, M., Gladkova, I., Aizenman, H., Syvitski, J. P., & Foufoula-Georgiou, E. (2015, 8). Profiling risk and sustainability in coastal deltas of the world. *Science*, *349*(6248), 638–643. https://doi.org/10.1126/SCIENCE.AAB3574

Tessler, Z. D., Vörösmarty, C. J., Overeem, I., & Syvitski, J. P. (2018, 3). A model of water and sediment balance as determinants of relative sea level rise in contemporary and future deltas. *Geomorphology*, *305*, 209–220. https://doi.org/10.1016/J.GEOMORPH.2017.09.040

Todd, T. W. (1968, 9). Dynamic diversion; influence of longshore current-tidal flow interaction on chenier and barrier island plains. *Journal of Sedimentary Research*, *38*(3), 734–746. https://doi.org/10.1306/74D71A5A-2B21-11D7-8648000102C1865D

Torrence, C., & Compo, G. P. (1998). A practical guide to wavelet analysis. *Bulletin of the American Meteorological Society*, *79*, 61–78. https://doi.org/10.1175/1520-0477(1998)079⟨0061:APGTWA⟩2.0.CO;2

van Kouwen, N. C., Ton, A. M., Vos, S. E., Vijverberg, T., Reniers, A. J., & Aarninkhof, S. G. (2023, 9). Quantifying spit growth and its hydrodynamic drivers in wind-dominated lake environments. *Geomorphology*, *437*, 108799. https://doi.org/10.1175/1520-0477(1998)079⟨0061:APGTWA⟩2.0.CO;210.1016/J.GEOMORPH.2023.108799

Van Maren, D. S. (2005). Barrier formation on an actively prograding delta system: The Red River Delta, Vietnam. *Marine Geology*, *224*, 123–143. https://doi.org/10.1016/j.margeo.2005.07.008

van Maren, D. S. (2007, 2). Water and sediment dynamics in the Red River mouth and adjacent coastal zone. *Journal of Asian Earth Sciences*, *29*(4), 508–522. https://doi.org/10.1016/J.JSEAES.2006.03.012

Vespremeanu-Stroe, A., & Preoteasa, L. (2015). Morphology and the Cyclic Evolution of Danube Delta Spits. *Coastal Research Library*, *12*, 327–339. Retrieved from `https://link.springer.com/chapter/10.1007/978-3-319-13716-2_18`

Vespremeanu-Stroe, A., Preoteasa, L., Zăinescu, F., Rotaru, S., Croitoru, L., & Timar-Gabor, A. (2016, 9). Formation of Danube delta beach ridge plains and signatures in morphology. *Quaternary International*, *415*, 268–285. https://doi.org/10.1016/J.QUAINT.2015.12.060

Vulis, L., Tejedor, A., Ma, H., Nienhuis, J. H., Broaddus, C., Brown, J., ... Foufoula-Georgiou, E. (2023). River delta morphotypes emerge from multiscale characterization of shorelines. *Geophysical Research Letters*. https://doi.org/10.1029/2022GL102684

Willis, B. J., Sun, T., & Ainsworth, R. B. (2021, 3). Contrasting facies patterns between river-dominated and symmetrical wave-dominated delta deposits. *Journal of Sedimentary Research*, *91*(3), 262–295. https://doi.org/10.2110/JSR.2020.131

Willis, B. J., Sun, T., & Ainsworth, R. B. (2022, 6). Sharp-based shoreface successions reconsidered in three-dimensions: A forward stratigraphic modelling perspective. *The Depositional Record*, *8*(2), 685–717. https://doi.org/10.1002/DEP2.177

Xu, Z., & Plink-Björklund, P. (2023, 10). Quantifying Formative Processes in River- and Tide-Dominated Deltas for Accurate Prediction of Future Change. *Geophysical Research Letters*, *50*(20), e2023GL104434. https://doi.org/10.1029/2023GL104434

Zăinescu, F., Anthony, E., & Vespremeanu-Stroe, A. (2021, 8). River Jets Versus

Wave-Driven Longshore Currents at River Mouths. *Frontiers in Marine Science*, *8*, 708258. https://doi.org/10.3389/fmars.2021.708258

Zăinescu, F., Storms, J. E. A., Vespremeanu-Stroe, A., Vegt, H. V. D., Schuster, M., & Anthony, E. (2024, 10). Wave-Influenced Delta Morphodynamics, Long-Term Sediment Bypass and Trapping Controlled by Relative Magnitudes of Riverine and Wave-Driven Sediment Transport. *Geophysical Research Letters*, *51*(19), e2024GL111069. https://doi.org/10.1029/2024GL111069

Zainescu, F., Vespremeanu-Stroe, A., & Tatui, F. (2016, 3). Comparative spit dynamics. the case of deltaic river mouth spits. *Journal of Coastal Research*, *1*(75), 800–804. https://doi.org/10.2112/SI75-161.1

Supporting Information for "Processes controlling wave-influenced delta growth and the role of fine-grained cohesive sediment"

Connor Broaddus[1], Jaap H. Nienhuis[2], Douglas A. Edmonds[3], Efi Foufoula-Georgiou[1,4]

[1]Department of Civil and Environmental Engineering, University of California Irvine, USA

[2]Department of Physical Geography, Utrecht University, NL

[3]Department of Earth and Atmospheric Sciences, Indiana University, USA

[4]Department of Earth System Science, University of California Irvine, USA

Contents of this file

1. Text S1 to S2
2. Figures S1 to S2
3. Movies S1 to S5

Additional Supporting Information (Files uploaded separately)

Introduction This document includes information detailing how fill fraction and lagoon birthdays are measured and computed. These descriptions are accompanied by schematics. Finally, we include captions for movies that demonstrate the growth of river-dominated and wave-dominated end-member simulations.

Text S1. Measurement of fill fraction To analyze the temporal characteristics of the barrier-spit accretion process, we define a time varying metric measuring the fraction of initially available accommodation space that is occupied by subaqueous sediment deposits in areas near the delta front, which we refer to as the fill fraction (F).

The first step is defining the delta front – the area over which to measure F ("area of interest" in Figure S1a). The area of interest (AOI) is defined separately for each time step of the simulation because the delta progrades through time. We define the AOI as a contiguous region bounded by a 2.5 km shoreline buffer. The AOI does not extend indefinitely along the delta flanks; rather, the lower bounds of the AOI are located 1/3 of the distance between the most basinward point of the shoreline and the initial shoreline ($0.33*L_d$, where L_d is the maximum length of the delta). These lower bounds are oriented perpendicular to the shoreline.

Within the AOI, we define the F as the volume of subaqueous sediment deposits (V_{ss}) divided by the volume of initially available accomodation space (V_{acc}) in the same region. We exclude from this calculation regions where sediment accumulation is less than 0.5 meters to avoid spurious changes in F as a result of the constantly changing AOI. Figure S1b shows how these volumes are defined for an example cross-section.

Text S2. Computation of lagoon birthdays To facilitate temporal comparison between the barrier-spit accretion process and lagoon preservation on the delta plain, we compute the periods of lagoon formation as discrete points in time (which we refer to as "birthdays") for the simulation used in the temporal analysis (Figure S2a).

To compute lagoon birthdays, we first define binary maps of lagoon presence for each output timestep of the simulation. Lagoons are defined as areas within the delta plain with depth greater than 0.5 meters that are not part of the channel network. We take the time sum of these lagoon presence maps and divide by the total number of simulation time steps to define persistence (Figure S2b), which is the fraction of total simulation time that a cell spent classified as a lagoon.

From the final lagoon presence map (Figure S2c) we identify individual lagoons using image analysis tools in MATLAB. Because lagoons do not form instantaneously, each lagoon has a distribution of persistence values. For each lagoon, we subtract the maximum value of its persistence distribution from the total simulation time to define its birthday (Figure S2d).

Birthdays are only computed for lagoons that exist at the end of the simulation. While this may result in the exclusion of some lagoons that form and are later ”erased” by deposition, it allows us to focus on lagoons that persist on the delta plain, which is the purpose of this analysis. Regardless, for the simulation of interest there do not appear to be any lagoons which are excluded from the analysis; some areas of identified lagoons do indeed fill in, but other areas remain and are used in the birthday calculation.

Movie S1. Animation showing the bed level evolution for a simulation with $W = 5e - 3$ and $C_{mud} = 0.01$. Delta growth is typified by channel bifurcation as a result of mouth bar formation, and channel avulsions.

Movie S2. Animation showing the bed level evolution for a simulation with $W = 1$ and $C_{mud} = 0.01$. Delta growth is typified by cyclical accretion of barrier spits, which enclose large, shore-parallel lagoons that are incorporated into the delta plain.

Movie S3. Animation showing the bed level evolution for a simulation with $W = 1e - 2$ and $C_{mud} = 1$. Delta growth is typified by channel progradation as a result of levee growth, unstable bifurcations that rapidly lead to closure of one limb, and channel avulsions.

Movie S4. Animation showing the bed level evolution for a simulation with $W = 1$ and $C_{mud} = 1$. Delta growth is typified by cyclical accretion of barrier spits. In most cases the associated lagoons are not preserved, instead filling with fine grained sediment prior to barrier-spit amalgamation with the existing delta plain.

Movie S5. Animation showing the bed level evolution for a simulation with $W = 1$ and $C_{mud} = 1$. This simulation differs from the others reported here in that the discharge boundary condition is held constant at 500 m^3 s^{-1}. Delta growth proceeds in a manner identical to that of Movie S4, demonstrating that the barrier-spit accretion process is not a product of variations in discharge or fluvial sediment delivery.

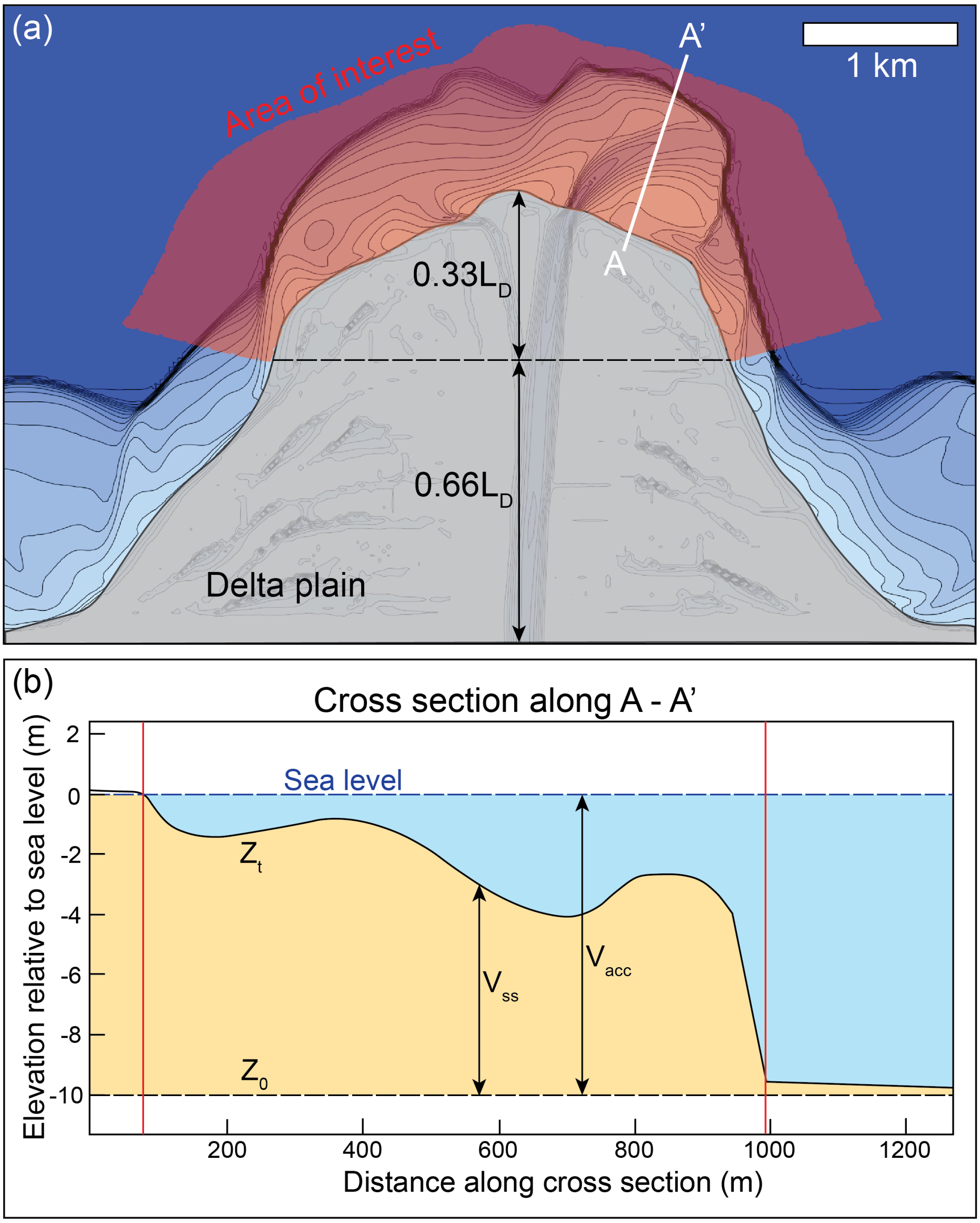

Figure S1. Schematic demonstrating how fill fraction is calculated. (a) shows the area of interest for a single timestep (red area), defined based on a fraction of total delta length (L_d) and a 2.5km buffer around the intial shoreline. (b) shows an example of the quantities defining the volume of subaqueous sediment (V_{ss}) and the volume of initial accomodation space (V_{acc}) based on the initial bed level (Z_0) and the bed level for a given timestep (Z_t). Note that these volumes are computed over the entire AOI, with the cross section merely serving as an example for visualization purposes. The white line (A-A') in (a) shows the location of the cross section shown in (b).

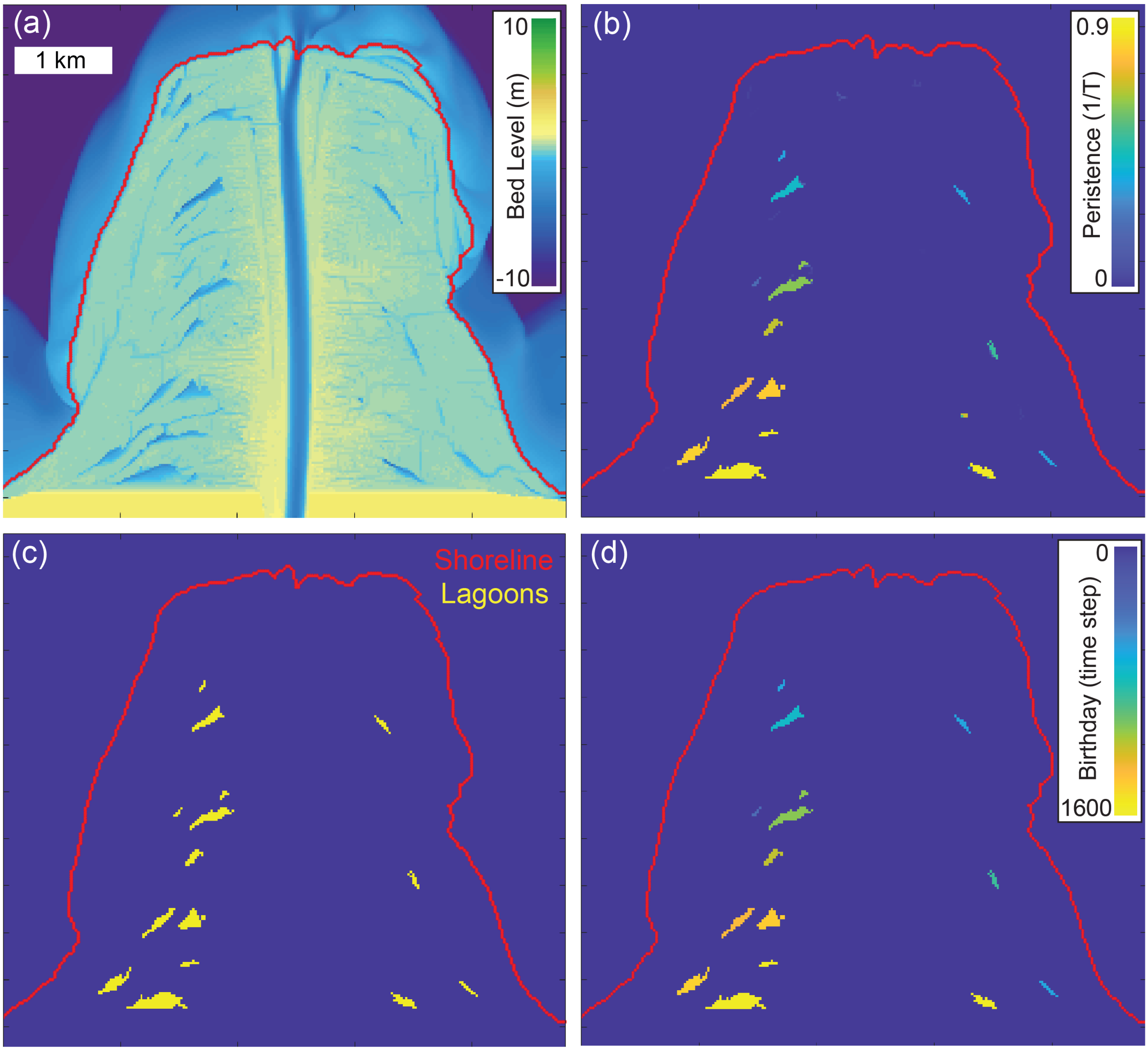

Figure S2. Maps demonstrating the lagoon birthdays calculation, including (a) final bed levels for the simulation of interest, (b) lagoon persistence, (c) lagoon presence for the final timestep, (d) lagoon birthdays in terms of number of timesteps. Scale and extent are identical for all panels.